RENEWABLE ELECTRIC POWER SYSTEMS ENERGY YIELD AND PERFORMANCE ESTIMATION

BY

SAIRAJ VIJAYKUMAR DHOPLE

DISSERTATION

Submitted in partial fulfillment of the requirements
for the degree of Doctor of Philosophy in Electrical and Computer Engineering
in the Graduate College of the
University of Illinois at Urbana-Champaign, 2012

Urbana, Illinois

Doctoral Committee:

Assistant Professor Alejandro D. Domínguez-García, Chair
Professor Philip T. Krein
Professor Peter W. Sauer
Assistant Professor Lee DeVille
Assistant Professor Robert Pilawa-Podgurski

ABSTRACT

This dissertation presents models for reliability assessment, energy yield estimation, and uncertainty analysis of renewable electric power systems. We propose system *performability* models that describe system attributes while acknowledging failures and repairs in constituent elements. Two broad classes of models are investigated: i) Markov reliability and reward models, and ii) stochastic hybrid systems (SHS) models. Conventional Markov models capture attributes that are largely static—the only dynamics are due to changes in system configuration due to failures and repairs in constituent elements. On the other hand, SHS can model a wide variety of dynamic phenomena, and provide significant flexibility over Markov models.

From an applications perspective, we propose Markov reward models to estimate the performability of photovoltaic energy conversion systems (PVECS) and wind energy conversion systems (WECS). A major impediment in formulating these models is the lack of precise data on model parameters, e.g., component failure and repair rates. Additionally, inputs to these models (e.g., incident insolation in PVECS and wind speed in WECS) are inherently uncertain. Therefore, to ensure validity of the results, we propose set-theoretic and probabilistic methods for uncertainty analysis in these models.

With regard to SHS, we first demonstrate how Markov reliability/reward models are a type of SHS. We also present applications to stochastic small-signal modeling of power systems. Case studies demonstrate how to quantify the impact of renewable resources uncertainty on power system dynamics.

To Pappa and Ayee

ACKNOWLEDGMENTS

I owe a debt of gratitude to Alejandro for his advice, assistance, insights, and all-round good humor. I have been incredibly fortunate to learn from Professor Krein and Professor Sauer—thanks go out to them for sparking my interest in power and energy systems. Thanks also go out to Lee, for explaining (among other things) the difference between f, $f(x)$, and $f(\cdot)$. I also want to take this opportunity to wish Robert the very best with all his academic endeavors. Of course, this would not have been possible without the support of my family and friends.

TABLE OF CONTENTS

Chapter 1 INTRODUCTION 1
1.1 Markov Reliability and Reward Models 2
1.2 Stochastic Hybrid Systems 6
1.3 Organization of this Dissertation and a Primer to the Case Studies . 9

Chapter 2 FUNDAMENTALS OF MARKOV RELIABILITY AND REWARD MODELS 11
2.1 Markov Reliability Models 11
2.2 Markov Reward Models 13
2.3 Stationary Distribution and Group Inverse of CTMCs 14
2.4 Sensitivity to Model Parameters 15
2.5 Dynamic Reward Models 17

Chapter 3 PROBABILISTIC UNCERTAINTY ANALYSIS IN MARKOV RELIABILITY AND REWARD MODELS 19
3.1 Problem Formulation 19
3.2 Single Parameter Case 21
3.3 Multiple-Parameter Case 25
3.4 Uncertainty in Markov Reward Models 31
3.5 Case Studies Covering Common Reliability Models 33

Chapter 4 UNKNOWN-BUT-BOUNDED UNCERTAINTY ANALYSIS IN MARKOV RELIABILITY AND REWARD MODELS 42
4.1 Problem Formulation 42
4.2 Taylor-Series Expansion of the Stationary Distribution 44
4.3 First-Order Approximation 46
4.4 Second-Order Approximation 47
4.5 Case Studies Covering Common Reliability Models 51

Chapter 5 STOCHASTIC HYBRID SYSTEMS FRAMEWORK FOR REWARD MODELING 59
5.1 Preliminaries 59

5.2 Markov Reward Models defined as SHS 61
5.3 Test Function and Extended Generator of SHS 63
5.4 Recovering Differential Equations for Conditional Moments from Test Functions 65
5.5 Evolution of the Accumulated Reward 66
5.6 Case Studies Covering Common Reward Models 72
5.7 Moment Closure for Markov Reward Models 79

Chapter 6 ESTIMATING PHOTOVOLTAIC ENERGY CONVERSION SYSTEMS PERFORMABILITY METRICS 82
6.1 Reliability and Performability Metrics of Interest in PVECS 83
6.2 Utility-Scale Installations 85
6.3 Optimum Repair Strategies for Residential PV Systems 89
6.4 Emerging Distributed Inverter Systems 92
6.5 Extensions and Future Work 95

Chapter 7 ESTIMATING WIND ENERGY CONVERSION SYSTEMS PERFORMABILITY METRICS 97
7.1 Overview of Proposed Framework 97
7.2 Quantifying Uncertainty in Wind Speed 99
7.3 Quantifying Uncertainty in Failure and Repair Rates 106
7.4 Case Studies that Demonstrate Impact of Input and Parametric Uncertainty 113

Chapter 8 IMPACT OF RENEWABLE RESOURCE VARIABILITY ON POWER SYSTEM DYNAMICS—AN SHS APPROACH 117
8.1 Linearized Power System Dynamics 118
8.2 Linearized Power System Dynamics as SHS 119
8.3 Renewable Resource Variability 120
8.4 Moment Evolution 123
8.5 Three-machine Nine-bus Power System 126

Chapter 9 CONCLUDING REMARKS AND FUTURE WORK 132
9.1 Concluding remarks 132
9.2 Future Work 133

Appendix A DERIVATIONS OF IMPORTANT RESULTS 135
A.1 Derivation of Result in (2.9) 135
A.2 Derivation of Stationary Distribution Sensitivities in (2.14)-(2.15) . 136
A.3 Derivation of Result in (3.22) 138
A.4 The Case of Dependent Model Parameters Considered in (3.25) . . . 140
A.5 Derivation of Linearized Power-System Model in (8.2) 141

REFERENCES 143

Chapter 1

INTRODUCTION

This dissertation presents system *performability* models for reliability assessment, energy yield estimation, and uncertainty analysis of renewable electric power systems. System performability models describe notions of system *perform*ance while acknowledging system reli*ability* due to failures and repairs in constituent elements. Two broad classes of models are investigated: i) Markov reliability and reward models, and ii) stochastic hybrid systems (SHS) models.

The methods we develop apply across the board to a wide class of systems. In light of this, the theoretical developments are presented with a high level of generality and accompanied by a variety of numerical/analytical case studies. From an applications perspective, we develop Markov models for photovoltaic energy conversion systems (PVECS) and wind energy conversion systems (WECS). A major impediment in formulating these models is the lack of precise data on model parameters, e.g., component failure and repair rates. Additionally, inputs to these models are inherently uncertain, e.g., incident insolation in PVECS and wind speed in WECS. Therefore, to ensure validity of the results, we propose set-theoretic and probabilistic methods for uncertainty analysis. In the development of Markov models, we will note that these are largely static in nature—the only dynamics are due to changes in system configuration due to failures and repairs in constituent elements. To provide an improved performability modeling framework, we will introduce SHS. In the realm of SHS, we demonstrate how these can be used to derive very general reward formalisms. We also show that Markov models are in fact an instance of SHS. Additionally, we present applications of SHS to stochastic small-signal modeling of power systems. The problem we study here is to quantify the impact of renewable resources uncertainty on the dynamics of electromechanical states of power system dynamic models.

1.1 Markov Reliability and Reward Models

Markov reliability models are ubiquitous in power system reliability assessment [1,2], and have been applied to study a wide array of systems including: WECS [3,4], small hydro power plants [5], PVECS [6–8], and substation/distribution equipment [9,10]. The efficacy of reliability and performability indices obtained from Markov reliability models hinges on the accuracy of component failure and repair rate data. However, due to scarcity of incidents, it is seldom possible to obtain accurate values of failure and repair rates for the system under investigation [11]. Therefore, in order to quantify the impact of imperfect information, uncertainty analysis must supplement reliability studies which are usually performed at single-point best estimates of the model parameter values [1,12–14].

Common approaches that have been explored to tackle parametric uncertainty in Markov models include: i) set-theoretic methods, in which parameters are modeled as unknown quantities bounded around a nominal value, and ii) probabilistic methods, in which parameters are modeled as random variables with known distributions. The main contribution of this dissertation pertains to the development of Taylor series expansions for the Markov chain stationary distribution that are then utilized in set-theoretic and probabilistic methods to propagate parametric uncertainty. Additionally, from an applications perspective, we demonstrate how these approaches to sensitivity and uncertainty analysis can be applied in PVECS and WECS.

1.1.1 Methods to Quantify Probabilistic Parametric Uncertainty

Chapter 3 presents a general framework for probabilistic uncertainty analysis in Markov reliability and reward models. Failure and repair rates are modeled as random variables (in lieu of precise numbers) with distributions determined by various methods, e.g., utilizing known confidence intervals and distributions of aleatory uncertainties such as the mean time to failure [15], applying the maximum entropy principle if only the range of the uncertain parameters is known [16], or based on expert opinions, engineering experience, and field data [17], [12]. Given the probability density functions (pdfs) of the uncertain parameters, we propose a framework to compute the pdfs of the Markov reliability model stationary distribution, and Markov reward model performability indices, both for repairable systems, in which the underlying Markov chains are ergodic.

The proposed framework involves the use of Taylor series expansions to approximate the entries of the Markov chain stationary distribution vector, i.e., the steady-state occupational probabilities of different states, as polynomial functions of the uncertain parameters, which are modeled as random variables. A significant contribution of this work is the derivation of the Taylor series coefficients, which are expressed in closed form as functions of the generator-matrix group inverse [18]. Subsequently, random variable transformations are applied to numerically compute the pdfs of the Markov chain steady-state probabilities and performability indices. Additionally, closed-form expressions for the expectation and variance of these indices are derived from a direct analysis of lower-order approximations of the Taylor series expansion. Note that if closed-form expressions for the relevant indices as a function of the model parameters were readily available, Taylor series expansions would be unnecessary; however, in general, it is difficult to obtain these expressions in closed form.

The use of Taylor series expansions to study parametric uncertainty in Markov reward models has been proposed in [16], [19]. In these works, the Taylor series coefficients are expressed in terms of the inverse of the underlying Markov chain generator matrix. However, since the generator matrix of ergodic Markov chains is singular, it is unclear how the ideas in [16], [19] can be implemented in practice. Additionally, while the approach is sketched out, it is not applied directly in the case studies. Methods to propagate uncertainty based on the Markov chain transient solution sensitivity to model parameters are outlined in [12], [20], [21], and [22]. By contrast, since we focus on repairable systems, our method focuses directly on the stationary distribution of ergodic Markov chains which are used to model repairable systems. Note also that our framework not only proposes closed-form approximations for the expectation and variance of reliability and performability indices, but also provides a numerical method to derive the pdfs of these indices. The sensitivities could be computed following alternative methods (see e.g., [12], [20] and the references therein) before applying the techniques proposed here to obtain the pdfs of the reliability/performability indices. Finally, a significant advantage of the proposed framework is that the only required input is the Markov chain generator matrix; i.e., closed-form expressions for the stationary distribution and performability indices as a function of the model parameters are not required a priori.

We demonstrate the application of the proposed framework in analyzing Markov reliability and reward models with several case studies, including: i) a two-state

model for a single component with two operating modes, ii) a three-state model for a two-component load-sharing system with common-cause failures, and iii) an $n+1$ state model for n components, each with two operating modes. In the first two case studies, we illustrate the accuracy of the proposed method by comparing results with Monte Carlo simulations (and the exact analytical result when available). The expectation and variance derived from the analytical expressions are also compared with those obtained numerically from the derived pdfs. The final case study presented in this chapter compares the execution time of the proposed approach with Monte Carlo simulations to compute the pdf of a particular performability metric. The execution time of the proposed Taylor series method is noted to be lower than Monte Carlo simulations for large models with a few uncertain parameters.

1.1.2 Methods to Quantify Worst-Case Parametric Uncertainty

In Chapter 4, we propose a set-theoretic method to propagate parametric uncertainty to reliability and performability indices that result from Markov reliability models. Instead of assuming that parameter probability distributions are available (or can be obtained from field data), we assume that only upper and lower bounds around nominal values are known. Thus, the values that these parameters can take are constrained within a set. Bounds on performability indices are obtained by propagating the set that describes all possible values the parameters can take through the stationary distribution of the Markov chain. This represents a worst-case uncertainty analysis as no assumptions are made on the failure-/repair-rate statistics. This method is more suited to reliability assessment when extensive failure/repair-rate data—that would enable constructing probability distributions—are unavailable. In summary, probabilistic parametric uncertainty models can be used to obtain statistics of reliability/performability indices; i.e., instead of obtaining a single-point estimate, we can obtain the distribution of the relevant indices. On the other hand, unknown-but-bounded parametric uncertainty models do not yield any statistical information of reliability/performability indices. Instead, they yield a bounding set that contains all possible values the relevant indices can take; i.e., in an unknown-but-bounded model, there is no notion of a *most likely* value, but we know with certainty that the *actual value* is contained in this bounding set [23].

In the proposed method, we assume that the uncertain parameters take values in a parallelotope, i.e., an extension of a parallelogram (in two dimensions) or a paral-

lelepiped (in three dimensions) to any dimension [24]. The center of the parallelotope corresponds to the nominal values that the parameters can take. A minimum-volume ellipsoid is constructed to upper-bound this parallelotope. Then, by using set operations, this ellipsoid is propagated through a second-order Taylor series expansion of the Markov chain stationary distribution.[1] This facilitates computation of approximate bounds on reliability and performability indices that arise from the Markov chain stationary distribution. The Taylor series coefficients are evaluated *only once* for the nominal values that the parameters take, and therefore, the approach is computationally inexpensive compared to repeated simulations, i.e., computing the relevant indices for all possible parameter values. A significant contribution of this work is a numerical method to propagate ellipsoidal sets through second-order polynomial systems—previous work in this area has been largely focused on linear systems [23]. This is relevant, as second-order Taylor-series expansions enable studies that can gauge the impact of larger uncertainties in parameter values, and as demonstrated in the case studies and examples in Chapter 4, they provide more accurate bounds than those obtained with first-order approximations.

Methods to assess the impact of unknown-but-bounded parametric uncertainty that exploit the sensitivity of the Markov chain transient solution to model parameters are proposed in [12,20]. By contrast, we focus directly on the stationary distribution of ergodic Markov chains employed in modeling repairable systems [13]. Techniques based on interval arithmetic (see, e.g., [25]) have been proposed in [26,27]. In these methods, the unknown parameters are assumed to belong to an interval—which is propagated through the Markov model using methods from interval arithmetics.

Heuristic methods based on fuzzy set theory have also been explored to quantify the impact of unknown-but-bounded parametric uncertainty [10,28,29]. However, it has been acknowledged that modeling uncertain transition rates by fuzzy membership functions requires computationally expensive fuzzy logic calculations [10]. The alternative is to derive explicit, closed-form equations for the reliability/performability indices (before applying fuzzy arithmetic). However, it turns out that this is infeasible for large models with multiple parameters [10]. The main advantage of our method is that the Markov chain generator matrix is the only required input; i.e., closed-form expressions for the stationary distribution or performability indices as a function of the model parameters are not required a priori. Based on

[1] Ellipsoids are preferred instead of the original parallelotope that they bound because set operations with ellipsoids involve simple matrix algebra.

these features, the proposed method is best suited to analyze parametric uncertainty in multi-state, multi-parameter Markov models, where closed-form expressions for the relevant indices are difficult to obtain, and exhaustive simulation of all possible parameter values is computationally expensive.

We demonstrate the application of the proposed method with two case studies in Chapter 4 : i) a two-component shared-load system with common-cause failures, and ii) an electric-power distribution transformer with deterioration and preventative maintenance. In the first case study, we quantify the impact of parametric uncertainty on a notion of reward defined for the two-component system, and in the second, we explore the optimal preventative maintenance rate to maximize transformer availability, while taking into account the effect of parametric uncertainty. We also compare the execution time of the proposed method by exhaustively simulating all possible parameter values as the model order grows.

1.2 Stochastic Hybrid Systems

Stochastic hybrid systems provide a reward modeling framework that not only encompasses Markov reward models but can capture a variety of other system performability notions. The framework foundations are a set of theoretical tools developed to analyze a class of stochastic processes referred to as piecewise-deterministic Markov processes [30]. Fundamentals of SHS and several applications to system performability modeling are presented in Chapter 5.

The state space of an SHS is comprised of a discrete state and a continuous state; the pair formed by these is what we refer to as the combined state of the SHS. The transitions of the discrete state are stochastic and the rates at which these transitions occur are (in general) a function of time and the value of the continuous state. For each value that the discrete state takes, the evolution of the continuous state is described by a stochastic differential equation (SDE). The SDEs associated with each value that the discrete states take need not be the same; indeed, in most applications they differ significantly. Additionally, associated with each discrete-state transition, there is a reset map that defines how the pre-transition discrete and continuous states map into the post-transition discrete and continuous states. Within the context of performability modeling, the set in which the discrete state takes values describes the possible configurations/modes that a system can adopt,

which not only includes the nominal (non-faulty) operational mode, but also those operational modes that arise due to faults (and repairs) in the components that comprise the system. The continuous state captures the evolution of some variables associated with the system performance, and as such, can be used to define specific reward measures that capture notions of system performability. Finally, the reset maps can define instantaneous gains and losses in reward measures that result from transitions due to failures and repairs.

In order to fully characterize an SHS-based reward model, we need to obtain the distribution of the combined state. However, this is an intractable problem, due to the coupling between the evolution of the discrete and continuous states and the reset maps. This can be solved only in a few special cases. For instance, if we assume that the discrete state does not depend on the continuous state, the evolution of the former can be written as a continuous-time Markov chain (CTMC); and as such, its probability distribution is fully characterized by the solution of the Chapman-Kolmogorov equations. However, unless we also assume that the resets do not change the value of the continuous state, it is not straightforward to obtain the continuous-state probability distribution.

Given the difficulty in obtaining the distribution of the combined state, we settle for a method that allows the computation of any arbitrary number of their raw moments. To this end, we rely on the extended generator of the SHS, which together with Dynkin's formula can be used to obtain a differential equation that describes the evolution of the expectation of any function of the combined state, as long as such a function is in the domain of the extended generator. Following the approach outlined in [31,32], we show that under certain general assumptions, monomial functions are always in the domain of the extended generator, and thus, Dynkin's formula holds. Additionally, for SHS where the reset maps, transition rates, and the vector fields defining the SDEs are polynomial, the generator maps the set of monomial functions to itself. Therefore Dynkin's formula gives a closed set of ordinary differential equations (ODEs) that describes the evolution of each moment in terms of the values of the other moments. Since there are infinitely many monomial functions, this formally produces an infinite-dimensional system of ODEs in what is referred to in the stochastic process literature as a closure problem.

The examples and case studies presented in Chapter 5 demonstrate how the proposed SHS framework applies to reward models where the rate at which the reward grows is: i) constant—this case is referred as the rate reward model [33], ii) gov-

erned by a first-order linear differential equation—we refer to this case as a first-order reward model, and iii) governed by a linear SDE—this case is referred as the second-order reward model [34]. The SHS framework can specify even more general reward models, but we restrict attention to the above cases as they have been previously studied in the literature which allows us to validate and verify our results. We will show that the structure of the standard reward models described above is such that there are finite-dimensional truncations of the ODEs governing the moment evolution that are closed; i.e., there are finite subsets of moments such that the evolution of any member of this subset is a function only of the other members of this subset. In other words, these conventional reward models do not lead to a closure problem, and therefore we only have to solve a finite-dimensional ODE to determine the evolution of the reward moments.

The SHS formalism not only applies to the reward models introduced above, but as we will show subsequently, it provides a framework to specify even more general reward models. Furthermore, while it is relatively simple to obtain analytical expressions for the reward distribution in rate and first-order reward models, for more general reward models, e.g., second-order reward models with impulses and/or losses in the accumulated reward, it is very difficult to obtain explicit, closed-form, analytical solutions for the partial differential equations (PDEs) that describe the evolution of the reward distributions [35]. In practice, in order to analyze such reward models, numerical methods are utilized to integrate the PDEs governing the evolution of the accumulated reward pdf [35,36]. However, as reported in the literature, these methods are oftentimes slow and inaccurate [34]. An alternative to numerical integration for characterizing the distribution of the reward is to compute its moments. The moments can then be used, e.g., to compute bounds on the probabilities of different events of interest using Markov/Chebyshev inequalities [37]. A number of methods have been proposed in the literature for computing moments in reward models. For example, techniques based on the Laplace transform of the accumulated-reward distribution are proposed in [33,34,38,39]. Rate reward models with impulses are specified as stochastic activity networks in [40], while in [41], the first moment of the accumulated reward in these models is computed following a method based on the frequency of transitions in the underlying Markov chain. A numerical procedure based on the uniformization method is proposed to compute the moments of the accumulated reward in [42]. In [43], Taylor-series approximations of the vector fields and transition rates that govern the evolution of the continuous state are used to

obtain a set of coupled differential equations whose solutions yield the moments of interest. In the same vein of these earlier works, the SHS-based framework proposed in this dissertation provides a method to compute any desired number of moments of the reward. This method is relatively straightforward to implement in a computer as it involves solving a linear ODE, for which there are very efficient numerical integration methods.

It is worth noting that in the nuclear engineering risk analysis literature there is a related body of work referred to as dynamic probabilistic risk assessment (DPRA) (see, e.g., [43–45] and the references therein). As in SHS, DPRA models are comprised of discrete and continuous dynamics; however, in DPRA models, the continuous dynamics associated to each discrete state is described by an ordinary differential equation (ODE). Additionally, although the transitions between discrete states in DPRA models are stochastic, they do not depend on the value that the continuous state takes. In fact, it is easy to verify that DPRA models are a particular instance of SHS. In these works, as in second-order reward models, the Chapman- Kolmogorov equations with appropriate Markovian assumptions are utilized to derive PDEs that govern the continuous states; however, even in this body of work, it has been acknowledged that closed-form analytical solutions to the PDEs can only be derived for simple models [44, 45]. In practice, most techniques for analyzing DPRA models are based on Monte Carlo simulation.

1.3 Organization of this Dissertation and a Primer to the Case Studies

This dissertation is organized as follows. In Chapter 2, we present fundamentals of Markov reliability and reward models. Chapters 3 and 4 present methods to quantify the impact of probabilistic and unknown-but-bounded parametric uncertainty, respectively, on performability indices recovered from Markov models. Fundamentals of SHS and their application to system performability modeling are presented in Chapter 5. Note that in Chapters 3, 4, and 5, we present several case studies pertaining to common reliability models which are very general and apply to a wide variety of systems (i.e., not limited to renewable electric power systems).

We utilize the models (and their derivatives) in Chapters 6, 7, and 8, to demonstrate several applications to reliability assessment, energy yield estimation, and

uncertainty analysis of renewable electric power systems. A primer to these case studies is provided below.

In Chapter 6, we present a modeling framework to integrate reliability considerations into energy-yield and cost estimations of PVECS using Markov reward model formalisms. Here, we use the analytical approach for parametric sensitivity analysis based on generalized matrix inversion techniques introduced in Chapter 2. In Chapter 7, we propose a framework to quantify the impact of parametric and input uncertainty on the reliability/performability of WECS. Parametric uncertainty in these models relates to the uncertainty in failure and repair rates of the constituent wind turbines in the farm. Input uncertainty is due to uncertainty in wind speed. The methods utilized here to quantify the impact of parametric uncertainty are adopted from Chapter 3. Finally, in Chapter 8, we explore a stochastic small-signal power system model cast in the SHS framework. The general DAE model that describes the evolution of the electromechanical states of the power system is linearized around nominal values of real/reactive power injections (corresponding to some nominal mode). As the discrete state evolves, so do the real/reactive power injections—we describe how this can be used to model renewable resource variability. Subsequently, we apply results from Chapter 5 to obtain the moments of the electromechanical states of the power system. Concluding remarks and directions for future work are summarized in Chapter 9.

Chapter 2

FUNDAMENTALS OF MARKOV RELIABILITY AND REWARD MODELS

In this chapter, we present some fundamentals of Markov reliability models, Markov reward models, the group inverse of ergodic Markov chains, and the sensitivity of the stationary distribution of Markov chains to model parameter variations. Our discussion is limited to mathematical fundamentals, and interested readers are referred to [18,46–48], for a more detailed account on these topics. The building blocks introduced in this chapter are used in uncertainty analysis methods described in Chapters 3-4.

2.1 Markov Reliability Models

Let $Q = \{Q(t),\, t \geq 0\}$ denote a stochastic process taking values in a set $\mathcal{Q}$.

- The stochastic process Q is called a *continuous time Markov chain* (CTMC) if it satisfies the so called Markov property, which is to say that [48]

$$\Pr\{Q(t_n) = i | Q(t_{n-1}) = j_{n-1}, \ldots, Q(t_1) = j_1\}$$

$$= \Pr\{Q(t_n) = i | Q(t_{n-1}) = j_{n-1}\},\ \forall i,\, j_1, \ldots,\, j_{n-1} \in \mathcal{Q},\, \forall t < \cdots < t_n. \quad (2.1)$$

- The chain Q is said to be *homogeneous* if it satisfies

$$\Pr\{Q(t) = i | Q(s) = j\} = \Pr\{Q(t-s) = i | Q(0) = j\},\ \forall i,\, j \in \mathcal{Q},\, 0 < s < t. \quad (2.2)$$

  Homogeneity of Q implies that the times between transitions are exponentially distributed.

- The chain Q is said to be *irreducible* if

$$\Pr\{Q(t) = i | Q(0) = j\} > 0, \forall i,\, j \in \mathcal{Q}, \text{for some}\, t > 0. \tag{2.3}$$

  Said in words, every state in an irreducible chain is accessible from every other state.

- The chain Q is said to be *ergodic* if it is irreducible, and the set $\mathcal{Q}$ is finite. Ergodic Markov chains have a unique stationary distribution independent of initial conditions [47].

In the context of reliability/reward modeling, we consider the class of CTMCs that are homogeneous, irreducible, and take values in a finite set $\mathcal{Q} = \{0,\, 1,\, 2, \ldots,\, N\}$, where $0,\, 1,\, 2, \ldots,\, N-1$ index system configurations that arise due to component faults, and N indexes the nominal, non-faulty configuration. Let Q denote a chain belonging to this class. In light of the definitions above, the chain Q is ergodic and has a unique stationary distribution.

Let $\pi_i(t)$, $t \geq 0$, be the probability that the chain is in state i at time t, and define the corresponding probability vector as $\pi(t) = [\pi_0(t),\, \pi_1(t), \ldots,\, \pi_N(t)]$. The evolution of $\pi(t)$ is governed by the Chapman-Kolmogorov equations

$$\dot{\pi}(t) = \pi(t)\Lambda, \tag{2.4}$$

with $\pi_N(0) = 1$, $\pi_i(0) = 0$, $i = 0,\, 1, \ldots,\, N-1$, and where $\Lambda \in \mathbb{R}^{N+1 \times N+1}$ is the Markov chain generator matrix whose entries are a function of component failure and repair rates [46]. By construction, all the row sums in Λ are zero, which implies that Λ is not invertible. The steady-state solution of (2.4) is referred to as the stationary distribution of the chain; it is denoted by π, and is obtained as the solution of

$$\pi\Lambda = 0, \quad \pi e^T = 1, \tag{2.5}$$

where $e \in \mathbb{R}^{N+1}$ is a row vector with all entries equal to one. The stationary distribution of an ergodic Markov chain is unique (independent of initial conditions), and a function of the generator-matrix parameters (interchangeably referred to as model parameters) which are denoted by θ_j, $j = 1,\, 2, \ldots,\, m$. To explicitly represent parametric dependence, the generator matrix and stationary distribution are expressed as $\Lambda(\theta)$ and $\pi(\theta) = [\pi_0(\theta), \ldots,\, \pi_N(\theta)]$, respectively, where $\theta = [\theta_1,\, \theta_2, \ldots, \theta_m]$ is the

vector of model parameters.

2.2 Markov Reward Models

A Markov reward model is defined by a Markov chain taking values in a finite set $\mathcal{Q}$ and a *reward function* $\varrho : \mathcal{Q} \to \mathbb{R}$ that maps each state $i \in \mathcal{Q}$ into a real-valued quantity ρ_i, which captures some performance metric of interest while in state i. At time t, the value that ϱ takes can be described by a random variable $P(t)$. The *instantaneous reward*, denoted by $\xi(t)$, is a probabilistic measure of system performance given by the expected value of $P(t)$

$$\xi(t) := \mathrm{E}[P(t)] = \sum_{i=0}^{n} \pi_i(t)\rho_i = \pi(t)\rho^T, \tag{2.6}$$

where $\rho := [\rho_0, \rho_1, \ldots, \rho_n]$. The *reward*, denoted by ξ, is a long-term measure of system performance, and it is defined as

$$\xi := \lim_{t\to\infty} \xi(t) = \lim_{t\to\infty} \sum_{i=0}^{N} \pi_i(t)\rho_i = \sum_{i=0}^{N} \pi_i\rho_i = \pi\rho^T, \tag{2.7}$$

where $\pi = [\pi_0, \pi_1, \ldots, \pi_N]$ is the Markov chain stationary distribution. If the values that the reward function ϱ takes are defined in per-unit time, then ξ describes the average rate at which the system delivers/consumes some quantity that captures a measure of system performance. The *accumulated reward*, denoted by γ, is a quantity measuring system performance in a period $[0, \tau]$, and it is defined as

$$\gamma := \int_0^\tau \mathrm{E}[P(t)]dt = \int_0^\tau \pi(t)\rho^T dt. \tag{2.8}$$

For the systems we study, there is typically orders of magnitude difference in the failure and repair rates. Consequently, the CTMC reaches steady state very fast, and (2.8) can be approximated as

$$\gamma \approx \pi\rho^T\tau = \xi \cdot \tau, \tag{2.9}$$

where π is the CTMC stationary distribution. A derivation of this result is provided in Appendix A.1.

In subsequent discussions, the reward and accumulated reward are expressed as $\xi(\theta)$ and $\gamma(\theta)$, respectively, to clearly represent their dependence on model parameters.

2.3 Stationary Distribution and Group Inverse of CTMCs

For ergodic Markov chains, the generator-matrix group inverse enables the numerical calculation of $\partial^k \pi_i(\theta)/\partial\theta_j^k$, $i = 0, 1, \ldots, n$; $j = 1, 2, \ldots, m$; $k > 0$, as will be discussed in Section 2.4. The group inverse of $\Lambda = \Lambda(\theta)$ for some θ is denoted by $\Lambda^{\#}$, and is given by the unique solution of

$$\begin{cases} \Lambda\Lambda^{\#}\Lambda = \Lambda, \\ \Lambda^{\#}\Lambda\Lambda^{\#} = \Lambda^{\#}, \\ \Lambda\Lambda^{\#} = \Lambda^{\#}\Lambda, \end{cases} \tag{2.10}$$

if and only if $\text{rank}(\Lambda) = \text{rank}(\Lambda^2)$, which is a condition that always holds for generator matrices of ergodic Markov chains [49]. A number of techniques amenable for computer implementation have been proposed to compute the group inverse [18]. An approach involving the QR factorization of Λ yields the stationary distribution $\pi = \pi(\theta)$, and the group inverse $\Lambda^{\#}$ [50]. In this method, Λ is factored as $\Lambda = QR$, where, Q, $R \in \mathbb{R}^{N+1\times N+1}$. The matrix R is of the form

$$R = \begin{bmatrix} U & -Ue^T \\ 0 & 0 \end{bmatrix}, \tag{2.11}$$

where $U \in \mathbb{R}^{N\times N}$ is a nonsingular upper-triangular matrix, and $e \in \mathbb{R}^N$ is a row vector with all entries equal to one. The stationary distribution can be derived by normalizing the last column of Q

$$\pi_j = \frac{q_{j+1,N+1}}{\sum_{i=1}^{n+1} q_{i,\,N+1}},\ j = 0,\ 1, \ldots,\ N. \tag{2.12}$$

The group inverse is related to Q and R as follows:

$$\Lambda^{\#} = (I - e^T\pi) \begin{bmatrix} U^{-1} & 0 \\ 0 & 0 \end{bmatrix} Q^T (I - e^T\pi). \tag{2.13}$$

2.4 Sensitivity to Model Parameters

For Markov reliability models, the first-order sensitivity of stationary distributions to model parameters was derived in [8]. The ideas in [8] were extended to compute higher-order sensitivities in [13, 14]. These results are summarized below. A proof for the results below is included in Appendix A.2.

The k-order sensitivity of the i steady-state probability to the j parameter θ_j, is given by

$$\frac{\partial^k \pi_i(\theta)}{\partial \theta_j^k} = k!\,(-1)^k\,\pi(\theta)\left(\frac{\partial \Lambda}{\partial \theta_j}\Lambda^{\#}\right)^k e_i^T. \tag{2.14}$$

The second-order mixed partial derivative is given by

$$\frac{\partial \pi_i^2(\theta)}{\partial \theta_j \partial \theta_k} = \pi(\theta)^T \left(\frac{\partial \Lambda}{\partial \theta_j}\Lambda^{\#}\frac{\partial \Lambda}{\partial \theta_k}\Lambda^{\#} + \frac{\partial \Lambda}{\partial \theta_k}\Lambda^{\#}\frac{\partial \Lambda}{\partial \theta_j}\Lambda^{\#}\right) e_i^T, \tag{2.15}$$

where $e_i \in \mathbb{R}^{N+1}$ is a vector with 1 as the i entry and zero otherwise. Derivation of analytical expressions for general mixed partial derivatives is the focus of ongoing research. In the uncertainty analysis methods we propose in Chapters 3-4, we will only use the sensitivities above.

Note that sensitivities of the reward and accumulated reward can easily be computed from the expressions above. In particular, using (2.7) and (2.14), the sensitivity of the reward to the i parameter can be expressed as

$$\frac{\partial^k \xi(\theta)}{\partial \theta_i^k} = \frac{\partial^k \pi(\theta)}{\partial \theta_i^k}\rho^T = k!\,(-1)^k\,\pi(\theta)\left(\frac{\partial \Lambda}{\partial \theta_i}\Lambda^{\#}\right)^k \rho^T, \tag{2.16}$$

and similarly, from the definition of the accumulated reward in (2.9), we get

$$\frac{\partial^k \gamma(\theta)}{\partial \theta_i^k} = \frac{\partial^k \xi(\theta)}{\partial \theta_i^k}\tau = k!\,(-1)^k\,\pi(\theta)\left(\frac{\partial \Lambda}{\partial \theta_i}\Lambda^{\#}\right)^k \rho^T\tau. \tag{2.17}$$

We provide a short example next to illustrate the application of the group inverse

in computing the sensitivities of the stationary distribution to model parameter variations for a simple—albeit representative—Markov reliability model.

Example 1

Consider a component with two possible operational states. In state 1, the component performs its intended function, and in state 0, it has failed. The failure and repair rates of the component are denoted by λ and μ, respectively. The state of the component (functioning or failed) can be described by a two-state Markov chain. The state-transition diagram for this chain is illustrated in Fig. 2.1, from which it follows that the generator matrix is given by

$$\Lambda = \begin{bmatrix} -\mu & \mu \\ \lambda & -\lambda \end{bmatrix}.$$

The stationary distribution of the chain, $\pi = [\pi_0, \pi_1]$, obtained by solving $\pi\Lambda = 0$ with $\pi e^T = 1$, where $e = [1, 1]$, is given by

$$\pi_0 = \frac{\lambda}{\mu + \lambda}, \quad \pi_1 = \frac{\mu}{\mu + \lambda}, \tag{2.18}$$

from which the following sensitivities can be derived

$$\frac{\partial \pi_0}{\partial \mu} = -\frac{\partial \pi_1}{\partial \mu} = -\frac{\lambda}{(\lambda + \mu)^2}, \tag{2.19}$$

$$\frac{\partial \pi_0}{\partial \lambda} = -\frac{\partial \pi_1}{\partial \lambda} = \frac{\mu}{(\lambda + \mu)^2}. \tag{2.20}$$

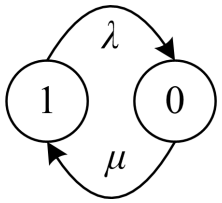

Figure 2.1: State-transition diagram of the two-state Markov model investigated in Example 1.

We will now verify that by using (2.14), the same result is obtained. Towards this end, the QR factorization of Λ yields

$$Q = \frac{1}{\sqrt{\lambda^2+\mu^2}} \begin{bmatrix} -\mu & \lambda \\ \lambda & \mu \end{bmatrix}, \tag{2.21}$$

$$R = \begin{bmatrix} \sqrt{\lambda^2+\mu^2} & -\sqrt{\lambda^2+\mu^2} \\ 0 & 0 \end{bmatrix}. \tag{2.22}$$

As described in (2.12), the stationary distribution can be obtained by normalizing the last column of Q in (2.21). Comparing (2.22) and (2.11), we see that $U = \sqrt{\lambda^2+\mu^2}$. Substituting U, (2.18), and (2.21) in (2.13) yields

$$\Lambda^{\#} = \frac{1}{(\lambda+\mu)^2} \begin{bmatrix} -\mu & \mu \\ \lambda & -\lambda \end{bmatrix}. \tag{2.23}$$

The sensitivity of the stationary distribution to μ and λ can be derived from (2.14) as

$$\begin{aligned} \frac{\partial \pi}{\partial \mu} &= -\pi \frac{\partial \Lambda}{\partial \mu} \Lambda^{\#} = \begin{bmatrix} -\frac{\lambda}{(\lambda+\mu)^2} & \frac{\lambda}{(\lambda+\mu)^2} \end{bmatrix}, \\ \frac{\partial \pi}{\partial \lambda} &= -\pi \frac{\partial \Lambda}{\partial \lambda} \Lambda^{\#} = \begin{bmatrix} \frac{\mu}{(\lambda+\mu)^2} & -\frac{\mu}{(\lambda+\mu)^2} \end{bmatrix}, \end{aligned}$$

where

$$\frac{\partial \Lambda}{\partial \mu} = \begin{bmatrix} -1 & 1 \\ 0 & 0 \end{bmatrix}, \ \frac{\partial \Lambda}{\partial \lambda} = \begin{bmatrix} 0 & 0 \\ 1 & -1 \end{bmatrix},$$

and $\pi = [\pi_0, \pi_1]$ is given by (2.18), and $\Lambda^{\#}$ is given by (2.23). Note that the sensitivities match those computed directly from the closed-form stationary distribution in (2.19)-(2.20).

2.5 Dynamic Reward Models

We end this chapter with a discussion of dynamic reward models. A dynamic Markov reward model is comprised of a Markov chain $Q(t)$ taking values in the set $\mathcal{Q}$, which describes the possible system operational modes; and a reward $Y(t)$, which captures some performance measure of interest and depends on each particular operational mode $q \in \mathcal{Q}$. The most commonly studied dynamic Markov reward models are rate-

reward models, and second-order reward models (see, e.g., [34,35] and the references therein). In rate-reward models, the accumulated reward evolves according to

$$dY(t) = a(q)dt, \, \forall q \in \mathcal{Q}, \, t \geq 0, \tag{2.24}$$

where $a\colon \mathcal{Q} \to \mathbb{R}$ is the (state-dependent) reward growth rate. In second-order reward models, the accumulated reward evolves according to

$$dY(t) = a(q)\, dt + c(q)\, dW_t, \, \forall q \in \mathcal{Q}, \, t \geq 0, \tag{2.25}$$

where $a\colon \mathcal{Q} \to \mathbb{R}$, $c\colon \mathcal{Q} \to \mathbb{R}$, and $W_t\colon \mathbb{R}^+ \to \mathbb{R}$ is the Wiener process. Impulses in the accumulated reward capture one-time effects due to the failure/repair of a constituent element in the system. As described in the introduction, various methods have been proposed to tackle impulses in first-order reward models. While not detailed in the original work in [34], computer tools by the same authors incorporate impulses in second-order reward models [35].

The SHS formalism studied in Chapter 5 generalizes and unifies a wide class of reward models. The state space in a SHS is comprised of a discrete state that represents the operational modes of the system under study, and a continuous state describing the reward dynamics. Reset maps capture the impact of transitions on the continuous state, which provides a systematic method to define initial conditions for the post-transition reward dynamics, and therefore enables the inclusion of impulses and losses in the reward when transitions occur. Furthermore, in the most general case, the vector fields that govern the evolution of the continuous state, the transition rates, and the reset maps are functions of time and/or (finite) polynomial functions of the continuous state. The generality of this modeling formalism facilitates wide applicability to a variety of reward models. In Chapter 5, we demonstrate how rate and second-order Markov reward models with impulses can be recovered as a special case of an SHS. Then in Chapter 8, we demonstrate how small-signal stochastic stability of power systems can be studied within the SHS formalism. This approach can be adopted to examine the impact of renewable resources variability on power systems dynamics.

Chapter 3

PROBABILISTIC UNCERTAINTY ANALYSIS IN MARKOV RELIABILITY AND REWARD MODELS

In this chapter, we propose numerical methods to compute the pdfs of the Markov chain stationary distribution, the reward, and the accumulated reward, given the parametrized Markov chain generator matrix and the model-parameter pdfs. This is the first of two methods we propose for uncertainty analysis in Markov reliability and reward models (in Chapter 4, we investigate a set-theoretic model). The methods we develop in this chapter are applied to investigate the performability of wind energy conversion systems in Chapter 7. We also present several case studies here applied to common reliability/reward models. The material we present subsequently has been published in [13].

First, we demonstrate how the pdfs of the stationary distribution can be derived for the case where a single parameter in the generator matrix is uncertain. Then, for the more general multiple-parameter case, we leverage the results of the single-parameter case to show how the pdfs of the stationary distribution, the reward, and the accumulated reward can be computed. Additionally, we also derive closed-form expressions that approximate the expectation and variance of the stationary distribution, the reward, and the accumulated reward.

3.1 Problem Formulation

Let $\Theta = [\Theta_1, \Theta_2, \ldots \Theta_m]$ be the vector of random variables that describes the model parameters, and let $f_{\Theta_j}(\theta_j)$ denote the pdf of Θ_j, $j = 1, 2, \ldots, m$. It is assumed that the Θ_j's are independent continuous random variables with known pdfs.[1] Therefore, the steady-state probabilities are random variables that can be collectively described by a random vector $\Pi = [\Pi_0, \Pi_1, \ldots, \Pi_N]$, where $\Pi_i = \pi_i(\Theta)$. Similarly, the reward,

[1] As shown in Section 3.3.1, this restriction can be relaxed if the joint distribution of the parameters, $f_{\Theta_1,\ldots,\Theta_m}(\theta_1, \ldots, \theta_m)$, is known.

$\Xi = \xi(\Theta)$, and the accumulated reward, $\Gamma = \gamma(\Theta) = \Xi \cdot \tau$, are random variables with pdfs $f_\Xi(\xi)$ and $f_\Gamma(\gamma)$, respectively.

If closed-form expressions for the stationary distribution as a function of the model parameters were available and if the expressions were invertible, then $f_{\Pi_i}(\pi_i)$, $f_\Xi(\xi)$, and $f_\Gamma(\gamma)$ could be determined through the well-known random-variable-transformation method stated in the following Lemma (see [51] for a proof).

Lemma 1

Consider a random variable X with pdf $f_X(x)$, and a differentiable, real-valued function $g(x)$. The pdf of the random variable $Y = g(X)$, $f_Y(y)$, is given by

$$f_Y(y) = \sum_{i=1}^{r} \frac{f_X(x_i)}{|g'(x_i)|},\ g'(x_i) := \left.\frac{dg}{dx}\right|_{x=x_i} \neq 0, \tag{3.1}$$

where $x_1, x_2, \ldots x_r$ are r real roots of $y = g(x)$.

The main impediment in directly applying the above Lemma to our problem is that it is seldom possible to obtain closed-form expressions for the Markov chain stationary distribution, $\pi(\theta)$ ($g(x)$ in the context of Lemma 1). Furthermore, the number of roots of $y = g(x)$ depends on the value of y, and might not be finite unless $g(x)$ is a polynomial.

In our method, to derive $f_{\Pi_i}(\pi_i)$ and $f_\Xi(\xi)$, the functions $\pi_i(\Theta)$ and $\xi(\Theta)$ are first approximated by polynomials by truncating their Taylor series expansions. Since we model these functions as polynomials, we are guaranteed to have a finite number of roots. The Taylor series coefficients are the sensitivities $\partial^k \pi_i(\theta)/\partial\theta^k$ and $\partial^k \xi(\theta)/\partial\theta^k$. In general, obtaining these sensitivities is a difficult task; however, they can be computed from the generator-matrix group inverse as shown in (2.14)-(2.16). Once the polynomial characterization is available, Lemma 1 (and its extension to the multiple-parameter case) can be applied to compute $f_{\Pi_i}(\pi_i)$ and $f_\Xi(\xi)$ by evaluating the roots of the polynomial approximations, which are easy to obtain numerically. Since the accumulated reward Γ is the product of the reward Ξ, and a constant τ, $f_\Gamma(\gamma)$ can be easily expressed as a function of $f_\Xi(\xi)$ and τ.

3.2 Single Parameter Case

Consider the case where a single parameter in the generator matrix is uncertain. This parameter is denoted by θ, and described by a random variable Θ, whose pdf $f_\Theta(\theta)$, is known.[2] To derive the pdf of the steady-state probability $\Pi_i = \pi_i(\Theta)$, we begin by expressing Θ as

$$\Theta = m_\Theta + \Delta\Theta, \tag{3.2}$$

where m_Θ is the mean of Θ, and $\Delta\Theta$ is a zero-mean random variable such that $f_{\Delta\Theta}(\Delta\theta) = f_\Theta(m_\Theta + \Delta\theta)$. We can expand $\pi_i(\Theta)$ around the mean of Θ using a Taylor series expansion as follows:

$$\Pi_i = \pi_i(m_\Theta + \Delta\Theta) = \pi_i(m_\Theta) + \sum_{k=1}^{\infty} \frac{a_{ki}}{k!}\Delta\Theta^k. \tag{3.3}$$

The k-order Taylor series coefficient, a_{ki}, follows from (2.14):

$$a_{ki} \;=\; \left.\frac{d^k\pi_i(\theta)}{d\theta^k}\right|_{\theta=m_\Theta} = k!\,(-1)^k\,\pi(\theta)\left(\frac{d\Lambda(\theta)}{d\theta}\Lambda^{\#}\right)^k e_i^T\Bigg|_{\theta=m_\Theta}, \tag{3.4}$$

where $e_i \in \mathbb{R}^{N+1}$ is a row vector with a 1 as the i entry and zero otherwise.

3.2.1 Probability Density Function of Π_i

Since the exact, analytical, closed-form expression for $\pi_i(\Delta\Theta)$ is not known, to apply the result in Lemma 1, Π_i is first expressed as $\Pi_i = p_i(\Delta\Theta)$, where p_i is a polynomial with real coefficients obtained by truncating the Taylor series in (3.3) at the t term

$$\Pi_i = p_i(\Delta\Theta) = \pi_i(m_\Theta) + \sum_{k=1}^{t} \frac{a_{ki}}{k!}\Delta\Theta^k. \tag{3.5}$$

Then, applying (3.1), $f_{\Pi_i}(\pi_i)$ can be computed as

$$f_{\Pi_i}(\pi_i) = \sum_{j=1}^{r} \frac{f_{\Delta\Theta}(\Delta\theta_j)}{|p_i'(\Delta\theta_j)|}, \tag{3.6}$$

[2] While we have defined $\theta = [\theta_1, \theta_2, \ldots, \theta_m]$ as the vector of model parameters, in this subsection, we abuse notation and denote the single uncertain model parameter by θ.

where $\Delta\theta_1, \Delta\theta_2, \ldots, \Delta\theta_r$ are the $r \leq t$ real roots of $\pi_i = p_i(\Delta\theta)$, and

$$p_i'(\Delta\theta_j) := \left.\frac{dp_i(\Delta\theta)}{d\Delta\theta}\right|_{\Delta\theta=\Delta\theta_j} = \sum_{k=1}^{t} \frac{a_{ki}}{(k-1)!}\Delta\theta_j^{k-1}. \tag{3.7}$$

3.2.2 Computer Implementation

Algorithm 1 provides the pseudocode for computer implementation of the method outlined in (3.2)-(3.7) to compute $f_{\Pi_i}(\pi_i)$, $i = 0, 1, \ldots, N$. Since (3.6) has to be evaluated pointwise, π_i is appropriately discretized between 0 and 1 in steps of $d\pi_i$ to obtain the vector $\bar{\pi}_i = [0 : d\pi_i : 1]$. A first-order Taylor series expansion can be utilized if the function $\pi_i(\theta)$ is not far from linear within one standard deviation away from the mean m_Θ [52]. Alternatively, higher-order expansions can be utilized. Given the parametrized generator matrix, it is easy to compute $\partial\Lambda/\partial\theta$ and obtain the QR factorization of the generator matrix at the mean of Θ, $\Lambda(m_\Theta)$. Next $\pi_i(m_\Theta)$ is obtained as shown in (2.12) by normalizing the last column of Q, the group inverse $\Lambda^\#$ is obtained from (2.13), and the Taylor series coefficients, a_{ki}, $k = 1, 2, \ldots, t$, are computed using (3.4). In the for loop, $f_{\Pi_i}(\pi_i)$ is evaluated point wise for each entry of $\bar{\pi}_i$. This involves computing the r real roots of the equation $\bar{\pi}_i(l) = p_i(\Delta\theta)$, $\forall l$, where $\bar{\pi}_i(l)$ is the l entry in $\bar{\pi}_i$, and then applying (3.6)-(3.7).

Algorithm 1 Computation of $f_{\Pi_i}(\pi_i)$ for the single-parameter case.

define $\bar{\pi}_i = [0 : d\pi_i : 1]$
define Taylor series order t
compute $\frac{\partial\Lambda}{\partial\theta}$ and $QR = \Lambda(m_\Theta)$
compute $\pi_i(m_\Theta)$ from (2.12), $\Lambda^\#$ from (2.13), and a_{ki}, $k = 1, 2, \ldots, t$ from (3.4)
for $\hat{\pi}_i = 0 : d\pi_i : 1$ **do**
  compute real roots of $\pi_i(m_\Theta) - \hat{\pi}_i + \sum_{k=1}^{t} \frac{a_{ki}}{k!}\Delta\theta^k = 0$, $\Delta\theta_j$, $j = 1, \ldots, r$
  for $j = 1$ to r **do**
    compute $f_{\Delta\Theta}(\Delta\theta_j)$ and $p_i'(\Delta\theta_j) = \sum_{k=1}^{t} \frac{a_{ki}}{(k-1)!}\Delta\theta_j^{k-1}$
  end for
  compute $f_{\Pi_i}(\hat{\pi}_i) = \sum_{j=1}^{r} \frac{f_{\Delta\Theta}(\Delta\theta_j)}{|p_i'(\Delta\theta_j)|}$
end for

3.2.3 Expectation and Variance of Π_i

While the method outlined in (3.2)-(3.7) provides the pdf of the Markov chain stationary distribution, it might be sufficient—for the purpose of back-of-the-envelope calculations—to compute the expected value and variance of Π_i. These could then be used together with Markov and Chebyshev inequalities to get accurate upper bounds on the probabilities of various events of interest [37]. The expected value of Π_i, denoted by m_{Π_i}, can be derived from (3.5) as

$$m_{\Pi_i} := \mathrm{E}[\Pi_i] = \pi_i(\mu_\Theta) + \sum_{k=1}^{t} \frac{a_{ki}}{k!} \mathrm{E}\left[\Delta\Theta^k\right]. \tag{3.8}$$

Since the pdf of $\Delta\Theta$ is known, it is easy to compute the expectations $\mathrm{E}[\Delta\Theta^k]$, $k > 0$. The variance of Π_i, denoted by $\sigma^2_{\Pi_i}$, can be derived from (3.5) and (3.8) as

$$\sigma^2_{\Pi_i} := \mathrm{Var}\left(\Pi_i\right) = \sum_{k=1}^{t} \left(\frac{a_{ki}}{k!}\right)^2 \mathrm{Var}(\Delta\Theta^k) + \sum_{k=1}^{t} \sum_{m=1,\, m\neq k}^{t} \frac{a_{ki}}{k!}\frac{a_{mi}}{m!} \cdot \mathrm{Cov}\left(\Delta\Theta^k, \Delta\Theta^m\right), \tag{3.9}$$

where $\mathrm{Var}\left(\Delta\Theta^k\right)$, and $\mathrm{Cov}\left(\Delta\Theta^k, \Delta\Theta^m\right)$ are given by

$$\mathrm{Var}(\Delta\Theta^k) = \mathrm{E}\left[\Delta\Theta^{2k}\right] - \left(\mathrm{E}\left[\Delta\Theta^k\right]\right)^2, \tag{3.10}$$

$$\mathrm{Cov}(\Delta\Theta^k, \Delta\Theta^m) = \mathrm{E}\left[\Delta\Theta^{k+m}\right] - \mathrm{E}\left[\Delta\Theta^k\right]\mathrm{E}\left[\Delta\Theta^m\right]. \tag{3.11}$$

We now present an example that illustrates the ideas described so far.

Example 2

Consider the two-state Markov chain studied in Example 1. Recall that in state 1, the component performs its intended function, and in state 0, it has failed. The failure rate of the component is denoted by λ, and the repair rate is denoted by μ. The state of the component (functioning or failed) can be described by a two-state Markov chain. The generator matrix for this chain is given by $\Lambda = \begin{bmatrix} -\mu & \mu \\ \lambda & -\lambda \end{bmatrix}$. Denote the stationary distribution of the chain by $\pi = [\pi_0, \pi_1]$. Recall from (2.18), that the stationary distribution of this chain is given by $\pi_0 = \lambda/(\mu+\lambda)$, $\pi_1 = \mu/(\mu+\lambda)$. Suppose the failure rate λ is uncertain and described by a normal random variable L

with mean $m_L = 5.5$, and standard deviation $\sigma_L = 0.5$. The repair rate is assumed to be perfectly known and given by $\mu = 5.5$. Note that failure and repair rates have units of per-unit time. To streamline the presentation, we omit the units in the following discussion. In this example, we describe how Algorithm 1 can be applied to compute $f_{\Pi_1}(\pi_1)$. Subsequently, we will compare the result obtained from Algorithm 1 with the exact analytical result.

Figure 3.1 depicts the function $\pi_1 = \frac{\mu}{\mu+\lambda} = \frac{\mu}{\mu+(\Delta\lambda+m_L)}$ and three polynomial approximations ($t = 1, 2, 3$), from which it is clear that a third-order expansion is accurate enough. The QR factorization of $\Lambda(\lambda)$ for $\lambda = m_L = 5.5$ and $\mu = 5.5$, provides

$$Q = \begin{bmatrix} -0.7071 & -0.7071 \\ 0.7071 & -0.7071 \end{bmatrix}, R = \begin{bmatrix} 7.7782 & -7.7782 \\ 0 & 0 \end{bmatrix}. \tag{3.12}$$

As described in (2.12), by normalizing the last column of Q, we obtain the stationary distribution $\pi(m_L) = [\pi_0(m_L), \pi_1(m_L)] = [0.5, 0.5]$. From (2.11) and (3.12), $U = 7.7782$. Then, applying (2.13), we obtain the group inverse

$$\Lambda^{\#} = \begin{bmatrix} -0.0455 & 0.0455 \\ 0.0455 & -0.0455 \end{bmatrix}. \tag{3.13}$$

Using (3.4) to compute the Taylor-series coefficients provides the following third-order polynomial approximation:

$$\begin{aligned} p_1(\Delta\lambda) &= \pi_1(m_L) + a_{11}(\Delta\lambda) + \frac{1}{2}a_{21}(\Delta\lambda)^2 + \frac{1}{6}a_{31}(\Delta\lambda)^3 \\ &= 0.5 - 0.0455(\Delta\lambda) + 0.0041(\Delta\lambda)^2 - 3.7566\text{e-}4(\Delta\lambda)^3. \end{aligned} \tag{3.14}$$

In order to numerically compute $f_{\Pi_1}(\pi_1)$, $0 \leq \pi_1 \leq 1$, we discretize π_1 as $\bar{\pi}_1 = [0 : 0.0001 : 1]$. We then compute the roots of the equation $\bar{\pi}_1(l) = p_1(\Delta\lambda)$, $\forall l$, where $\bar{\pi}_1(l)$ denotes the l entry of $\bar{\pi}_1$. The real roots are subsequently used in (3.6) to obtain $f_{\Pi_1}(\pi_1)$. For example, for $\hat{\pi}_1 = 0.5$, the real root is $\Delta\lambda_1 = 0$, and there are two complex roots, $\Delta\lambda_{2,3} = 5.5 \pm 9.5263\,j$ which are discarded. Since L (and hence ΔL) is normally distributed, it follows that

$$f_{\Delta L}(\Delta\lambda_1) = \frac{1}{\sqrt{2\pi\sigma_L^2}} \exp\left(-\frac{\Delta\lambda_1^2}{2\sigma_L^2}\right) = 0.7979. \tag{3.15}$$

From (3.14) we obtain

$$p_1'(\Delta\lambda_1) = \left.\frac{dp_1(\Delta\lambda)}{d\Delta\lambda}\right|_{\Delta\lambda=\Delta\lambda_1} = -0.0455 + 0.0082(\Delta\lambda_1) - 0.0011(\Delta\lambda_1)^2 = -0.0455. \tag{3.16}$$

Substituting (3.15) and (3.16) in (3.6), we get $f_{\Pi_1}(\hat{\pi}_1 = 0.5) = 17.5363$. This procedure is repeated for all other entries of $\bar{\pi}_1$ and the results are plotted in Fig. 3.2.

We can also compare the numerical solution with the exact solution obtained by applying random-variable transformation to the function $\Pi_1 = \mu/(\mu + L)$, which results in

$$f_{\Pi_1}(\pi_1) = f_L(\tilde{\lambda})\frac{\left(\tilde{\lambda}+\mu\right)^2}{\mu}, \quad \tilde{\lambda} = \frac{\mu(1-\pi_1)}{\pi_1}. \tag{3.17}$$

Figure 3.2 also depicts $f_{\Pi_1}(\pi_1)$ computed using the exact analytical expression in (3.17). The results show a very good match between the approximation and the exact solution.

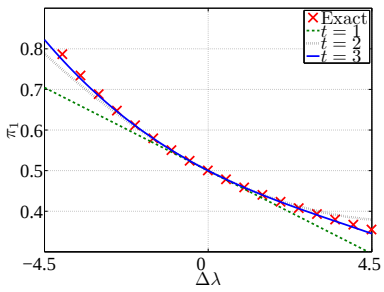

Figure 3.1: Polynomial approximations to model π_1.

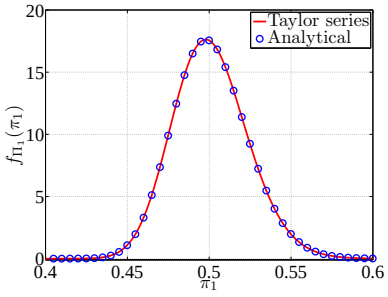

Figure 3.2: Taylor series and exact analytical results compared.

3.3 Multiple-Parameter Case

In this section, we consider the case where the generator matrix is a function of m parameters, $\theta_1, \theta_2, \ldots, \theta_m$, described by random variables $\Theta_1, \Theta_2, \ldots, \Theta_m$. We assume that the Θ_j's are independent, and that the pdfs $f_{\Theta_j}(\theta_j)$, $j = 1, 2, \ldots, m$ are known.

3.3.1 Probability Density Function of Π_i

To derive the pdf of Π_i, we propose a method that builds upon the single-parameter case. First, we pick a parameter, say Θ_1, and seek the Taylor series expansion of Π_i around the mean of Θ_1, m_{Θ_1}, with the other parameters fixed. Along these lines, express Θ as

$$\Theta = m_\Theta + \Delta\Theta, \tag{3.18}$$

where $m_\Theta = [m_{\Theta_1}, \theta_2, \ldots, \theta_m]$, and $\Delta\Theta = [\Delta\Theta_1, 0, \ldots, 0]$. We can expand $\pi_i(\Theta)$ around m_Θ using a Taylor series expansion as

$$\Pi_i = \pi_i(\Theta) = \pi_i(m_\Theta + \Delta\Theta) = \pi_i(m_\Theta) + \sum_{k=1}^{\infty} \frac{b_{ki}}{k!}\Delta\Theta_1^k. \tag{3.19}$$

The k-order Taylor series coefficient, b_{ki}, is given by:

$$b_{ki} \quad = \quad \left.\frac{\partial^k \pi_i(\theta)}{\partial\theta_1^k}\right|_{\theta=m_\Theta} = k!\,(-1)^k\,\pi(\theta)\left(\frac{\partial\Lambda(\theta)}{\partial\theta_1}\Lambda^{\#}\right)^k e_i^T\Bigg|_{\theta=m_\Theta}, \tag{3.20}$$

where $e_i \in \mathbb{R}^{N+1}$ is a row vector with 1 as the i entry and zero otherwise. We then express $\Pi_i = p_i(\Delta\Theta_1)$, where p_i is a polynomial function with real coefficients obtained by truncating the Taylor series in (3.19) at the t term

$$\Pi_i = p_i(\Delta\Theta_1) = \pi_i(m_\Theta) + \sum_{k=1}^{t} \frac{b_{ki}}{k!}\Delta\Theta_1^k. \tag{3.21}$$

Analogous to (3.6), we can derive the conditional pdf

$$f_{\Pi_i|\Theta_2,\ldots,\Theta_m}(\pi_i|\theta_2,\ldots,\theta_m) = \sum_{j=1}^{r} \frac{f_{\Delta\Theta_1}(\Delta\theta_{1,j})}{|p_i'(\Delta\theta_{1,j})|}, \tag{3.22}$$

where $\Delta\theta_{1,1}$, $\Delta\theta_{1,2}, \ldots \Delta\theta_{1,r}$ are the $r \leq t$ real roots of $\pi_i = p_i(\Delta\theta_1)$ and[3]

$$p_i'(\Delta\theta_{1,j}) = \left.\frac{dp_i(\Delta\theta_1)}{d\Delta\theta_1}\right|_{\Delta\theta_1=\Delta\theta_{1,j}} = \sum_{k=1}^{t} \frac{b_{ki}}{(k-1)!}\Delta\theta_{1,j}^{k-1}. \tag{3.23}$$

[3]Once the other parameters are fixed, p_i is a function of a single parameter $\Delta\theta_1$.

The derivation of (3.22) is provided in Appendix A.3. Applying the total probability theorem, and acknowledging the independence of $\Theta_2, \ldots, \Theta_m$, it follows that

$$f_{\Pi_i}(\pi_i) = \int_{\theta_2} \cdots \int_{\theta_m} f_{\Pi_i|\Theta_2,\ldots,\Theta_m}(\pi_i|\theta_2, \ldots, \theta_m)\, f_{\Theta_m}(\theta_m) d\theta_m \ldots f_{\Theta_2}(\theta_2) d\theta_2. \quad (3.24)$$

Remark

In the development above, the assumption of parameter independence is made from a modeling perspective. The proposed method is still mathematically tractable if the model parameters are dependent, and their joint distribution is known. In particular, the conditional pdf $f_{\Pi_i|\Theta_2,\ldots,\Theta_m}(\pi_i|\theta_2, \ldots, \theta_m)$ in this case is given by

$$f_{\Pi_i|\Theta_2,\ldots,\Theta_m}(\pi_i|\theta_2, \ldots, \theta_m) = \sum_{j=1}^{r} \frac{f_{\Delta\Theta_1|\Theta_2,\ldots,\Theta_m}(\Delta\theta_{1,j}|\theta_2, \ldots, \theta_m)}{|p_i'(\Delta\theta_{1,j})|}, \quad (3.25)$$

where $\Delta\theta_{1,1}$, $\Delta\theta_{1,2}, \ldots \Delta\theta_{1,r}$ are the $r \leq t$ real roots of $\pi_i = p_i(\Delta\theta_1)$. Appendix A.4 includes a short note on the computation of $f_{\Delta\Theta_1|\Theta_2,\ldots,\Theta_m}(\Delta\theta_{1,j}|\theta_2, \ldots, \theta_m)$ from the joint distribution of the model parameters, and the subsequent derivation of $f_{\Pi_i}(\pi_i)$ from the total probability theorem.

3.3.2 Computer implementation

Algorithm 2 provides the pseudocode for computer implementation of the method outlined in (3.18)-(3.24) to compute $f_{\Pi_i}(\pi_i)$, $i = 0, 1, \ldots, N$ given $f_{\Theta_j}(\theta_j)$, $j = 1, 2, \ldots, m$. The vectors $\bar{\theta}_j = [\theta_j^{start} : d\theta_j : \theta_j^{end}]$, $j = 2, \ldots, m$, are defined so that each vector spans several standard deviations on both sides of m_{Θ_j}, the mean of Θ_j. The nested for loops ensure that the conditional pdf in (3.22) is evaluated point wise for the entries in $\bar{\theta}_j$. The QR factorization of the generator matrix is evaluated for every[4] $\hat{\theta} = [m_{\Theta_1}, \hat{\theta}_2, \ldots, \hat{\theta}_m]$, where $\hat{\theta}_j$, $j = 1, 2, \ldots, m$, denotes an entry of the vector $\bar{\theta}_j$. Next $\pi_i(\hat{\theta})$ is obtained from (2.12) by normalizing the last column of Q, the group inverse $\Lambda^{\#}$ is obtained from (2.13), and the Taylor series coefficients, b_{ki}, $k = 1, 2, \ldots, t$, are computed using (3.20). The r real roots of the equation $\hat{\pi}_i = p_i(\Delta\theta_1)$ are computed, and the conditional $f_{\Pi_i|\Theta_2,\ldots,\Theta_m}\left(\hat{\pi}_i|\hat{\theta}_2, \ldots, \hat{\theta}_m\right)$

[4]Recall from Algorithm 1, that in the pseudocode we use the variable $\hat{\theta}_j$ to denote an entry in the vector $\bar{\theta}_j$, i.e., $\hat{\theta}_j = \bar{\theta}_j(l)$, for some l.

then follows from (3.6)-(3.7). The integrals at the end of each nested for loop can be implemented using some numerical integration scheme, e.g., the trapezoidal method.

Algorithm 2 Computation of $f_{\Pi_i}(\pi_i)$ for the multi-parameter case.

define $\bar{\pi}_i = [0 : d\pi_i : 1]$, $\bar{\theta}_2 = \left[\theta_2^{start} : d\theta_2 : \theta_2^{end}\right]$, $\ldots$, $\bar{\theta}_m = \left[\theta_m^{start} : d\theta_m : \theta_m^{end}\right]$
define Taylor series order t
compute $\frac{\partial \Lambda}{\partial \theta_j}$, $j = 2, \ldots, m$
for $\hat{\pi}_i = 0 : d\pi_i : 1$ **do**
  for $\hat{\theta}_2 = \theta_2^{start} : d\theta_2 : \theta_2^{end}$ **do**
    $\vdots$
    for $\hat{\theta}_m = \theta_m^{start} : d\theta_m : \theta_m^{end}$ **do**
      compute $QR = \Lambda(\hat{\theta})$, where $\hat{\theta} = [m_{\Theta_1}, \hat{\theta}_2, \ldots, \hat{\theta}_m]$
      compute $\pi_i(\hat{\theta})$ from (2.12), $\Lambda^{\#}$ from (2.13), b_{ki}, $k = 1, 2, \ldots, t$ from (3.20)
      compute real roots of $\pi_i(\hat{\theta}) - \hat{\pi}_i + \sum_{k=1}^{t} \frac{b_{ki}}{k!} \Delta\theta_1^k = 0$, $\Delta\theta_{1,j}$, $j = 1, \ldots, r$
      for $j = 1$ to r **do**
        compute $f_{\Delta\Theta_1}(\Delta\theta_{1,j})$, and $p_i'(\Delta\theta_{1,j}) = \sum_{k=1}^{t} \frac{b_{ki}}{(k-1)!} \Delta\theta_{1,j}^{k-1}$
      end for
      compute $f_{\Pi_i|\Theta_2,\ldots,\Theta_m}\left(\hat{\pi}_i|\hat{\theta}_2, \ldots, \hat{\theta}_m\right) = \sum_{j=1}^{r} \frac{f_{\Delta\Theta_1}(\Delta\theta_{1,j})}{|p_i'(\Delta\theta_{1,j})|}$
    end for
    compute $f_{\Pi_i|\Theta_2,\ldots,\Theta_{m-1}}\left(\hat{\pi}_i|\hat{\theta}_2, \ldots, \hat{\theta}_{m-1}\right)$
    $\vdots$
  end for
  compute $f_{\Pi_i}(\hat{\pi}_i) = \int_{\theta_2} f_{\Pi_i|\Theta_2}\left(\hat{\pi}_i|\hat{\theta}_2\right) f_{\Theta_2}(\hat{\theta}_2) d\theta_2$
end for

3.3.3 Expected Value and Variance of Π_i

To derive an expression for the expectation and variance of Π_i, consider the multiple-variable version of the Taylor series expansion

$$\begin{aligned} \Pi_i &= \pi_i(\Theta) = \pi_i(m_\Theta + \Delta\Theta) \\ &= \pi_i(m_\Theta) + \sum_{k_1=1}^{\infty} \cdots \sum_{k_m=1}^{\infty} \frac{\Delta\Theta_1^{k_1} \ldots \Delta\Theta_m^{k_m}}{k_1! \ldots k_m!} \cdot \left. \frac{\partial^{k_1+\ldots k_m} \pi_i(\theta)}{\partial\theta_1^{k_1} \ldots \partial\theta_m^{k_m}} \right|_{\theta=m_\Theta}, \end{aligned} \quad (3.26)$$

where $m_\Theta = [m_{\Theta_1}, \mu_{\Theta_2}, \ldots, \mu_{\Theta_m}]$. While closed-form expressions for the partial derivatives $\partial^k \pi_i(\theta)/\partial\theta^k$ are available (see Appendix A.2), derivation of analytical expressions for the mixed partial derivatives of the form $\partial^{k_1+\cdots+k_m}\pi_i(\theta)/\partial\theta_1^{k_1}\ldots\partial\theta_m^{k_m}$ is the focus of ongoing research. Therefore, we will focus on lower-order Taylor series expansions to approximate the expectation and variance of Π_i. Towards this end, let us consider a second-order expansion for $\pi_i(\Theta)$

$$\Pi_i \approx \pi_i(m_\Theta) + \Delta\Theta\ \nabla\pi_i(\theta)^T\big|_{\theta=m_\Theta} + \frac{1}{2}\Delta\Theta\ \nabla^2\pi_i(\theta)\big|_{\theta=m_\Theta}\ \Delta\Theta^T, \tag{3.27}$$

where $m_\Theta = [m_{\Theta_1}, \mu_{\Theta_2}, \ldots, \mu_{\Theta_m}]$, and the gradient $\nabla\pi_i(\theta)$, and Hessian $\nabla^2\pi_i(\theta)$, are given by

$$\nabla\pi_i(\theta) = \left[\frac{\partial\pi_i(\theta)}{\partial\theta_1}, \frac{\partial\pi_i(\theta)}{\partial\theta_2}, \ldots, \frac{\partial\pi_i(\theta)}{\partial\theta_m}\right], \tag{3.28}$$

$$\nabla^2\pi_i(\theta) = \begin{bmatrix} \frac{\partial^2\pi_i(\theta)}{\partial\theta_1^2} & \frac{\partial^2\pi_i(\theta)}{\partial\theta_1\partial\theta_2} & \cdots & \frac{\partial^2\pi_i(\theta)}{\partial\theta_1\partial\theta_m} \\ \frac{\partial^2\pi_i(\theta)}{\partial\theta_2\partial\theta_1} & \frac{\partial^2\pi_i(\theta)}{\partial\theta_2^2} & \cdots & \frac{\partial^2\pi_i(\theta)}{\partial\theta_2\partial\theta_m} \\ \vdots & \vdots & \ddots & \vdots \\ \frac{\partial^2\pi_i(\theta)}{\partial\theta_m\partial\theta_1} & \frac{\partial^2\pi_i(\theta)}{\partial\theta_m\partial\theta_2} & \cdots & \frac{\partial^2\pi_i(\theta)}{\partial\theta_m^2} \end{bmatrix}. \tag{3.29}$$

Substituting the gradient and Hessian in (3.27) and taking into account i) the independence of the Θ_j's, and ii) the fact that $\mathrm{E}[\Delta\Theta_j] = 0\,\forall j = 1, 2, \ldots, m$, the expected value of Π_i is given by

$$\begin{aligned} m_{\Pi_i} &= \pi_i(m_\Theta) + \frac{1}{2}\sum_{k=1}^{m}\mathrm{E}[\Delta\Theta_k^2]\cdot\left.\frac{\partial^2\pi_i(\theta)}{\partial\theta_k^2}\right|_{\theta=m_\Theta} \\ &+ \sum_{j=1}^{m}\sum_{k=1,\,k\neq j}^{m}\mathrm{E}[\Delta\Theta_j]\cdot\mathrm{E}[\Delta\Theta_k]\cdot\left.\frac{\partial\pi_i^2(\theta)}{\partial\theta_j\partial\theta_k}\right|_{\theta=m_\Theta} \\ &= \pi_i(m_\Theta) + \frac{1}{2}\sum_{k=1}^{m}\mathrm{E}[\Delta\Theta_k^2]\cdot\left.\frac{\partial^2\pi_i(\theta)}{\partial\theta_k^2}\right|_{\theta=m_\Theta}. \end{aligned} \tag{3.30}$$

Similarly, assuming a first-order expansion for $\pi_i(\Theta)$,

$$\Pi_i \approx \pi_i(m_\Theta) + \Delta\Theta\ \nabla\pi_i(\theta)^T\big|_{\theta=m_\Theta}, \tag{3.31}$$

the variance of Π_i is given by

$$\sigma^2_{\Pi_i} = \sum_{k=1}^{m} \mathrm{Var}[\Delta\Theta_k] \left(\frac{\partial \pi_i(\theta)}{\partial \theta_k} \right)^2 \Bigg|_{\theta = m_\Theta} . \tag{3.32}$$

Algorithm 3 Computation of $f_\Xi(\xi)$ and $f_\Gamma(\gamma)$ for the multiple-parameter case.

define $\rho = [\rho_0, \rho_1, \ldots, \rho_n]$, τ, $\bar{\xi} = [0 : d\xi : \|\rho\|_1]$, $\bar{\gamma} = [0 : d\gamma : \tau \cdot \|\rho\|_1]$, $\bar{\theta}_2 = \left[\theta_2^{start} : d\theta_2 : \theta_2^{end}\right]$,..., $\bar{\theta}_m = \left[\theta_m^{start} : d\theta_m : \theta_m^{end}\right]$
define Taylor series order t
compute $\frac{\partial \Lambda}{\partial \theta_j}$, $j = 2, \ldots, m$
for $\hat{\xi} = 0 : d\xi : \|\rho\|_1$ **do**
  for $\hat{\theta}_2 = \theta_2^{start} : d\theta_2 : \theta_2^{end}$ **do**
    $\vdots$
    for $\hat{\theta}_m = \theta_m^{start} : d\theta_m : \theta_m^{end}$ **do**
      compute $QR = \Lambda(\hat{\theta})$ where $\hat{\theta} = [m_{\Theta_1}, \hat{\theta}_2, \ldots, \hat{\theta}_m]$
      compute $\xi(\hat{\theta}) = \pi(\hat{\theta})\rho^T$ (2.12), $\Lambda^{\#}$ (2.13), c_k, $k = 1, \ldots, t$ (3.35)
      compute real roots of $\xi(\hat{\theta}) - \hat{\xi} + \sum_{k=1}^{t} \frac{c_k}{k!} \Delta\theta_1^k = 0$, $\Delta\theta_{1,j}$, $j = 1, \ldots, r$
      for $j = 1$ to r **do**
        compute $f_{\Delta\Theta_1}(\Delta\theta_{1,j})$, and $x'(\Delta\theta_{1,j}) = \sum_{k=1}^{t} \frac{c_k}{(k-1)!} \Delta\theta_{1,j}^{k-1}$
      end for
      compute $f_{\Xi|\Theta_2,\ldots,\Theta_m}\left(\hat{\xi}|\hat{\theta}_2, \ldots, \hat{\theta}_m\right) = \sum_{j=1}^{r} \frac{f_{\Delta\Theta_1}(\Delta\theta_{1,j})}{|x'(\Delta\theta_{1,j})|}$
    end for
    compute $f_{\Xi|\Theta_2,\ldots,\Theta_{m-1}}\left(\hat{\xi}|\hat{\theta}_2, \ldots, \hat{\theta}_{m-1}\right)$
    $\vdots$
  end for
  compute $f_\Xi(\hat{\xi}) = \int_{\theta_2} f_{\Xi|\Theta_2}(\hat{\xi}|\hat{\theta}_2) f_{\Theta_2}(\hat{\theta}_2) d\theta_2$
end for
for $\hat{\gamma} = 0 : d\gamma : \tau \cdot \|\rho\|_1$ **do**
  $f_\Gamma(\hat{\gamma}) = \frac{f_\Xi(\hat{\gamma}/\tau)}{\tau}$
end for

3.4 Uncertainty in Markov Reward Models

In this section, we show how the pdfs of the reward $\Xi = \Pi\rho^T$, and accumulated reward $\Gamma = \Xi \cdot \tau$—denoted by $f_\Xi(\xi)$ and $f_\Gamma(\gamma)$, respectively—can be computed for the multiple-parameter case. We also propose closed-form approximations for the expectation and variance of Ξ and Γ.

3.4.1 Probability Density Function of Ξ and Γ

To derive the pdf of Ξ, we follow a procedure similar to the one outlined in Section 3.3. First, we pick a parameter, say Θ_1, and seek the Taylor series expansion of ξ around the mean of Θ_1, with the other parameters fixed. As before, splitting Θ as

$$\Theta = m_\Theta + \Delta\Theta, \tag{3.33}$$

where $m_\Theta = [m_{\Theta_1}, \theta_2, \ldots, \theta_m]$ and $\Delta\Theta = [\Delta\Theta_1, 0, \ldots, 0]$, we can express

$$\begin{aligned} \Xi &= \xi(\Theta) = \xi(m_\Theta + \Delta\Theta) \\ &= \xi(m_\Theta) + \sum_{k=1}^{\infty} \frac{c_k}{k!}\Delta\Theta_1^k = \pi(m_\Theta)\rho^T + \sum_{k=1}^{\infty} \frac{c_k}{k!}\Delta\Theta_1^k. \end{aligned} \tag{3.34}$$

The k-order Taylor series coefficient c_k is given by

$$c_k = \left.\frac{\partial^k \xi(\theta)}{\partial\theta_1^k}\right|_{\theta=m_\Theta} = \left.\frac{\partial^k \pi(\theta)}{\partial\theta_1^k}\rho^T\right|_{\theta=m_\Theta} = k!\,(-1)^k\,\pi(\theta)\left(\frac{\partial\Lambda(\theta)}{\partial\theta_1}\Lambda^{\#}\right)^k\rho^T\Bigg|_{\theta=m_\Theta} \tag{3.35}$$

We then truncate the Taylor series in (3.34) at the t term as follows:

$$\Xi = x(\Delta\Theta_1) = \pi(m_\Theta)\rho^T + \sum_{k=1}^{t} \frac{c_k}{k!}\Delta\Theta_1^k. \tag{3.36}$$

Then, analogous to (3.22), we get

$$f_{\Xi|\Theta_2,\ldots,\Theta_m}(\xi|\theta_2, \ldots, \theta_m) = \sum_{j=1}^{r} \frac{f_{\Delta\Theta_1}(\Delta\theta_{1,j})}{|x'(\Delta\theta_{1,j})|}, \tag{3.37}$$

where $\Delta\theta_{1,1}$, $\Delta\theta_{1,2}, \ldots \Delta\theta_{1,r}$ are the $r \leq t$ roots of $\xi = x(\Delta\theta_1)$. Applying the total probability theorem, and acknowledging the independence of $\Theta_2, \ldots, \Theta_m$,

$$f_{\Xi}(\xi) = \int_{\theta_2} \ldots \int_{\theta_m} f_{\Xi|\Theta_2,\ldots,\Theta_m}(\xi|\theta_2, \ldots, \theta_m) f_{\Theta_m}(\theta_m) d\theta_m \ldots f_{\Theta_2}(\theta_2) d\theta_2. \tag{3.38}$$

From the definition of $\Gamma = \Xi \cdot \tau$, it follows that

$$f_{\Gamma}(\gamma) = \frac{f_{\Xi}(\gamma/\tau)}{\tau}. \tag{3.39}$$

3.4.2 Computer Implementation

Algorithm 3 provides the pseudocode for computer implementation of the method outlined in (3.33)-(3.39) to compute $f_{\Xi}(\xi)$ and $f_{\Gamma}(\gamma)$ given $f_{\Theta_j}(\theta_j)$, $j = 1, 2, \ldots, m$. The pseudocode follows along similar lines to that in Algorithm 2. Note that the vectors $\bar{\xi} = [0 : d\xi : \|\rho\|_1]$ and $\bar{\gamma} = [0 : d\gamma : \tau \cdot \|\rho\|_1]$ are formulated based on the one-norm of ρ, since $\xi = \pi\rho^T$, $\gamma = \xi \cdot \tau = \pi \cdot \rho^T \cdot \tau$ and $0 \leq \pi_i \leq 1$, $\forall i = 0, 1, \ldots, N$.

3.4.3 Expected Value and Variance of Ξ and Γ

Similar to (3.30), assuming a second-order expansion for $\xi(\Theta)$, we can express the expected value of Ξ, denoted by m_{Ξ}, as

$$m_{\Xi} := \mathrm{E}[\Xi] = \pi(m_{\Theta})\rho^T + \frac{1}{2}\sum_{k=1}^{m} \mathrm{E}[\Delta\Theta_k^2] \left.\frac{\partial^2 \pi(\theta)}{\partial \theta_k^2}\right|_{\theta=m_{\Theta}} \rho^T. \tag{3.40}$$

Additionally, similar to (3.32), assuming a first-order expansion for $\xi(\Theta)$, the variance of Ξ, denoted by σ_{Ξ}^2, is given by

$$\sigma_{\Xi}^2 \quad := \quad \mathrm{Var}(\Xi) = \sum_{k=1}^{m} \mathrm{Var}\left(\Delta\Theta_k\right) \left.\left(\frac{\partial \pi(\theta)}{\partial \theta_k}\rho^T\right)^2\right|_{\theta=m_{\Theta}}. \tag{3.41}$$

From the definition of $\Gamma = \Xi \cdot \tau$, we get

$$m_{\Gamma} := \mathrm{E}[\Gamma] = \mathrm{E}[\Xi \cdot \tau] = m_{\Xi} \cdot \tau, \tag{3.42}$$

$$\sigma_{\Gamma}^2 := \mathrm{Var}(\Gamma) = \mathrm{Var}(\Xi \cdot \tau) = \sigma_{\Xi}^2 \cdot \tau^2. \tag{3.43}$$

3.5 Case Studies Covering Common Reliability Models

In this section, we present three case studies that demonstrate the applicability of the proposed method in quantifying the impact of probabilistic parametric uncertainty in common Markov reliability models. The first case study returns to the two-state Markov model discussed in Example 2. While the example examined the case with a single uncertain parameter, in this case study, we consider the case where both parameters are uncertain. It is still fairly straightforward to derive an analytical expression for the pdfs of the stationary distribution, the reward, and hence, the accumulated reward, because the steady-state probabilities are simple functions of the model parameters. The availability of an analytical solution allows us to validate the Taylor series approach. The second case study explores a two-component load-sharing system with common-cause failures [46]. In this case, it is not possible to derive the pdfs of the steady-state probabilities and the reward from the analytical expressions of the stationary distribution. Therefore the results from the Taylor series approach are compared with those obtained from repeated Monte Carlo simulations. In the final case study, we examine computer execution times for an $n+1$ state reward model for a system of n identical components, each with two operating modes.

In all the case studies that follow, we model the failure rates with normal distributions and repair rates with uniform distributions. This is based on the presumption that typically the mean and variance of the failure rate might be available from field data; however, due to the involvement of myriad human factors, only a range of repair times might be known. We denote $N \sim \mathcal{N}(\mu_N, \sigma_N^2)$ to be a normal random variable with mean μ_N and variance σ_N^2. Additionally, we denote $U \sim \mathcal{U}(a_U, b_U)$ to be a uniform random variable over the interval $[a_U, b_U]$. Also, note that failure and repair rates have units of per-unit time. To streamline the presentation, we omit the units in the following discussion.

3.5.1 Single Component with Two Operating States

Consider the two-state reliability model of Example 2. We define a reward model by choosing a reward vector $\rho = [\rho_0, \rho_1]$, where ρ_0 and ρ_1 are constants that capture some notion of performance while in states 0 and 1, respectively. As described in (2.7), the long-term reward is given by $\xi = \rho_0\pi_0 + \rho_1\pi_1$, and as described in (2.8),

the accumulated reward at time τ is given by $\gamma = \xi \cdot \tau$.

Since the failure and repair rates are not perfectly known, it is assumed that they are described by random variables L and M with (known) pdfs $f_L(\lambda)$ and $f_M(\mu)$, respectively. Further, it is assumed that L and M are independent. Consequently, the stationary distribution is described by random variables Π_0 and Π_1, and the reward and accumulated reward are described by random variables Ξ and Γ, respectively.

Through random variable transformations, the following expressions for $f_{\Pi_0}(\pi_0)$, $f_{\Pi_1}(\pi_1)$, and $f_\Xi(\xi)$ can be derived from the closed-form expressions for π_0 and π_1 given in (2.18):

$$f_{\Pi_0}(\pi_0) = \int_\lambda \frac{\lambda}{\pi_0^2} \cdot f_M\left(\frac{\lambda(1-\pi_0)}{\pi_0}\right) \cdot f_L(\lambda) d\lambda, \tag{3.44}$$

$$f_{\Pi_1}(\pi_1) = \int_\lambda \frac{\lambda}{(1-\pi_1)^2} \cdot f_M\left(\frac{\lambda\pi_1}{(1-\pi_1)}\right) \cdot f_L(\lambda) d\lambda, \tag{3.45}$$

$$f_\Xi(\xi) = \int_\lambda \left|\frac{\lambda(\rho_1-\rho_0)}{(\rho_1-\xi)^2}\right| \cdot f_M\left(\frac{\lambda(\xi-\rho_0)}{(\rho_1-\xi)}\right) \cdot f_L(\lambda) d\lambda. \tag{3.46}$$

Recall that $f_\Gamma(\gamma)$ can be obtained from $f_\Xi(\xi)$ using (3.39).

For illustration, let us consider that the failure rate is normally distributed and that the repair rate is uniformly distributed, i.e., $L \sim \mathcal{N}(m_L, \sigma_L^2)$, $M \sim \mathcal{U}(a_M, b_M)$. Figures 3.3 and 3.4 depict the pdfs $f_{\Pi_0}(\pi_0)$, $f_{\Pi_1}(\pi_1)$, $f_\Xi(\xi)$, and $f_\Gamma(\gamma)$ computed: i) numerically using a third-order Taylor series expansion with the methods outlined in Sections 3.3.2 and 3.4.2, ii) analytically using (3.44), (3.45), (3.46), and iii) numerically from a 1,000,000-sample Monte Carlo simulation performed as described next. We first sample the distribution of the random vector Θ that describes the values that the model parameters can take. For each sample θ, we obtain the corresponding generator matrix $\Lambda(\theta)$ by substituting for the corresponding values. Then, by using a QR factorization of $\Lambda(\theta)$, we obtain the stationary distribution of the chain $\pi(\theta)$ without having to solve the Chapman-Kolmogorov equations (for the specific $\Lambda(\theta)$ as $t \to \infty$).

The simulation parameters are $m_L = 0.55$, $\sigma_L^2 = 0.1^2$, $a_M = 1$, $b_M = 10$, $\rho = [\rho_0, \rho_1] = [0.25, 0.75]$, and $\tau = 6$. The results indicate that the pdfs computed via the Taylor series method accurately match the exact analytical results and those from Monte Carlo simulations. Tables 3.1-3.2 list the analytically com-

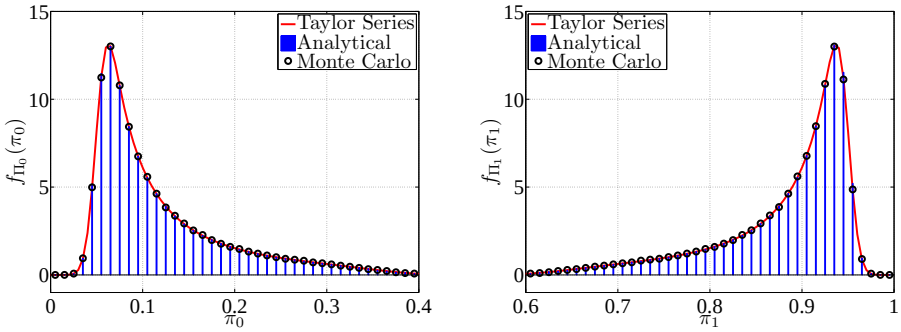

(a) (b)

Figure 3.3: $f_{\Pi_0}(\pi_0)$, $f_{\Pi_1}(\pi_1)$ for $L \sim \mathcal{N}(0.55,\, 0.1^2)$ and $M \sim \mathcal{U}(1,\, 10)$.

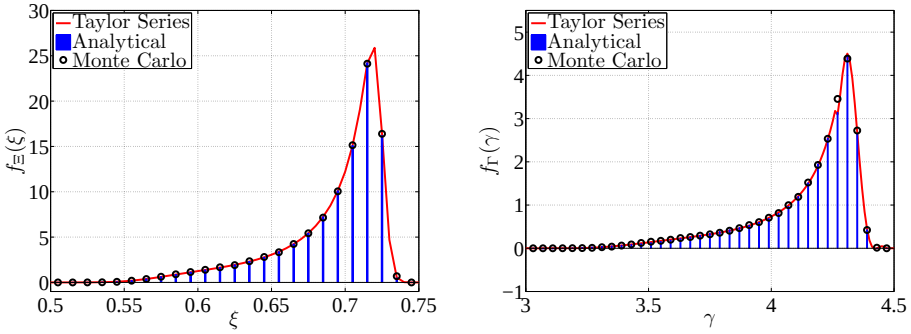

(a) (b)

Figure 3.4: $f_{\Xi}(\xi)$, $f_{\Gamma}(\gamma)$ for $L \sim \mathcal{N}(0.55,\, 0.1^2)$, $M \sim \mathcal{U}(1,\, 10)$, $\rho = [0.25,\, 0.75]$, and $\tau = 6$.

puted expectations and variances, respectively, for Π_0, Π_1, Ξ, and Γ for two sets of parameter distributions: $L \sim \mathcal{N}(0.55,\, 0.1^2)$, $M \sim \mathcal{U}(1,\, 10)$, and $L \sim \mathcal{N}(0.55,\, 0.1^2)$, $M \sim \mathcal{U}(100,\, 109)$. Recall that the analytical expressions for the expectation and variance are based on lower-order approximations derived in Sections 3.3.3 and 3.4.3. For comparison, the expectations and variances computed numerically from their pdfs—derived using the third-order Taylor series expansion—are also computed. The expectations computed analytically match those computed numerically in both cases. However, the analytically computed variance matches the exact numerical result only when the mean repair rate is several orders of magnitude larger than the mean failure rate. Note that since the expectation and variance are computed

Table 3.1: Analytical and numerical expectations compared for the model studied in Section 3.5.1.

Case	R.v.	m: Analytical	m: Numerical
$L \sim \mathcal{N}(0.55,\, 0.1^2)$ $M \sim \mathcal{U}(1,\, 10)$	Π_0	0.1019	0.1167
	Π_1	0.8981	0.8833
	Ξ	0.6991	0.6916
	Γ	4.1943	4.1328
$L \sim \mathcal{N}(0.55,\, 0.1^2)$ $M \sim \mathcal{U}(100,\, 109)$	Π_0	0.0052	0.0052
	Π_1	0.9948	0.9948
	Ξ	0.7474	0.7474
	Γ	4.4843	4.4954

assuming second- and first-order truncations of the Taylor-series expansion, respectively, there might be an error introduced in the computed values if higher-order terms are dominant. For the examples we explore in the case studies, the higher-order terms are negligible if the mean repair rate is several orders of magnitude higher than the mean failure rate—consequently, the analytical results match the numerical values better in these cases. While the results may be inaccurate, the analytical expressions can be evaluated with minimum effort, and thus serve useful for back-of-the-envelope calculations. On the other hand, the pdfs computed following the Taylor-series method are accurate (even if the analytically computed moments are not accurate). This is because the method proposed to obtain the pdfs of the reliability indices does not constrain the order of the Taylor-series expansion. We obtain very accurate estimates for the mean and variance of the indices from the computed pdfs—at the expense of computation time.

3.5.2 Two-Component Load-Sharing System with Common-Cause Failures

This example, adapted from [46], explores a system composed of two identical components that share a common load. The component failure rate is denoted by λ, and the repair rate is denoted by μ. In addition, the system is susceptible to common-cause failures which cause all operational components to fail at the same time. The common-cause failure rate is denoted by λ_C. The state transition diagram for this

Table 3.2: Analytical and numerical variances compared for the model studied in Section 3.5.1.

Case	R.v.	σ^2: Analytical	σ^2: Numerical
$L \sim \mathcal{N}(0.55,\, 0.1^2)$ $M \sim \mathcal{U}(1,\, 10)$	Π_0	0.0012	0.0053
	Π_1	0.0012	0.0053
	Ξ	3.1151×10^{-4}	0.0013
	Γ	0.0112	0.0477
$L \sim \mathcal{N}(0.55,\, 0.1^2)$ $M \sim \mathcal{U}(100,\, 109)$	Π_0	9.1312×10^{-7}	9.1501×10^{-7}
	Π_1	9.1312×10^{-7}	9.1501×10^{-7}
	Ξ	2.2828×10^{-7}	2.2875×10^{-7}
	Γ	8.2181×10^{-6}	8.1940×10^{-6}

system is shown in Fig. 3.5. Both components are operational in state 2, a single component is operational in state 1, and in state 0, both components have failed. Repairs restore the operation of one component at a time. From the state-transition diagram in Fig. 3.5, the generator matrix can be derived as

$$\Lambda = \begin{bmatrix} -\mu & \mu & 0 \\ \lambda + \lambda_C & -(\lambda + \lambda_C + \mu) & \mu \\ \lambda_C & 2\lambda & -(2\lambda + \lambda_C) \end{bmatrix}. \tag{3.47}$$

Denote the stationary distribution of the chain by $\pi = [\pi_0,\, \pi_1,\, \pi_2]$. Solving (2.5), we obtain

$$\pi_0 = \frac{(\lambda + \lambda_C)(2\lambda + \lambda_C) + \lambda_C\mu}{(\lambda + \lambda_C + \mu)(2\lambda + \lambda_C) + \lambda_C\mu + \mu^2}, \tag{3.48}$$

$$\pi_1 = \frac{(2\lambda + \lambda_C)\mu}{(\lambda + \lambda_C + \mu)(2\lambda + \lambda_C) + \lambda_C\mu + \mu^2}, \tag{3.49}$$

$$\pi_2 = \frac{\mu^2}{(\lambda + \lambda_C + \mu)(2\lambda + \lambda_C) + \lambda_C\mu + \mu^2}. \tag{3.50}$$

Notice how involved the analytical closed-form expressions are even for this simple system. Consider that the performance of the system is proportional to the number of operational components. Then, we can define a reward model for this system by choosing $\rho = [\rho_0,\, \rho_1,\, \rho_2] = [0,\, 1,\, 2]$. The long-term reward is given by $\xi = \pi \cdot \rho^T = \pi_1 + 2\pi_2$.

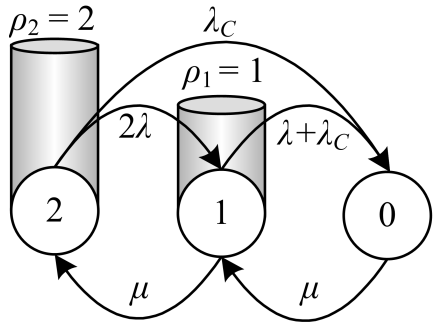

Figure 3.5: State-transition diagram for the three-state load-sharing system with common-cause failures.

Table 3.3: Analytical and numerical expectations compared for the model studied in Section 3.5.2.

Case	R.v.	m: Analytical	m: Numerical
	Π_0	0.0330	0.0430
$L \sim \mathcal{N}(0.5, 0.1^2)$	Π_1	0.1777	0.1822
$L_C \sim \mathcal{N}(0.05,\ 0.01^2)$	Π_2	0.7892	0.7748
$M \sim \mathcal{U}(1,\ 10)$	Ξ	1.7562	1.7318
	Π_0	1.6579×10^{-4}	1.6683×10^{-4}
$L \sim \mathcal{N}(1.6\text{e-}4,\ (25\text{e-}6)^2)$	Π_1	0.0027	0.0027
$L_C \sim \mathcal{N}(2\text{e-}5,\ (5\text{e-}6)^2)$	Π_2	0.9971	0.9968
$M \sim \mathcal{U}(0.1, 0.15)$	Ξ	1.9969	1.9964

Suppose the failure rate, repair rate, and common-cause failure rate are described by random variables L, M, and L_C with (known) pdfs $f_L(\lambda)$, $f_M(\mu)$, and $f_{L_C}(\lambda_C)$, respectively. Additionally, it is assumed that L, M, and L_C are independent. Consequently, the components of the stationary distribution $\Pi = [\Pi_0\,, \Pi_1,\ \Pi_2]$ are random variables with distributions $f_{\Pi_0}(\pi_0)$, $f_{\Pi_1}(\pi_1)$, and $f_{\Pi_2}(\pi_2)$. Similarly, the reward, $\Xi = \Pi \cdot \rho^T = \Pi_1 + 2\Pi_2$ is a random variable with distribution $f_\Xi(\xi)$. Unlike the two-state example explored in Section 3.5.1, it is clear from the expressions of the steady-state probabilities that closed-form expressions for the pdfs cannot be obtained. Therefore, we recourse to the Taylor series approach to derive the pdfs of the steady-state probabilities and the reward.

Let us consider $L \sim \mathcal{N}(0.5,\ 0.1^2)$, $L_C \sim \mathcal{N}(0.05,\ 0.01^2)$, and $M \sim \mathcal{U}(1,\ 10)$.

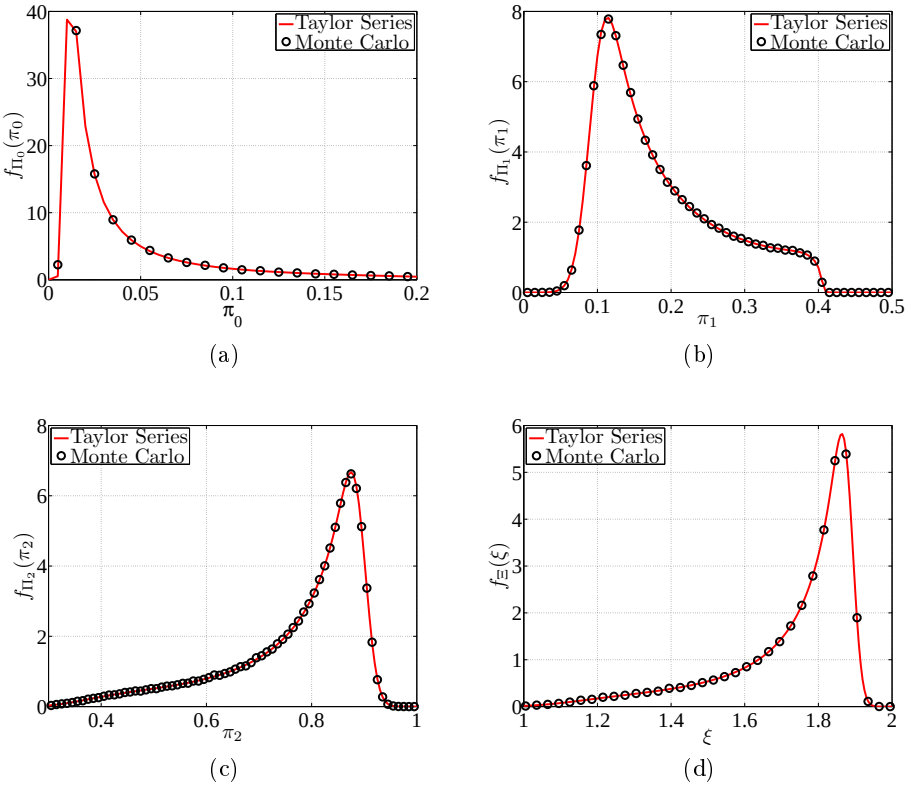

Figure 3.6: $f_{\Pi_0}(\pi_0)$, $f_{\Pi_1}(\pi_1)$, $f_{\Pi_2}(\pi_2)$, and $f_{\Xi}(\xi)$ for $L \sim \mathcal{N}(0.5,\, 0.1^2)$, $L_C \sim \mathcal{N}(0.05,\, 0.01^2)$, $M \sim \mathcal{U}(1,\, 10)$, $\rho = [0,\, 1,\, 2]$.

Figure 3.6 depicts the pdfs $f_{\Pi_0}(\pi_0)$, $f_{\Pi_1}(\pi_1)$, $f_{\Pi_2}(\pi_2)$, and $f_{\Xi}(\xi)$, all computed using a third-order Taylor series expansion with the methods outlined in Sections 3.3.2 and 3.4.2. Additionally, results from a 1,000,000-sample Monte Carlo simulation are also shown. The figures indicate that the pdfs computed via the Taylor series method accurately match those obtained through Monte Carlo simulations.

Tables 3.3-3.4 list the analytically computed expectations and variances for Π_0, Π_1, Π_2, and Ξ for two sets of parameter distributions: $L \sim \mathcal{N}(0.5, 0.1^2)$, $L_C \sim \mathcal{N}(0.05,\, 0.01^2)$, $M \sim \mathcal{U}(1,\, 10)$, and $L \sim \mathcal{N}(1.6\text{e-}4,\, (25\text{e-}6)^2)$, $L_C \sim \mathcal{N}(2\text{e-}5,\, (5\text{e-}6)^2)$, $M \sim \mathcal{U}(0.1, 0.15)$. Recall that the analytical expressions for the expectation and variance are based on lower-order approximations derived in Sections 3.3.3 and 3.4.3. For comparison, the expectations and variances computed numerically from their pdfs—derived with the third-order Taylor series approach—are also computed. As before, while the expectations computed analytically match those computed numer-

Table 3.4: Analytical and numerical variances compared for the model studied in Section 3.5.2.

Case	R.v.	σ^2: Analytical	σ^2: Numerical
	Π_0	3.8745×10^{-5}	0.0024
$L \sim \mathcal{N}(0.5, 0.1^2)$	Π_1	6.6013×10^{-4}	0.0070
$L_C \sim \mathcal{N}(0.05,\ 0.01^2)$	Π_2	0.0010	0.0167
$M \sim \mathcal{U}(1,\ 10)$	Ξ	0.0014	0.0312
	Π_0	1.9755×10^{-9}	2.1305×10^{-9}
$L \sim \mathcal{N}(1.6\text{e-}4,\ (25\text{e-}6)^2)$	Π_1	2.5731×10^{-7}	2.6977×10^{-7}
$L_C \sim \mathcal{N}(2\text{e-}5,\ (5\text{e-}6)^2)$	Π_2	2.7533×10^{-7}	2.8889×10^{-7}
$M \sim \mathcal{U}(0.1, 0.15)$	Ξ	2.9730×10^{-7}	3.1215×10^{-7}

ically in both cases, the analytically computed variance matches the exact numerical result only when the mean repair rate is several orders of magnitude larger than the mean failure rate.

3.5.3 System of n Components

The final case study compares the execution time t_e, of the proposed Taylor series method with Monte Carlo simulations for a system of n identical components, each with two operating modes (functioning/failed). The state-transition diagram that models the reliability of this system is depicted in Fig. 3.7. The component failure rate is denoted by λ, and the repair rate is denoted by μ. Repairs restore the operation of all failed components simultaneously. The performance of the system is proportional to the number of operational components. A reward model for this system is formulated by choosing $\rho = [\rho_0,\ \rho_1,\ \ldots \rho_i, \ldots,\ \rho_n] = \left[0,\ \frac{1}{n},\ \ldots \frac{i}{n}, \ldots,\ 1\right]$. The long-term reward is given by $\xi = \pi\rho^T = \frac{1}{n}\pi_1 + \frac{2}{n}\pi_2 + \cdots + \frac{i}{n}\pi_i + \cdots + \pi_n$. Suppose the failure rate and repair rate are described by random variables $L \sim \mathcal{N}(0.55,\ 0.1^2)$ and $M \sim \mathcal{U}(1,\ 10)$, respectively. Consequently, the components of the stationary distribution $\Pi = [\Pi_0,\ \Pi_1,\ \ldots,\ \Pi_i, \ldots,\ \Pi_n]$ are random variables, and the reward, $\Xi = \Pi\rho^T$ is a random variable with pdf $f_\Xi(\xi)$.

This case study explores the impact of the number of samples in the Monte Carlo simulation n_s, and the dimension of the state space n, on the time to compute $f_\Xi(\xi)$

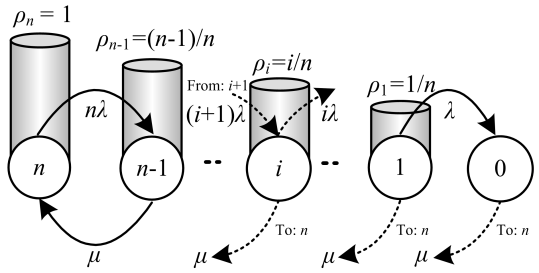

Figure 3.7: State-transition diagram for system of n components.

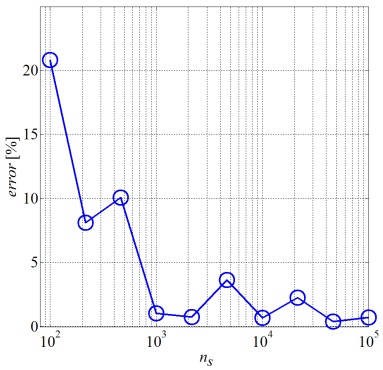

Figure 3.8: Percentage error in σ_Ξ as a function of n_s, $n = 2$.

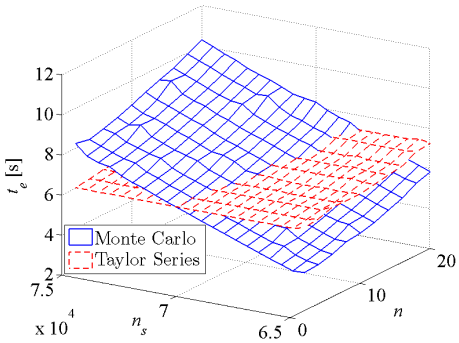

Figure 3.9: Execution time t_e, as a function of model order n, and number of samples n_s.

through: i) third-order Taylor series approach following the pseudocode outlined in Section 3.4.2, ii) Monte Carlo simulations involving repeated sampling from n_s-length random samples of the failure and repair-rate distributions. The experiment is performed on a PC with a 2.66 GHz Intel Core$^{\text{TM}}$2 Quad CPU processor with 4 GB memory in the MATLAB environment. Figure 3.8 plots the percentage difference in the variance of Ξ, σ_Ξ, as a function of n_s for $n = 2$ for one experimental run. The result demonstrates the significance of n_s on the accuracy of Monte Carlo simulations. Figure 3.9 plots the execution time of the two methods as a function of n and n_s. In the experiment, n is increased from 2 to 20 in steps of 2, and n_s is increased from 65,000 to 75,000 in steps of 500. The Taylor series method execution time is lower than Monte Carlo simulations over a wide range of n_s (prominent for $n_s > 70,000$). For large models ($n > 20$) and a sufficiently large number of samples ($n_s > 75,000$), Fig. 3.9 clearly indicates that the proposed Taylor series method outperforms Monte Carlo simulation.

Chapter 4

UNKNOWN-BUT-BOUNDED UNCERTAINTY ANALYSIS IN MARKOV RELIABILITY AND REWARD MODELS

Recall that in Chapter 3, we described a probabilistic uncertainty model—in particular, parameters were modeled as random variables with known distributions. Here, we explore the set theoretic counterpart of the probabilistic model, i.e., we assume the model parameters are constrained to lie within a set. Given this set, we then compute the set that bounds the reliability/performability indices of interest. The ideas presented in this chapter constitute the second (of two) methods to propagate parametric uncertainty through Markov models. The material we present subsequently is partially adopted from [13].

First, we present some fundamentals, and then describe the ellipsoidal-propagation method to quantify the impact of unknown-but-bounded parametric uncertainty in Markov reliability and reward models.

4.1 Problem Formulation

With regard to the standard terminology introduced in Chapter 2, assume that the model parameters, θ_j, $j = 1, 2, \ldots, m$, are not perfectly known, but are constrained to a range. The parameter vector can be expressed as $\theta = \bar{\theta} + \Delta\theta$, where $\bar{\theta}$ is the vector of nominal parameter values and $\Delta\theta \in \mathcal{X} \subseteq \mathbb{R}^m$, where $\mathcal{X}$ is a parallelotope defined as

$$\mathcal{X} := \left\{ \Delta\theta : \left| \kappa_i^T \Delta\theta \right| \leq 1, \forall i = 1, \ldots, m \right\}. \tag{4.1}$$

The vertices of $\mathcal{X}$ are determined by the parameter value ranges, while the vectors κ_i define the edges of $\mathcal{X}$ [53]. Given this unknown-but-bounded parametric uncertainty model, we are interested in characterizing the uncertainty in the stationary distribution $\pi(\theta)$. In particular, we are interested in determining the set $\mathcal{Y}$ such that $\Delta\pi = \pi - \bar{\pi} \in \mathcal{Y} \subseteq \mathbb{R}^{N+1}$, where $\bar{\pi} := \pi(\bar{\theta}) = [\bar{\pi}_0, \bar{\pi}_1, \bar{\pi}_2, \ldots, \bar{\pi}_N]^T$ is the

stationary distribution corresponding to the nominal parameter values. Notice that the reward $\xi(\theta) = \pi(\theta)^T \rho$ is a linear projection of the stationary distribution $\pi(\theta)$ onto the direction specified by the vector ρ. Therefore, to bound the values that the reward can take, we need to obtain the set $\mathcal{Y}$ and then apply a linear transformation to recover a set $\mathcal{C} \in \mathbb{R}$, such that $\xi(\theta) = \pi(\theta)^T \rho \in \mathcal{C}$. A similar method applies to obtain the set that bounds the accumulated reward γ.

The brute-force solution to the problem discussed here is to repeatedly compute the stationary distribution and the associated reward (by solving (2.5), (2.7), respectively) for a range of parameter values in the set $\{\bar{\theta}\} \oplus \mathcal{X}$. However, this approach is bound to be computationally expensive as the dimension of the state space N, or the number of model parameters m, increases. Therefore, in this work, we seek an analytical approach based on the Taylor-series expansion of the stationary distribution. To illustrate ideas, we provide a short representative example below.

Example 3

Figure 4.1 graphically describes the problem discussed above in the context of the two-state Markov reliability model for a single component with two operating modes—failed in state 0 and operational in state 1. Recall that we studied this model in Examples 1 and 2. The probability that the component has failed is given by $\pi_0(\lambda, \mu) = \lambda/(\lambda + \mu)$, and the probability that it is operational is given by $\pi_1(\lambda, \mu) = \mu/(\lambda + \mu)$, where λ is the component failure rate, and μ is the repair rate. The set $\mathcal{X}$ describes the values that the parameters λ and μ may take. We are interested in recovering the set $\mathcal{Y}$ that captures all values that the stationary distribution $\pi = [\pi_0, \pi_1]$ may take, due to uncertainty in the values of λ and μ. In the proposed method, we describe parametric uncertainty by an ellipsoidal set $\mathcal{E}$ (an

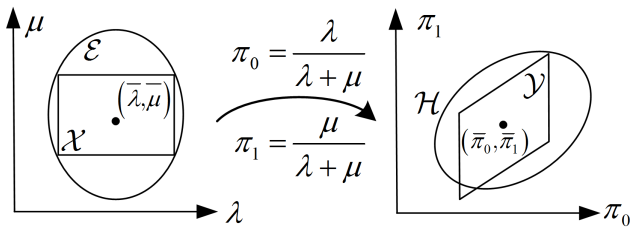

Figure 4.1: Illustrating the set-theoretic method for the two-state Markov reliability model examined in Example 3.

upper bound to the set $\mathcal{X}$). Then, we recover the set $\mathcal{H}$ by propagating $\mathcal{E}$ through a second-order Taylor series expansion of $\pi_0(\lambda, \mu)$ and $\pi_1(\lambda, \mu)$ about the nominal values of λ and μ ($\bar{\lambda}$ and $\bar{\mu}$, respectively). The set $\mathcal{H}$ captures variability in π_1 and π_0 up to second order. In general, for multi-state, multi-parameter models, it is difficult to obtain closed-form expressions for the stationary distribution—let alone analytically probe the impact of parametric uncertainty on such expressions.[1] The proposed method addresses this problem by: i) expressing the stationary distribution with a Taylor-series expansion as a function of the model parameters, and ii) providing a general method to propagate ellipsoidal-shaped sets through a second-order Taylor-series expansion. We must note, that as hinted in the figure, if the parametric uncertainty is large, the set $\mathcal{H}$ may not upper-bound the set $\mathcal{Y}$.

Next, we characterize the Markov-chain stationary-distribution Taylor-series expansion. Then, we propose methods to propagate ellipsoidal-shaped sets through first- and second-order Taylor series expansions of the Markov chain stationary distribution.

4.2 Taylor-Series Expansion of the Stationary Distribution

To characterize uncertainty in the entries of the stationary distribution $\pi(\theta)$, we can omit $\pi_0(\theta)$ and only consider the other N (out of the $N+1$) entries of $\pi(\theta)$. This is because $\pi_0(\theta) = 1 - \sum_{i=1}^{N} \pi_i(\theta)$. For small perturbations around the nominal parameter values, $\pi_i(\theta)$, $i = 1, 2, \ldots, N$, can be approximated by a second-order Taylor series expansion:

$$\pi_i(\theta) = \pi_i(\bar{\theta}) + \Delta\pi_i \approx \bar{\pi}_i + \nabla\pi_i(\bar{\theta})\Delta\theta + \frac{1}{2}\Delta\theta^T\nabla^2\pi_i(\bar{\theta})\Delta\theta, \tag{4.2}$$

where $\Delta\theta = [\Delta\theta_1, \Delta\theta_2, \ldots, \Delta\theta_m]^T = [\theta_1 - \bar{\theta}_1, \theta_2 - \bar{\theta}_2, \ldots, \theta_m - \bar{\theta}_m]^T \in \mathbb{R}^m$. In (4.2), the gradient $\nabla\pi_i(\bar{\theta})$, and Hessian $\nabla^2\pi_i(\bar{\theta})$, are given by

$$\nabla\pi_i(\bar{\theta}) = \left[\frac{\partial\pi_i(\bar{\theta})}{\partial\theta_1}, \frac{\partial\pi_i(\bar{\theta})}{\partial\theta_2}, \ldots, \frac{\partial\pi_i(\bar{\theta})}{\partial\theta_m}\right], \tag{4.3}$$

[1] To appreciate this aspect, readers are referred to (4.22)-(4.24) in Section 4.5.1—closed-form expressions for the stationary distribution of a two-component shared-load system with common-cause failures.

$$\nabla^2\pi_i(\bar{\theta}) = \begin{bmatrix} \frac{\partial^2\pi_i(\bar{\theta})}{\partial\theta_1^2} & \frac{\partial^2\pi_i(\bar{\theta})}{\partial\theta_1\partial\theta_2} & \cdots & \frac{\partial^2\pi_i(\bar{\theta})}{\partial\theta_1\partial\theta_m} \\ \frac{\partial^2\pi_i(\bar{\theta})}{\partial\theta_2\partial\theta_1} & \frac{\partial^2\pi_i(\bar{\theta})}{\partial\theta_2^2} & \cdots & \frac{\partial^2\pi_i(\bar{\theta})}{\partial\theta_2\partial\theta_m} \\ \vdots & \vdots & \ddots & \vdots \\ \frac{\partial^2\pi_i(\bar{\theta})}{\partial\theta_m\partial\theta_1} & \frac{\partial^2\pi_i(\bar{\theta})}{\partial\theta_m\partial\theta_2} & \cdots & \frac{\partial^2\pi_i(\bar{\theta})}{\partial\theta_m^2} \end{bmatrix}. \tag{4.4}$$

Since the generator matrix Λ is singular, it is easy to verify that the entries of the matrices in (4.3)-(4.4) cannot be obtained by direct differentiation of (2.5). However, as demonstrated in Chapter 2, the group inverse of Λ, denoted by $\Lambda^{\#}$, is a powerful kernel to study the sensitivity of the stationary distribution to parameter variations.[2] In particular, the sensitivities $\partial\pi_i(\bar{\theta})/\partial\theta_j$, $\partial^2\pi_i(\bar{\theta})/\partial\theta_j^2$, and $\partial^2\pi_i(\bar{\theta})/\partial\theta_j\partial\theta_k$, $\forall i = 0, 1, \ldots, n$, $\forall j, k = 1, 2, \ldots, m$, are given by

$$\frac{\partial\pi_i(\bar{\theta})}{\partial\theta_j} = -\pi(\bar{\theta})^T \frac{\partial\Lambda}{\partial\theta_j}\Lambda^{\#}e_i, \tag{4.5}$$

$$\frac{\partial\pi_i^2(\bar{\theta})}{\partial\theta_j^2} = 2\pi(\bar{\theta})^T \left(\frac{\partial\Lambda}{\partial\theta_j}\Lambda^{\#}\right)^2 e_i, \tag{4.6}$$

$$\frac{\partial\pi_i^2(\bar{\theta})}{\partial\theta_j\partial\theta_k} = \pi(\bar{\theta})^T \left(\frac{\partial\Lambda}{\partial\theta_j}\Lambda^{\#}\frac{\partial\Lambda}{\partial\theta_k}\Lambda^{\#} + \frac{\partial\Lambda}{\partial\theta_k}\Lambda^{\#}\frac{\partial\Lambda}{\partial\theta_j}\Lambda^{\#}\right) e_i, \tag{4.7}$$

where $\pi(\bar{\theta})$ is the stationary distribution evaluated at the nominal parameter values, $\Lambda^{\#}$ is the group inverse of the generator matrix, and $e_i \in \mathbb{R}^{N+1}$ is a vector with 1 as the i entry and zero otherwise. The derivation of (4.5)-(4.7) is provided in Appendix A.1. Both the group inverse $\Lambda^{\#}$, and the stationary distribution for the nominal parameter values $\pi(\bar{\theta})$, can be obtained by a QR factorization of the generator matrix Λ [50]. This method was summarized in Section 2.3. The nominal stationary distribution and the sensitivities have to be computed just once to provide a complete characterization of the second-order Taylor-series expansion.

As described in the introduction to this chapter, the values the model parameters can take are unknown but lie within a parallelotope $\mathcal{X}$ centered around $\bar{\theta}$, i.e., $\theta = \bar{\theta} + \Delta\theta$, where $\Delta\theta \in \mathcal{X} \subseteq \mathbb{R}^m$. We are interested in propagating the set $\mathcal{X}$ through the system defined in (4.2) to obtain the set $\mathcal{Y}$ that contains all possible values that $\Delta\pi = [\Delta\pi_1, \ldots, \Delta\pi_N]^T$ can take. To address this problem, we build on results for unknown-but-bounded analysis in affine systems [23], which provides a

[2]Recall that the group inverse of Λ is denoted by $\Lambda^{\#}$, and is given by the unique solution of i) $\Lambda\Lambda^{\#}\Lambda = \Lambda$, ii) $\Lambda^{\#}\Lambda\Lambda^{\#} = \Lambda^{\#}$, and iii) $\Lambda\Lambda^{\#} = \Lambda^{\#}\Lambda$, if and only if $\text{rank}(\Lambda) = \text{rank}(\Lambda^2)$, which is a condition that always holds for generator matrices of ergodic Markov chains [49].

straightforward solution to the problem when (4.2) is truncated after the first-order term. A major contribution of our work is to extend these results and include the effect of unknown-but-bounded input uncertainty in second-order polynomial systems; i.e., we address the case where (4.2) is not truncated. This is relevant, since we cannot guarantee linear (or almost linear) behavior of $\pi(\theta)$ with variations of θ around the nominal value $\bar{\theta}$. As demonstrated in the case studies, second-order approximations are far more accurate.

4.3 First-Order Approximation

Consider (4.2) truncated after the first-order term

$$\pi(\theta) = \pi(\bar{\theta}) + \Delta\pi \approx \pi(\bar{\theta}) + J\Delta\theta, \tag{4.8}$$

where $\pi(\theta) = [\pi_1(\theta), \ldots, \pi_N(\theta)]^T$ (note that the first entry of the stationary distribution is omitted, but we persist with the same notation), and $J = \left[\frac{\partial \pi_i(\bar{\theta})}{\partial \theta_j}\right] \in \mathbb{R}^{N\times m}$ is the Jacobian matrix of $\pi(\theta)$ excluding $\pi_0(\theta)$. Given the uncertainty in the values that θ can take, we are interested in determining the values that π can take, i.e., we wish to characterize the set $\mathcal{Y}$ such that $\Delta\pi = [\Delta\pi_1, \ldots, \Delta\pi_N]^T = \pi - \bar{\pi} \in \mathcal{Y} \subseteq \mathbb{R}^N$.

Assume that each entry in $\Delta\theta = [\Delta\theta_1, \Delta\theta_2, \ldots, \Delta\theta_m]^T$ is constrained to a symmetric interval (around 0), which implies that the set $\mathcal{X}$ which contains all possible values of $\Delta\theta$ is a parallelotope. A parallelotope can be tightly bound by the intersection of a family of ellipsoids that satisfy some criteria, e.g., minimum volume or tightness along a given direction in the input space [54]. In this work, we bound the uncertain parameters by a single minimum-volume ellipsoid $\mathcal{E}$ as follows:

$$\Delta\theta \in \mathcal{X} \subseteq \mathcal{E} = \left\{\Delta\theta : \Delta\theta^T \Psi^{-1} \Delta\theta \leq 1\right\}, \tag{4.9}$$

where Ψ is a positive definite matrix that determines the shape of $\mathcal{E}$. In particular, the eigenvectors of Ψ determine the orientation of $\mathcal{E}$, while the eigenvalues of Ψ determine the lengths of the semimajor axes of $\mathcal{E}$ in the direction of the corresponding eigenvectors [23]. The volume of the ellipsoid is proportional to $(\det \Psi)^{1/2}$; therefore,

Ψ can be determined by solving the following optimization program [55]:

$$\begin{aligned} \min \quad & (\det \Psi)^{1/2} \\ \text{s.t.} \quad & v^T \Psi^{-1} v \leq 1, \, \forall v \in \mathcal{V}, \end{aligned} \tag{4.10}$$

where $\mathcal{V}$ is the set of vertices that define $\mathcal{X}$. The program in (4.10) can be efficiently solved using convex optimization techniques [55].

Define $\mathcal{F}$ as the set that bounds $\Delta\pi = J\Delta\theta$ resulting from variations in $\Delta\theta$ as described in (4.9), i.e., $\Delta\pi \in \mathcal{Y} \subseteq \mathcal{F}$. Then, it follows that $\mathcal{F}$ is an ellipsoid (see e.g., [23]) described by

$$\mathcal{F} = \left\{ \Delta\pi : \Delta\pi^T \Gamma^{-1} \Delta\pi \leq 1 \right\}, \tag{4.11}$$

where the shape matrix Γ is given by

$$\Gamma = J \Psi J^T. \tag{4.12}$$

4.4 Second-Order Approximation

Here, we extend the ideas presented in Section 4.3 to the second-order Taylor-series approximation in (4.2). As before, the set $\mathcal{X}$ that contains all possible values that $\Delta\theta$ can take is bounded by a minimum-volume ellipsoid $\mathcal{E}$ as described in (4.9). Following the method in Section 4.3, the linear component of (4.2), i.e., $J\Delta\theta$, is bounded by the ellipsoid $\mathcal{F}$ defined in (4.11). We handle the second-order term, i.e., $\frac{1}{2}\Delta\theta^T \nabla^2 \pi_i(\bar{\theta}) \Delta\theta$, as follows. First, for each i, we solve[3]

$$\begin{aligned} \Delta\pi_i^{min} \quad = \quad & \min \quad \frac{1}{2}\Delta\theta^T \nabla^2 \pi_i(\bar{\theta}) \Delta\theta \\ & \text{s.t.} \quad \Delta\theta \in \mathcal{X}, \end{aligned} \tag{4.13}$$

$$\begin{aligned} \Delta\pi_i^{max} \quad = \quad & \max \quad \frac{1}{2}\Delta\theta^T \nabla^2 \pi_i(\bar{\theta}) \Delta\theta \\ & \text{s.t.} \quad \Delta\theta \in \mathcal{X}. \end{aligned} \tag{4.14}$$

[3] If the Hessian is negative (positive) definite—a condition that can be checked a priori—we only need to solve (4.13) ((4.14)).

Since we are interested in a worst-case bound, we can guarantee that

$$\frac{1}{2}\Delta\theta^T\nabla^2\pi_i(\bar{\theta})\Delta\theta \in \mathcal{S}_i, \tag{4.15}$$

where $\mathcal{S}_i = [-s_i,\, s_i]$, and $s_i = \max\left\{|\Delta\pi_i^{max}|\,,\, \left|\Delta\pi_i^{min}\right|\right\}$. Repeating this procedure for $i = 1, 2, \ldots, N$, we obtain a set $\mathcal{S} = \mathcal{S}_1 \times \mathcal{S}_2 \times \cdots \times \mathcal{S}_N \subseteq \mathbb{R}^N$ that bounds the second-order term. Then, we can obtain a minimum-volume ellipsoid $\mathcal{G}$ that contains $\mathcal{S}$. The set $\mathcal{Y} \in \mathbb{R}^N$ (which contains $\Delta\pi$) can be upper-bounded by the Minkowski sum of the ellipsoids $\mathcal{F}$ and $\mathcal{G}$, i.e., $\mathcal{Y} \subseteq \mathcal{F} \oplus \mathcal{G}$. In general, $\mathcal{F} \oplus \mathcal{G}$ is not an ellipsoid, but we can obtain a family of ellipsoids $\mathcal{H}_\gamma = \left\{\Delta\pi : \Delta\pi^T\Phi_\gamma^{-1}\Delta\pi \leq 1\right\}$ that upper bounds $\mathcal{F} \oplus \mathcal{G}$ by choosing

$$\Phi_\gamma = (1-\gamma)^{-1}\Sigma + \gamma^{-1}\Gamma, \quad 0 < \gamma < 1, \tag{4.16}$$

which ensures that $\mathcal{Y} \subseteq \mathcal{F} \oplus \mathcal{G} \subseteq \bigcap \mathcal{H}_\gamma$. The result in (4.16) follows from a special type of Holder's inequality as discussed in [23]. Figure 4.2 illustrates the concepts introduced so far: a single ellipsoid $\mathcal{H}_\gamma$ bounding $\mathcal{Y}$ is depicted in the figure, whereas a family of ellipsoids bounding $\mathcal{Y}$ (note that $\mathcal{Y}$ is not depicted in the figure) may be obtained by varying γ between 0 and 1. The intersection of the ellipsoids in this family would yield a tighter upper bound to the set $\mathcal{Y}$.

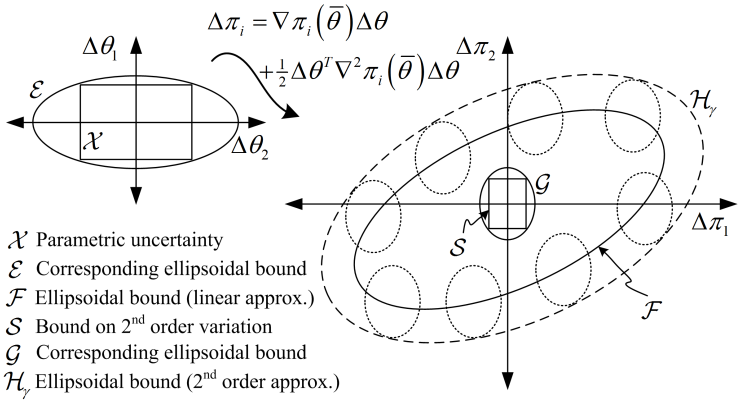

Figure 4.2: Ellipsoidal bounds for the Markov chain stationary distribution.

We now illustrate the ideas presented in Sections 4.3 and 4.4 with two simple numerical examples. The first example examines a second-order system (for which the Taylor-series expression is exact), and therefore the method proposed in Section 4.4 provides an upper bound on all possible values that the output can take. The second

example investigates a third-order system, in which case a second-order Taylor-series expansion is an approximation. Therefore, while the method outlined in Section 4.4 improves the linear approximation, the intersection of the $\mathcal{H}_\gamma$'s does not provide, in general, an upper bound for all possible output variations. Note that the examples *do not correspond* to the stationary distribution of actual Markov chains, but are constructed primarily to illustrate the notation and the concepts introduced so far.

Example 4

Consider the second-order system

$$\begin{cases} \pi_1(\theta_1,\, \theta_2) = 2\theta_1^2 + 3\theta_1\theta_2 + \theta_2^2, \\ \pi_2(\theta_1,\, \theta_2) = \theta_1 + \theta_2 - 9\theta_1^2 - 9\theta_2^2. \end{cases} \tag{4.17}$$

Suppose the nominal parameter values are given by $\bar{\theta} = [\bar{\theta}_1,\, \bar{\theta}_2]^T = [1,\, 1]^T$; then from (4.17), it follows that $\bar{\pi} = [\bar{\pi}_1,\, \bar{\pi}_2]^T = [6,\, -16]^T$. The gradients $\nabla\pi_1(\bar{\theta})$ and $\nabla\pi_2(\bar{\theta})$ are given by

$$\begin{cases} \nabla\pi_1(\bar{\theta}) = [4\bar{\theta}_1 + 3\bar{\theta}_2,\, 3\bar{\theta}_1 + 2\bar{\theta}_2] = [7,\, 5], \\ \nabla\pi_2(\bar{\theta}) = [1 - 18\bar{\theta}_1,\, 1 - 18\bar{\theta}_2] = [-17,\, -17], \end{cases} \tag{4.18}$$

and $\nabla^2\pi_1(\bar{\theta})$ and $\nabla^2\pi_2(\bar{\theta})$ are given by

$$\nabla^2\pi_1(\bar{\theta}) = \begin{bmatrix} 4 & 3 \\ 3 & 2 \end{bmatrix},\ \nabla^2\pi_2(\bar{\theta}) = \begin{bmatrix} -18 & 0 \\ 0 & -18 \end{bmatrix}. \tag{4.19}$$

Suppose $\theta_1 \in [0.1,\, 1.9]$ and $\theta_2 \in [0.1,\, 1.9]$, i.e., the parameters θ_1 and θ_2 vary by up to 90% around their nominal values, which implies that $\Delta\theta_1 \in [-0.9,\, 0.9]$ and $\Delta\theta_2 \in [-0.9,\, 0.9]$. The set $\mathcal{X}$ is depicted in Fig. 4.3a, where we can see that it is tightly bounded by the minimum volume ellipsoid $\mathcal{E}$, also depicted in Fig. 4.3a. Corresponding to $\mathcal{E}$, and assuming a linear approximation as in Section 4.3, we obtain the bounding ellipsoid $\mathcal{F}$ with shape matrix $\Gamma = J\Psi J^T$, where $J = [\nabla\pi_1(\bar{\theta}),\, \nabla\pi_2(\bar{\theta})]^T$ is the Jacobian matrix, the entries of which are given in (4.18). Figure 4.3b depicts $\mathcal{F}$ which captures uncertainty up to first order. In the figure, we also plot a cloud of points that results from solving (4.17) for all possible values of θ_1 and θ_2. As expected, since the system is second order, this bound fails to capture all possible values that $\Delta\pi$ can take. To improve the linear bound, we follow the

procedure in Section 4.4 to determine an ellipsoidal bound for the second-order term. First, the solution to (4.13)-(4.14) yields the sets $\mathcal{S}_1$ and $\mathcal{S}_2$, and a corresponding minimum-volume ellipsoidal bound $\mathcal{G}$, all illustrated in Fig. 4.3c. Finally, we obtain the ellipsoids $\mathcal{H}_\gamma$, with shape matrices Φ_γ computed from (4.16), for a set of values γ chosen in the interval (0, 1). These are plotted in Fig. 4.3d, superimposed on the exact values that $\pi(\theta)$ can take, obtained by exhaustively taking samples from the set $\mathcal{X}$. Since the function is second order, the Taylor-series characterization is exact. Therefore, each $\mathcal{H}_\gamma$ captures the entire range of values that $\pi(\theta)$ can take. An intersection of the $\mathcal{H}_\gamma$'s provides a tighter bound.

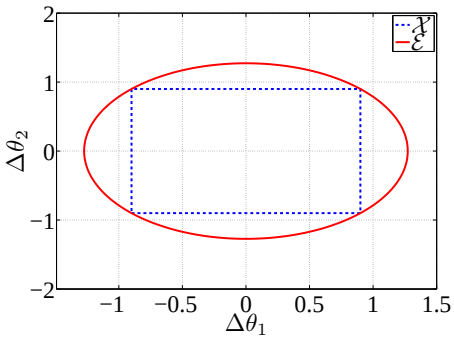

(a) Set that describes parametric uncertainty $\mathcal{X}$, and corresponding minimum-volume ellipsoidal bound $\mathcal{E}$.

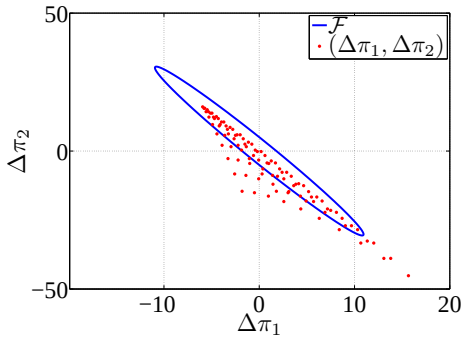

(b) Exact solution to output uncertainty and ellipsoidal bound obtained from linear approximation.

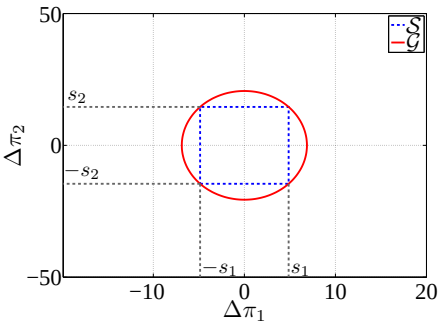

(c) Set that describes second-order uncertainty $\mathcal{S}$, and corresponding minimum-volume ellipsoidal bound $\mathcal{G}$.

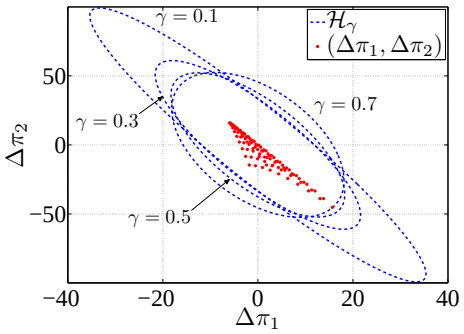

(d) Exact solution to output uncertainty and ellipsoidal bounds that capture second-order variations for different values of γ.

Figure 4.3: Results for second-order system studied in Example 4.

Example 5

Consider the following third-order system:

$$\begin{cases} \pi_1(\theta_1,\, \theta_2) = 2\theta_1 + \theta_2^2 + \theta_1\theta_2, \\ \pi_2(\theta_1,\, \theta_2) = \theta_1^2 + \theta_2^3. \end{cases} \tag{4.20}$$

Suppose θ_1 and θ_2 vary by up to 90% around their nominal values, $\bar{\theta}_1 = 1$, $\bar{\theta}_2 = 1$. Figure 4.4a plots a cloud of points obtained by solving (4.20) for all possible values of θ_1 and θ_2, as well as the linear bound $\mathcal{F}$. As expected, this bound does not capture all possible values that $\pi(\theta)$ can take, since the system is of third order. To improve the linear bound, we determine the ellipsoids $\mathcal{H}_\gamma$ for a set of values γ chosen from the range $(0,\, 1)$. These are plotted and superimposed in Fig. 4.4b. Since the system is of third order, we see that the intersection of the $\mathcal{H}_\gamma$'s—while significantly better than the first-order bound—fails to capture all possible values of $\pi(\theta)$; in particular, there is a single point (emphasized for clarity in Fig. 4.4b) that lies outside the intersection of the $\mathcal{H}_\gamma$'s. This example demonstrates that the validity of the proposed approach is contingent on how closely a second-order Taylor-series expansion approximates the original function.

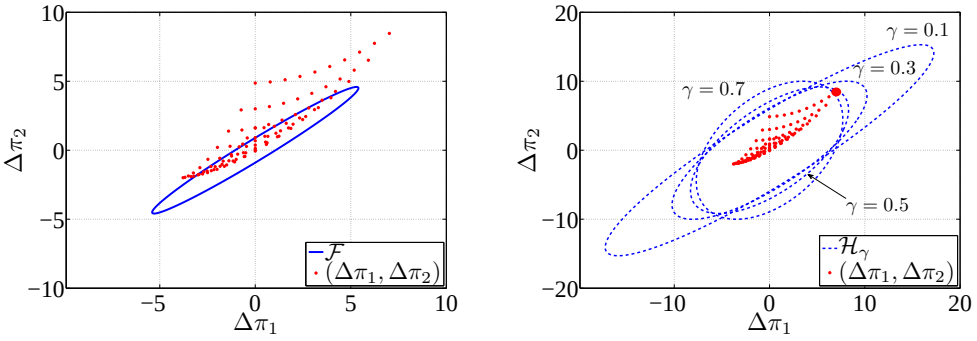

(a) Exact solution and ellipsoidal bound obtained from linear approximation.

(b) Exact solution and ellipsoidal bounds that capture second-order variations.

Figure 4.4: Results for third-order system studied in Example 5.

4.5 Case Studies Covering Common Reliability Models

In this section, we examine the impact of parametric uncertainty in two reliability models. In both case studies, we compare the results obtained using the ellipsoidal-

shaped sets with repeated simulations. The repeated simulations are performed as follows. We first create vectors with evenly spaced values for each parameter θ_j (about the nominal values $\bar{\theta}_j$) $\forall\ j = 1, \ldots, m$. The set $\{\bar{\theta}\} \oplus \mathcal{X}$, where $\bar{\theta} = [\bar{\theta}_1, \ldots, \bar{\theta}_m]$, describes the Cartesian product of all the θ_j's. For each $\hat{\theta} \in \{\bar{\theta}\} \oplus \mathcal{X}$, we obtain the corresponding generator matrix $\Lambda(\hat{\theta})$ by substituting the corresponding values of the parameters. Then, through a QR factorization of $\Lambda(\hat{\theta})$, we obtain the stationary distribution of the chain $\pi(\hat{\theta})$ without having to solve the Chapman-Kolmogorov equations (for the specific $\Lambda(\hat{\theta})$ as $t \to \infty$). This is repeated for all elements in $\{\bar{\theta}\} \oplus \mathcal{X}$. For large number of parameters m, or as the number of values in each θ_j is increased (to increase the accuracy of the results), this process can get computationally expensive as demonstrated in the second case study.

4.5.1 Two Components with Shared Load

This example, adapted from [46], explores the Markov reliability model for a system of two identical components that share a common load. The failure and repair rates of the components are denoted by λ and μ, respectively. The probabilistic counterpart of this model was studied in Section 3.5.2. Additionally, the system is susceptible to common-cause failures which cause both components to fail at a rate λ_C. The state-transition diagram of the Markov chain describing the availability of this system is depicted in Fig. 4.5. Both components are operational in state 2, a single component is operational in state 1, and in state 0, both components have failed. Repairs restore the operation of one component at a time. From the

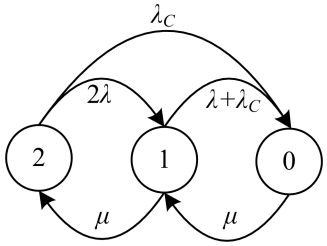

Figure 4.5: System of two identical components with shared load and common-cause failures.

state-transition diagram, the Markov chain generator matrix can be derived as

$$\Lambda = \begin{bmatrix} -\mu & \mu & 0 \\ \lambda + \lambda_C & -(\lambda + \lambda_C + \mu) & \mu \\ \lambda_C & 2\lambda & -(2\lambda + \lambda_C) \end{bmatrix}. \tag{4.21}$$

Solving (2.5) with Λ given in (4.21), it can be shown that [46]

$$\pi_0 = \frac{(\lambda + \lambda_C)(2\lambda + \lambda_C) + \lambda_C \mu}{(\lambda + \lambda_C + \mu)(2\lambda + \lambda_C) + \lambda_C \mu + \mu^2}, \tag{4.22}$$

$$\pi_1 = \frac{(2\lambda + \lambda_C)\mu}{(\lambda + \lambda_C + \mu)(2\lambda + \lambda_C) + \lambda_C \mu + \mu^2}, \tag{4.23}$$

$$\pi_2 = \frac{\mu^2}{(\lambda + \lambda_C + \mu)(2\lambda + \lambda_C) + \lambda_C \mu + \mu^2}. \tag{4.24}$$

This illustrates a major advantage of our proposed framework in that closed-form expressions of the sort in (4.22)-(4.24)—which are difficult to obtain in general—are not required a priori. Additionally, even if the expressions are available, given the information that the parameters λ, μ, and λ_c belong to some set, it is difficult to compute bounds on the stationary distribution without repeatedly solving (2.5) for all possible parameter values in the set.

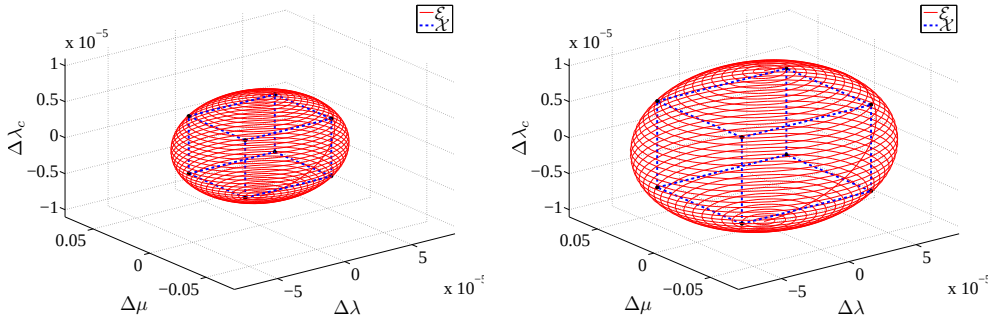

Figure 4.6: Ellipsoidal upper bounds to parameters with (a) 20% and (b) 30% uncertainty.

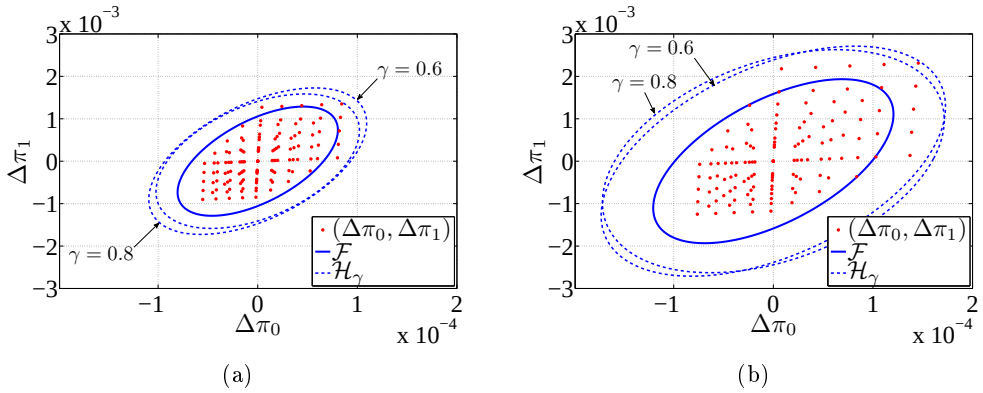

Figure 4.7: Linear- and second-order ellipsoidal bounds to stationary distribution assuming (a) 20% and (b) 30% uncertainty.

The nominal values of the failure rate, repair rate, and common-cause failure rate are given by: $\bar{\lambda} = 1.6 \times 10^{-4}$ hr^{-1}, $\bar{\mu} = 1.25 \times 10^{-1}$ hr^{-1}, and $\bar{\lambda}_c = 2 \times 10^{-5}$ hr^{-1}, respectively [46]. The nominal steady-state probabilities are given by $\bar{\pi}_0 = 1.63 \times 10^{-4}$, $\bar{\pi}_1 = 0.0027$, and $\bar{\pi}_2 = 0.9971$. Let $\theta_1 = \lambda$, $\theta_2 = \mu$, $\theta_3 = \lambda_c$, and consider that each parameter $\theta_i \in [\bar{\theta}_i - \frac{p}{100} \cdot \bar{\theta}_i, \bar{\theta}_i + \frac{p}{100} \cdot \bar{\theta}_i]$, $i = 1, 2, 3$, where $\bar{\theta}_i$ is the nominal value of the i parameter, and p describes the % variation in the value that the i parameter θ_i can take. Figures 4.6a and 4.6b depict the sets $\mathcal{X}$ and corresponding upper-bounding minimum-volume ellipsoids $\mathcal{E}$ that the parameters are constrained to, assuming uncertainty $p = 20\%$ and $p = 30\%$, respectively. Figures 4.7a and 4.7b depict linear and second-order ellipsoidal bounds ($\mathcal{F}$ and $\mathcal{H}_\gamma$, respectively) on the uncertainty in the steady-state probabilities. In both cases, we see that a linear approximation is insufficient. The intersection of the $\mathcal{H}_\gamma$'s accurately captures all possible variations for 20% uncertainty in the parameters. For 30% uncertainty, there is a single point that lies outside the intersection of the $\mathcal{H}_\gamma$'s.

Now, suppose that the performance of the system depends on the number of operational components. Define a reward model by choosing $\rho = [\rho_0, \rho_1, \rho_2]^T = [0, 1, 2]^T$. The long-term reward is then given by $\xi = \pi^T \rho = \pi_1 + 2\pi_2$. Since the parameters are uncertain, we can obtain bounds on ξ by simply projecting the ellipsoidal bounds for the stationary distribution onto the direction defined by ρ. Figure 4.8 depicts upper and lower bounds to the values that ξ can take as a function of the level of uncertainty p. Results from repeatedly solving (2.5)-(2.7) for all possible parameter values are superimposed. Notice that the ellipsoidal bounds accurately capture the impact of uncertainty on the values that ξ can take.

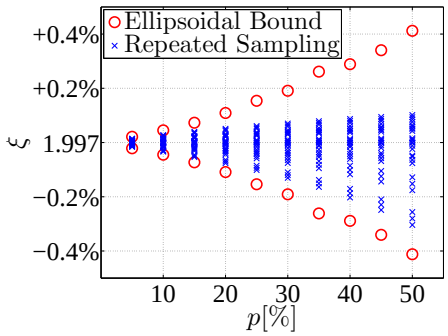

Figure 4.8: Uncertainty in reward as a function of parametric uncertainty.

4.5.2 Preventative Transformer Maintenance

This example examines the preventative maintenance of an electric-power distribution transformer (see [56] and the references therein for a detailed description of this model). Note that similar models have been used to study the impact of preventative maintenance in operational software systems [57]. The state-transition diagram that describes the Markov reliability model is depicted in Fig. 4.9. The transformer has an ideal operating state denoted by D_1, and two deteriorated states, denoted by D_2 and D_3, respectively. Denote the rate at which complete failure due to deterioration is expected by λ_1, which implies that transitions between the deterioration states occur at the rate $3\lambda_1$. Transformer failure due to deterioration is denoted by state F_1. Once in this state, repair at the rate μ_1 restores the transformer to the ideal operating state. Apart from gradual deterioration, a transition to a catastrophic failure state, denoted by F_0, at the rate λ_0 is possible from any of the deteriorated states. From this state, repair restores operation at a rate μ_0. Preventative maintenance can be performed on the transformer when it is in states D_i, $i = 1, 2, 3$. Preventative maintenance in state D_i $(i > 1)$ restores operation to state D_{i-1} after passing through the maintenance state M_i. Preventative maintenance is performed at a rate λ_m and the time required for maintenance is captured by μ_m.

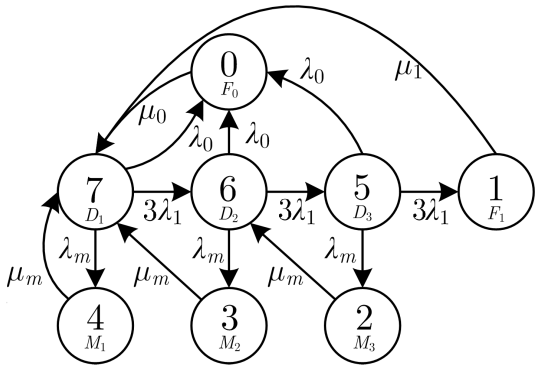

Figure 4.9: Reliability model for transformer with deterioration and preventative maintenance.

The availability of the transformer, $\xi = \pi_7 + \pi_6 + \pi_5$, i.e., the sum of the steady-state probabilities in states D_1, D_2, and D_3. Note that the availability is given by $\xi = \pi^T \rho$, where π is the stationary distribution and the reward vector $\rho = [0, 0, 0, 0, 0, 1, 1, 1]^T$. The problem of interest is to determine the optimal preventative maintenance rate λ_m, that maximizes the availability while taking into account the effect of parametric uncertainty. We show that the proposed method to uncertainty analysis can provide further insight into the problem.

The nominal parameter values are given by: $\bar{\lambda}_1 = 1/1000\,\text{days}^{-1}$, $\bar{\mu}_1 = 1/14\,\text{days}^{-1}$, $\bar{\mu}_m = 1/0.5\,\text{days}^{-1}$, $\bar{\lambda}_0 = 1/500\,\text{days}^{-1}$, and $\bar{\mu}_0 = 1/7\,\text{days}^{-1}$. Suppose the parameters λ_1, μ_1, and μ_m are unknown but bounded around their nominal values. Assuming 10% uncertainty around the nominal values, Fig. 4.10 depicts the set $\mathcal{X}$ (and corresponding upper-bounding minimum-volume ellipsoid $\mathcal{E}$) that contains all values that the parameters can take. Following the methods outlined in Section 4.4, we determine bounds on the stationary distribution. Figure 4.11 depicts linear and second-order ellipsoidal bounds ($\mathcal{F}$ and $\mathcal{H}_\gamma$, respectively) on the values that the steady-state probabilities can take (without loss of generality, we just depict variability in π_7, π_6, and π_0). The exact solution—determined by repeated simulation—is superimposed on the ellipsoidal bounds. We see that a linear approximation is insufficient, and the second-order approximation provides a better (albeit conservative) bound. For 10% uncertainty around the nominal parameter values, Fig. 4.12 plots the availability of the transformer as a function of λ_m. From this figure, we see that a maintenance rate in the order of 0.005 days^{-1} maximizes the transformer availability. Notice that the second-order bound is more conservative, and in general lower

bounds are more accurate than upper bounds.

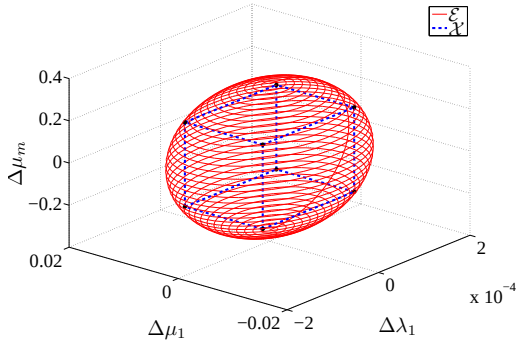

Figure 4.10: Ellipsoidal upper bound to parameters with 10% uncertainty.

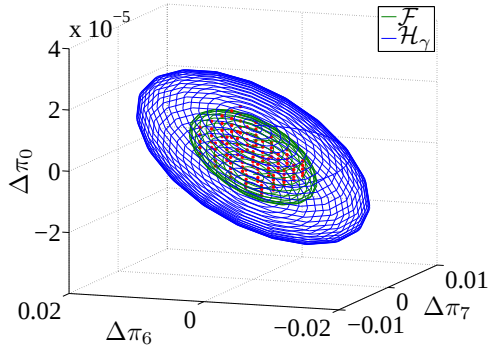

Figure 4.11: Ellipsoidal bounds to stationary distribution.

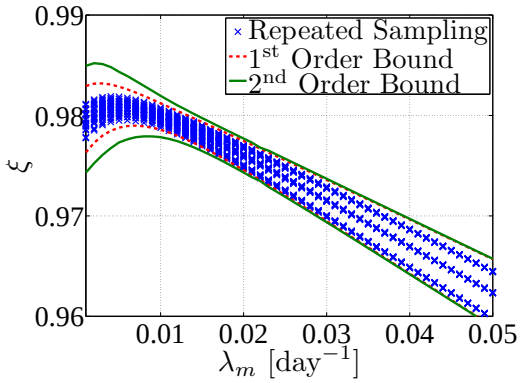

Figure 4.12: Transformer availability as a function of preventative maintenance rate assuming 10% parametric uncertainty.

Now, consider the state-transition diagram depicted in Fig. 4.9, except with an arbitrary number of deterioration states. We compare the execution time of the proposed method with the execution time involved in obtaining the solution by running repeated simulations as the model order is increased (i.e., as the number of deterioration states is increased). We utilize a first-order Taylor series expansion for this experiment because the programs in (4.13)-(4.14) are not optimized for execution time (this is grounds for future work). Consider that all parameters λ_m, μ_m, λ_1, μ_1, λ_0, μ_0 are uncertain up to 5% around their nominal values. To perform the repeated simulations, for each parameter we sample the nominal value and

two extreme values. The experiment is performed on a PC with a 2.66 GHz Intel Core^{TM}2 Quad CPU processor with 4 GB memory in the MATLAB environment. The execution time as a function of the number of deterioration states for the two methods is plotted in Fig. 4.14. Figure 4.13 superimposes the bounds obtained with the ellipsoidal method on the results of the repeated simulations. The results indicate that for large models (as the number of states is increased beyond 60 in this case), the proposed method has lower execution time compared to exhaustive simulation of all possible parameter values.

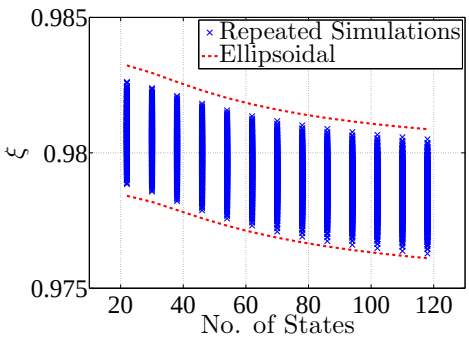

Figure 4.13: Ellipsoidal bounds and results from exhaustive simulations as a function of model order.

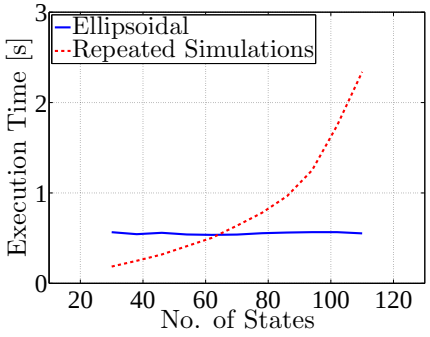

Figure 4.14: Execution time for the ellipsoidal method compared to exhaustive simulations as a function of model order.

Chapter 5

STOCHASTIC HYBRID SYSTEMS FRAMEWORK FOR REWARD MODELING

In this chapter, we propose a stochastic hybrid systems (SHS) formalism to tackle a wide class of reward models that describe system reliability/performability. Our discussion of the mathematical preliminaries is limited to fundamental mathematical concepts and definitions, and interested readers are referred to [30–32, 47, 48] for a detailed account. The main contribution of this chapter is to formulate the SHS framework for performability modeling (previous applications have included other domains). In doing so, we provide a modeling formalism for system reliability theory that extends traditional notions such as availability to factor in relevant aspects of system performance. In this chapter we present case studies covering common reliability problems. The framework in this chapter is then applied to study the impact of stochastic disturbances on power system dynamics in Chapter 8. The material presented here is partially adopted from [58].

5.1 Preliminaries

In the most general sense, an SHS is a combination of a continuous-time, discrete-state stochastic process $Q(t) \in \mathcal{Q}$, coupled with a continuous-time, continuous-state stochastic process $X(t) \in \mathbb{R}^d$. Additionally, we assume that this system is fully coupled, in the sense that the evolution of the continuous state depends on the discrete state, and the transitions among the discrete states depend on the continuous state. System reliability/performability is described by a reward which we denote by $Y(t)$, $Y : \mathbb{R}^+ \to \mathbb{R}$. In the forthcoming discussion, we will demonstrate how the reward is derived from the continuous state $X(t)$.

We provide an intuitive description of SHS next. Towards this end, consider the functions

$$\lambda_j \colon \mathcal{Q} \times \mathbb{R}^d \to \mathbb{R}^+, \quad \phi_j \colon \mathcal{Q} \times \mathbb{R}^d \to \mathcal{Q} \times \mathbb{R}^d, \quad j \in \mathcal{J} \tag{5.1}$$

which we call the *transition rates* and *transition reset maps* (interchangeably referred as *reset maps*, subsequently). The idea of these functions is that at any time, the system undergoes transition j with rate λ_j, and if it undergoes this transition, then it instantaneously applies the map ϕ_j to the current discrete and continuous states and discontinuously changes their values at that moment. More specifically, for any time $t > 0$, we say that the probability of transition j occurring in the time domain $[t, t+\Delta t)$ is $\lambda_j(Q(t), X(t))\Delta t + o(\Delta t)$, and if it does occur, then we define $(Q(t+\Delta t), X(t+\Delta t)) = \phi_j(Q((t+\Delta t)^-), X((t+\Delta t)^-))$, thus obtaining a new mode and state.[1] From this, we see that the probability of no transition occurring in $[t, t+\Delta t)$ is $1 - \Delta t \sum_{j\in\mathcal{J}} \lambda_j(q, x)$. Finally, between transitions, we prescribe that $X(t), Y(t)$ evolve according to the SDE

$$\begin{aligned} dX(t) &= f(Q(t),\, X(t),\, t)\, dt + g(Q(t),\, X(t),\, t)\, dW_t, \\ Y(t) &= h(Q(t),\, X(t),\, t), \end{aligned} \tag{5.2}$$

where $W_t : \mathbb{R}^+ \to \mathbb{R}^l$ is the l-dimensional Wiener process, $f : \mathcal{Q} \times \mathbb{R}^d \times \mathbb{R}^+ \to \mathbb{R}^d$, $g : \mathcal{Q} \times \mathbb{R}^d \times \mathbb{R}^+ \to \mathbb{R}^{d\times l}$, and $h : \mathcal{Q} \times \mathbb{R}^d \times \mathbb{R}^+ \to \mathbb{R}$.

This combination of the discrete and continuous processes $(Q(t),\, X(t))$ is commonly referred to as a SHS [31]. For the class of SHS studied in [31], the vector fields that govern the evolution of the continuous state (f, g, and h), the reset maps (ϕ_j), and the transition rates (λ_j), are required to be polynomial functions of the continuous state. In this case, as illustrated in Section 5.7, the evolution of the moments of the continuous state in such a system is governed by an infinite-dimensional system of ODEs, and moment closure methods have to be applied to obtain truncated state-space descriptions [32]. For the class of reward models we explore here, the vector fields that govern the evolution of the continuous state and the reset maps are linear, and, moreover, the transition rates are not assumed to be functions of the continuous state. As we show below, this implies that the differential equations that govern the evolution of the conditional moments in these models are finite dimensional and moment-closure methods are unnecessary.

The SHS formalism outlined above provides a unified and generalized modeling framework to tackle a wide variety of reward models (above and beyond the Markov reward models developed in Chapter 2). As discussed in the introduction, since this work presents the first application of SHS to system performability modeling, we

[1] We use the notation $a(t^-) = \lim_{s \nearrow t} a(s)$ to denote the left-hand limit of the function a.

restrict our attention to Markov reward models. We illustrate next how these are derived from the general setting described above.

5.2 Markov Reward Models defined as SHS

In the case studies and examples that follow, we explore a reward framework that is a special case of the SHS model described above, where we assume that: i) the SDEs describing the fixed-mode evolution are linear (or, more precisely, affine) in the state $X(t)$, ii) the transition rates governing the jumps among modes are independent of $X(t)$, and iii) the reward is a linear function of the state. More precisely, we assume that the SDE governing $X(t)$ is given by

$$\begin{aligned} dX(t) &= A(Q(t),\, t)\, X(t)dt + B(Q(t),\, t)dt + C(Q(t),\, t)\, dW_t, \\ Y(t) &= R(Q(t),\, t)\, X(t), \end{aligned} \tag{5.3}$$

where $W_t : \mathbb{R}^+ \to \mathbb{R}^l$ is the l-dimensional Wiener process, $A : \mathcal{Q} \times \mathbb{R}^+ \to \mathbb{R}^{d\times d}$, $B : \mathcal{Q} \times \mathbb{R}^+ \to \mathbb{R}^d$, $C : \mathcal{Q} \times \mathbb{R}^+ \to \mathbb{R}^{d\times l}$, and $R : \mathcal{Q} \times \mathbb{R}^+ \to \mathbb{R}^{1\times d}$.

We first note that under these assumptions, the discrete process $Q(t)$ is a CTMC—in particular, one can understand the pathwise evolution of $Q(t)$ without knowing $X(t), Y(t)$. Note that if we further assume that the transition rates are not a function of time, i.e., if $\lambda_j \colon \mathcal{Q} \to \mathbb{R}^+$, the Markov chain is homogeneous. In the context of this work, the CTMC $Q(t)$ describes the Markov reliability model, while $(Q(t),\, X(t),\, Y(t))$ describes the Markov reward model.

It should be noted that rate reward, first-order reward, and second-order reward models are all subsumed in this framework. In fact, to realize rate reward models, we choose $A = C = 0$ in (5.3); to realize first-order reward models, we choose $C = 0$ in (5.3). Expressed as such, (5.3) describes a second-order reward model; this is the most general model we explore in this work.

The results presented in [32] for SHS apply directly to the Markov reward models examined in this work. Of particular interest is the method to obtain the moments of the state (from which we can recover the accumulated-reward moments). As described subsequently in Section 5.3, this method is based on defining appropriate test functions and formulating the extended generator for the underlying stochastic processes. We end this section by illustrating the notation introduced so far with a simple example. We will revert to this example in Section 5.4 to demonstrate how

the moments of the accumulated reward are obtained from appropriately defined test functions.

Example 6

Consider a Markov reliability model described by a CTMC $Q(t)$, taking values in the set $\mathcal{Q} = \{0, 1\}$.[2] We give a schematic depiction of this model in Fig. 5.1. Associated with this Markov chain, we consider a first-order reward model. To this end, define$X(t) = [X_1(t), X_2(t), \ldots, X_d(t)]^T$, which evolves according to

$$\frac{dX(t)}{dt} = A(Q(t))X(t) =: A_{Q(t)}X(t), \tag{5.4}$$

where we denote $A_{Q(t)} = A_0 \in \mathbb{R}^{d\times d}$ if $Q(t) = 0$, and $A_{Q(t)} = A_1 \in \mathbb{R}^{d\times d}$ if $Q(t) = 1$. The accumulated reward $Y(t)$ is given by $Y(t) = R(Q(t))X(t) =: R_{Q(t)}X(t)$, where

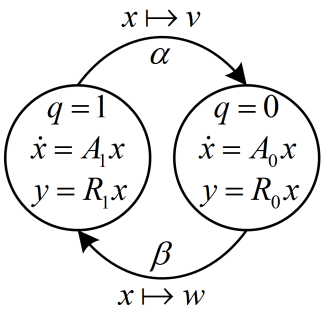

Figure 5.1: First-order reward model studied in Example 6.

$R_{Q(t)} = R_0 \in \mathbb{R}^{1\times d}$ if $Q(t) = 0$, and $R_{Q(t)} = R_1 \in \mathbb{R}^{1\times d}$ if $Q(t) = 1$. Now choose two numbers $\alpha, \beta \in \mathbb{R}^+$ and two vectors $v, w \in \mathbb{R}^d$; basically, α, v will govern the transitions from state $1 \to 0$, so that we transition from mode 1 to mode 0 with rate α, and when we do so, we reset the value of $X(t)$ to v, and similarly for β, w in the other direction. Following the notation introduced in Section 5.1, it is clear that we have two transitions ($\mathcal{J} = \{0, 1\}$), with transition rates[3]

$$\lambda_0(q, x) = \delta_{q,1}\alpha, \quad \lambda_1(q, x) = \delta_{q,0}\beta \tag{5.5}$$

[2]This example reverts to the two-state model examined in Examples 1, 2, and 3. The added flexibility afforded by the SHS modeling framework allows us to consider dynamic rewards in this case.

[3]In subsequent developments, we use the Kronecker delta notation, i.e., $\delta_{i,j} = 1$ if $i = j$, and $\delta_{i,j} = 0$ if $i \neq j$.

and reset maps

$$\phi_0(q,x) = (0, \delta_{q,1} v), \quad \phi_1(q,x) = (1, \delta_{q,0} w). \tag{5.6}$$

It turns out that there is another, more compact, way to formulate this in the SHS framework. To this end, we can say that there is exactly one transition and define the following transition rates and reset maps:

$$\lambda(q,x) = \begin{cases} \alpha, & q = 1, \\ \beta, & q = 0. \end{cases}, \quad \phi(q,x) = \begin{cases} (0,v), & q = 1, \\ (1,w), & q = 0, \end{cases} \tag{5.7}$$

which can be written more compactly using the Kronecker delta notation as

$$\lambda(q,x) = \delta_{q,1}\alpha + \delta_{q,0}\beta, \quad \phi(q,x) = (1-q, \delta_{q,1} v + \delta_{q,0} w). \tag{5.8}$$

These models are equivalent with probability one, since, if a transition has rate zero then it occurs with probability zero. We will find that both of these viewpoints are useful in different contexts.

From standard results in Markov chains, the residence (sojourn) time in each mode is exponentially distributed with the parameter given by the rate of transition out of that state. More precisely, choose $s > 0$ so that $Q(s) = 0$. Define the stopping time T by

$$T = \inf_{t>s} \{t : Q(t) = 1\}, \tag{5.9}$$

which then implies $\Pr\{T - s > t | Q(s) = 0\} = e^{-\beta t}$. A similar statement exists for the other transition. From this, for example, we can determine the probability distribution of $Q(t)$ for all $t > 0$, for how many transitions have occurred, etc., using standard results from Markov chains.

In Section 5.4, we will revisit this example and obtain ODEs that capture the evolution of the p-order uncentered moments of the accumulated reward $\mathrm{E}[Y^p(t)]$, $p \geq 1$.

5.3 Test Function and Extended Generator of SHS

For the reward model introduced in (5.3), define a *test function* $\psi(q, x, t)$, $\psi : \mathcal{Q} \times \mathbb{R}^d \times \mathbb{R}^+ \to \mathbb{R}$, where q represents the discrete state of the CTMC, and x represents the continuous state from which the accumulated reward is recovered. The

extended generator (referred interchangeably as *generator* subsequently) denoted by $(L\psi)(q, x, t)$ is the composition of the Lie derivative and the test function of the SHS, and it is given by

$$\begin{aligned}(L\psi)(q,\, x, t) \;&:=\; \frac{\partial}{\partial x}\psi(q,\, x,\, t)\cdot(A(q,\, t)x + B(q,\, t)) + \frac{\partial}{\partial t}\psi(q,\, x,\, t)\\ &+\; \frac{1}{2}\sum_{i,j}\left((CC^T)_{i,j}(q,t)\frac{\partial^2}{\partial x_i x_j}\psi(q,\, x,\, t)\right)\\ &+\; \sum_{j\in\mathcal{J}}\lambda_j(q,x,t)\left(\psi\left(\phi_j\left(q,\, x,\, t\right)\right) - \psi(q,\, x,\, t)\right), \end{aligned} \tag{5.10}$$

where $\partial\psi/\partial x \in \mathbb{R}^{1\times d}$ and $\partial^2\psi/\partial x^2 \in \mathbb{R}^{d\times d}$ denote the gradient and Hessian of $\psi(q,\, x,\, t)$ with respect to x, respectively, and the summation (in the third line) is over all transitions of the underlying CTMC [30,32]. The evolution of the expected value of the test function $\mathbb{E}\left[\psi(Q(t),\, X(t),\, t)\right]$ is governed by Dynkin's formula, which can be stated in differential form as follows [30,32]:

$$\frac{d}{dt}\mathbb{E}[\psi(Q(t),\, X(t),\, t)] = \mathbb{E}[(L\psi)(Q(t), Xx(t),\, t)]. \tag{5.11}$$

This holds for every ψ that is in the domain of the extended generator L.[4] We point out that in the current work, we will only consider those ψ that do not explicitly depend on time, and so the second term in (5.10) does not appear.

Said in words, (5.11) means that the time rate of change of the expected value of a test function evaluated on the stochastic process is given by the expected value of the generator. Intuitively, this makes sense: the first line in (5.10) captures the total derivative of the test function with respect to time, the second line captures the effect of the Wiener process, while the third term describes the impact of the reset maps (note that the second line in (5.10) is absent in rate and first-order reward models). In particular, for pure diffusions (with no jumps), the generator of the process is given by the first two lines of (5.10), and in the context of CTMCs (no continuous state), the generator of the process is the third line of (5.10).

Next, we summarize the general procedure outlined in [32] to specify a family of test functions from which the moments of the accumulated reward can be recovered by applying the results in (5.10)-(5.11).

[4]Describing the domain of this operator is, in general, technically difficult. However, it turns out that in the current framework (namely, SDEs that have affine drifts with additive noise, and state-independent transition rates) all functions polynomial in x are in the domain of L.

5.4 Recovering Differential Equations for Conditional Moments from Test Functions

For a Markov reward model where the underlying CTMC takes values in the set $\mathcal{Q} = \{0, 1, \ldots, N\}$, we define the family of test functions

$$\psi_i^m(q,\, x) := \delta_{i,q} x^m = \begin{cases} x^m & \text{if} \quad q = i \\ 0 & \text{if} \quad q \neq i \end{cases}, \forall i \in \mathcal{Q}, \tag{5.12}$$

where $m := (m_1,\, m_2, \ldots,\, m_d) \in \mathbb{N}^{1\times d}$, and $x^m := x_1^{m_1} x_2^{m_2} \ldots x_d^{m_d}$. We also define the *conditional moments* at time t, $\mu_i^m(t)$, $\forall i \in \mathcal{Q}$, by

$$\mu_i^m(t) := \mathrm{E}\left[\psi_i^m(q,\, x)\right] = \mathrm{E}\left[X^m(t) | Q(t) = i\right] \cdot \Pr\left\{Q(t) = i\right\}, \tag{5.13}$$

and for every $m \in \mathbb{N}^{1\times d}$, the *vector of conditional moments*

$$\mu^m(t) := \left[\mu_0^m(t),\, \mu_1^m(t),\, \ldots,\, \mu_N^m(t)\right]. \tag{5.14}$$

The last equality in (5.13) follows from the definition of the test functions in (5.12). By appropriately picking the m_i's, we can isolate the conditional moments of interest. We demonstrate this next, in the context of the reward model introduced in Example 6 in Section 5.2.

Example 6 (continued)

Recall the reward model introduced in Example 6 in Section 5.2. Associated with the two discrete states, define the following test functions:

$$\begin{aligned} \psi_0^{(m)}(q,\, x) &= \delta_{q,0} x^m = \begin{cases} x^m & \text{if} \quad q = 0 \\ 0 & \text{if} \quad q = 1 \end{cases}, \\ \psi_1^{(m)}(q,\, x) &= \delta_{q,1} x^m = \begin{cases} 0 & \text{if} \quad q = 0 \\ x^m & \text{if} \quad q = 1 \end{cases}, \end{aligned} \tag{5.15}$$

where $m \in \mathbb{N}^{1\times d}$ and $x^m = x_1^{m_1} x_2^{m_2} \ldots x_d^{m_d}$. As stated previously, by appropriately picking m, we can recover many conditional moments of interest. For instance,

choosing $m = (0, \ldots, 0)$ recovers the occupational probabilities of the modes,

$$\mu_i^{(0,\ldots,0)}(t) = \Pr\{Q(t) = i\} = \pi_i(t). \tag{5.16}$$

Similarly, picking $m = (2, \ldots, 0)$ isolates the second-order conditional moment of $X_1(t)$

$$\begin{aligned} \mu_i^{(2,\ldots,0)}(t) &= \mathrm{E}\left[X^{(2,\ldots,0)}(t)|Q(t) = i\right] \cdot \Pr\{Q(t) = i\} \\ &= \mathrm{E}\left[X_1^2(t)|Q(t) = i\right] \cdot \Pr\{Q(t) = i\} \end{aligned} \tag{5.17}$$

Finally, picking $m = (1, \ldots, 1)$ yields the conditional expectation of the product $\prod_{\ell=1}^{d} X_\ell(t)$

$$\begin{aligned} \mu_i^{(1,\ldots,1)}(t) &= \mathrm{E}\left[X^{(1,\ldots,1)}(t)|Q(t) = i\right] \cdot \Pr\{Q(t) = i\} \\ &= \mathrm{E}\left[\prod_{\ell=1}^{d} X_\ell(t)|Q(t) = i\right] \cdot \Pr\{Q(t) = i\}. \end{aligned} \tag{5.18}$$

5.5 Evolution of the Accumulated Reward

For a given m (which, as shown previously, can be defined to isolate the conditional moment of interest), we apply (5.10) to obtain expressions for $N+1$ extended generators, $\left(L\psi_i^{(m)}\right)(q, x)$, $i \in \mathcal{Q} = \{0, 1, \ldots, N\}$. From Dynkin's formula in (5.11), we then obtain a set of $N+1$ differential equations that govern the conditional moments

$$\frac{d}{dt}\mu_i^{(m)}(t) = \frac{d}{dt}\mathbb{E}\left[\psi_i^{(m)}(q, x)\right] = \mathbb{E}\left[\left(L\psi_i^{(m)}\right)(q, x)\right], \forall i \in \mathcal{Q} = \{0, 1, \ldots, N\}. \tag{5.19}$$

The problem of interest is to obtain the p-order moment of the accumulated reward $\mathrm{E}[Y^p(t)]$, from the conditional moments defined above. Recall that the accumulated reward is given by $Y(t) = R(Q(t), t)\, X(t) = \sum_{j=1}^{d} r_j(Q(t), t)\, X_j(t)$, which implies that $Y^p(t)$ is a polynomial function of $X_j(t)$, $j = 1, 2, \ldots, d$. In particular, applying the multinomial theorem, we can express

$$Y^p(t) = \sum_{m_1+m_2+\cdots+m_d=p} \binom{p}{m_1, m_2, \ldots, m_d} \prod_{1\le s\le d} \left(r_s(Q(t), t)\, X_s(t)\right)^{m_s}, \tag{5.20}$$

i.e., as a polynomial function of $X_j(t)$, $j = 1, 2, \ldots, d$. There is a more compact way to write the multinomial theorem that we will find useful below: given a vector of natural numbers $m = (m_1, \ldots, m_d)$, we define

$$|m| := \sum_{i=1}^{d} m_i, \quad \binom{p}{m} := \binom{p}{m_1,\, m_2, \ldots,\, m_d}. \tag{5.21}$$

Then (5.20) can be expressed as

$$Y^p(t) = \sum_{|m|=p} \binom{p}{m} (R(Q(t), t)\, X(t))^m, \tag{5.22}$$

where we use the notation

$$(R(Q(t), t)X(t))^m \quad = \quad R^m(Q(t), t)X^m(t) = \prod_{l=1}^{d} (r_l(Q(t), t)X_l(t))^{m_l}. \tag{5.23}$$

We will find (5.22) very useful since all of the powers in the right-hand side of (5.22) are less than or equal to p. Therefore, if we know all of the moments $\mu_j^{(m)}$ with $|m| \leq p$, $j \in \mathcal{Q}$, then we can obtain the p^{th} order moment of Y as follows:

$$\begin{aligned}
\mathrm{E}\left[Y^p(t)\right] &= \sum_{|m|=p} \binom{p}{m} \mathrm{E}\left[(R(Q(t), t)\, X(t))^m\right] \\
&= \sum_{|m|=p} \binom{p}{m} \sum_{i \in \mathcal{Q}} \mathrm{E}\left[(R(Q(t), t)\, X(t))^m \,|Q(t) = i\right] \Pr\{Q(t) = i\} \\
&= \sum_{|m|=p} \binom{p}{m} \sum_{i \in \mathcal{Q}} (R(i, t))^m \mathrm{E}\left[X^m(t) | Q(t) = i\right] \Pr\{Q(t) = i\} \\
&= \sum_{|m|=p} \binom{p}{m} \sum_{i \in \mathcal{Q}} (R(i, t))^m \mu_i^{(m)}(t) \\
&= \sum_{i \in \mathcal{Q}} \sum_{|m|=p} \binom{p}{m} (R(i, t))^m \mu_i^{(m)}(t).
\end{aligned} \tag{5.24}$$

Therefore, to compute $\mathrm{E}\left[Y^p(t)\right]$, all we need to know are the moments $\mu_i^{(m)}(t)$ with $i \in \mathcal{Q}$ and $|m| = p$.

Remark

As a special case, consider the Markov reward model described by the following scalar system (i.e., $d = 1$):

$$\begin{aligned} dX(t) &= (a(Q(t),\, t)\, X(t)dt + b(Q(t),\, t))\, dt + C(Q(t),\, t)\, dW_t, \\ Y(t) &= r \cdot X(t), \end{aligned} \tag{5.25}$$

where W_t is the l-dimensional Wiener process, $a : \mathcal{Q} \times \mathbb{R}^+ \to \mathbb{R}$, $b : \mathcal{Q} \times \mathbb{R}^+ \to \mathbb{R}$, $C : \mathcal{Q} \times \mathbb{R}^+ \to \mathbb{R}^{1\times l}$, and $r \in \mathbb{R}$. Using (5.24), we have that

$$\mathrm{E}\left[Y^p(t)\right] = r^p \sum_{i=0}^{N} \mu_i^{(p)}(t). \tag{5.26}$$

We now revert to Example 1 to illustrate how (5.24) applies in practice.

Example 6 (continued)

Let us again consider Example 6 in Section 5.2 but simply the case where $d = 2$. The accumulated reward is given by $Y(t) = R(Q(t))X(t) = r_1(Q(t))X_1(t) + r_2(Q(t))X_2(t)$. Suppose we are interested in computing the second-order moment of the reward, $\mathrm{E}\left[Y^2(t)\right]$. Using (5.24), we have

$$\mathrm{E}\left[Y^2(t)\right] = \sum_{i=0}^{1} \left(r_1^2(i)\mu_i^{(2,\,0)}(t) + r_2^2(i)\mu_i^{(0,\,2)}(t) + 2r_1(i)r_2(i)\mu_i^{(1,\,1)}(t) \right). \tag{5.27}$$

Note that there is no technical restriction to considering higher dimensional continuous state spaces (i.e., $d > 2$), but this would give many more terms in (5.27). First apply the law of total expectation to express the second-order moment of the reward

as a function of the (relevant) conditional moments

$$\begin{aligned}
\mathrm{E}\left[Y^2(t)\right] &= \mathrm{E}\left[Y^2(t)|Q(t)=0\right]\cdot\Pr\{Q(t)=0\} \\
&\quad +\mathrm{E}\left[Y^2(t)|Q(t)=1\right]\cdot\Pr\{Q(t)=1\} \\
&= \mathrm{E}[(d_1(0),X_1(t)+d_2(0),X_2(t))^2|Q(t)=0]\cdot\Pr\{Q(t)=0\} \\
&\quad +\mathrm{E}[(d_1(1),X_1(t)+d_2(1),X_2(t))^2|Q(t)=1]\cdot\Pr\{Q(t)=1\} \\
&= \sum_{i=0}^{1} d_1^2(i)\mathrm{E}[X_1(t)^2|Q(t)=i]\cdot\Pr\{Q(t)=i\} \\
&\quad +d_2^2(i)\mathrm{E}[X_2(t)^2|Q(t)=i]\cdot\Pr\{Q(t)=i\} \\
&\quad +2d_1(i)d_2(i)\mathrm{E}[X_1(t)X_2(t)|Q(t)=i]\cdot\Pr\{Q(t)=i\} \\
&= \sum_{i=0}^{1} d_1^2(i)\mu_i^{(2,0)}(t)+d_2^2(i)\mu_i^{(0,2)}(t)+2d_1(i)d_2(i)\mu_i^{(1,1)}(t). \qquad (5.28)
\end{aligned}$$

All that remains is to compute the evolution of $\mu_i^{(m)}(t)$ with $|m|=2$, for which we use (5.19). First, we need to derive the extended generator of the process. Towards this end, we use the definition of L from (5.10). There are two terms in the generator, namely[5]

$$(L\psi)(q,x)=\frac{\partial}{\partial x}\psi(q,x)\cdot A(q)x+\lambda(q,x)(\psi(\phi(q,x))-\psi(q,x)). \qquad (5.29)$$

We want to compute $(L\psi_i^{(m)})(q,x)$ for $|m|=2$. Towards this end, we consider each term in (5.29) in turn. Let us first write the coordinates of $A(q)$ as $A(q)=[a_q^{ij}]$. Then, we get

$$\frac{\partial}{\partial x}\psi_i^{(m)}(q,x)=\delta_{i,q}\begin{bmatrix} m_1x_1^{-1}x^m \\ m_2x_2^{-1}x^m \end{bmatrix}^T, \quad A(q)x=\begin{bmatrix} a_q^{11}x_1+a_q^{12}x_2 \\ a_q^{21}x_1+a_q^{22}x_2 \end{bmatrix}. \qquad (5.30)$$

[5]Recall that for this first-order model, $B=C=0$, and ψ does not explicitly depend on time.

So the first term in (5.29) is

$$\begin{aligned}
&\frac{\partial}{\partial x}\psi_i^{(m)}(q,x)\cdot A(q)x\\
=&\delta_{i,q}\left(m_1a_q^{11}x^m+m_1a_q^{12}x^m\frac{x_2}{x_1}+m_2a_q^{21}x^m\frac{x_1}{x_2}+m_2a_q^{22}x^m\right)\\
=&\delta_{i,q}\left((m_1a_q^{11}+m_2a_q^{22})x^m+m_1a_q^{12}x^{(m_1-1,m_2+1)}+m_2a_q^{21}x^{(m_1+1,m_2-1)}\right)\\
=&\delta_{i,q}\left((m_1a_q^{11}+m_2a_q^{22})x^m+m_1a_q^{12}x^{(m_1-1,m_2+1)}+m_2a_q^{21}x^{(m_1+1,m_2-1)}\right). \qquad (5.31)
\end{aligned}$$

This calculation shows us some patterns: i) the dynamics coming from the ODE between jumps does not cross-couple discrete states (i.e., all the subscripts in this equation are the same), ii) the off-diagonal terms in the matrix cross-couple moments (i.e., if A_q is diagonal, then all the superscripts in this equation are the same), and iii) while the subtractions in the exponents might make us think that we have to worry about negative-powered moments, notice that every time we subtract a power we multiply by an m-dependent factor (e.g., if $m_1=0$ then the second term in the last equation is multiplied by zero, even though it formally has a -1 exponent in the formula).

We now consider the second term of (5.29). Recalling (5.7), we have

$$\begin{aligned}
&\lambda(q,x)(\psi_i^{(m)}(\phi(q,x))-\psi_i^{(m)}(q,x))\\
=&(\delta_{q,1}\alpha+\delta_{q,0}\beta)\left(\psi_i^{(m)}(1-q,\delta_{q,1}v+\delta_{q,0}w)-\psi_i^{(m)}(q,x)\right)\\
=&(\delta_{q,1}\alpha+\delta_{q,0}\beta)\left(\delta_{1-q,i}(\delta_{q,1}v^m+\delta_{q,0}w^m)-\delta_{q,i}x^m\right)\\
=&\delta_{i,0}\left(\delta_{q,1}\alpha v^m\mathbf{1}(x)-\delta_{q,0}\beta x^m\right)+\delta_{i,1}\left(\delta_{q,0}\beta w^m\mathbf{1}(x)-\delta_{q,1}\beta x^m\right)\\
=&\delta_{i,0}\left(\alpha v^m\psi_1^{(0,0)}(q,x)-\beta\psi_0^{(m)}(q,x)\right)+\delta_{i,1}\left(\beta w^m\psi_0^{(0,0)}(q,x)-\alpha\psi_1^{(m)}(q,x)\right),
\end{aligned} \qquad (5.32)$$

where we add the $\mathbf{1}(x)$ to stress the places where the function is constant in x. Note that (5.32) works for general d and any vector m. Writing out the two cases, $i=0,1$, we have

$$\begin{aligned}
\lambda(q,x)(\psi_0^{(m)}(\phi(q,x))-\psi_0^{(m)}(q,x)) &= \alpha v^m\psi_1^{(0,0)}(q,x)-\beta\psi_0^{(m)}(q,x),\\
\lambda(q,x)(\psi_1^{(m)}(\phi(q,x))-\psi_1^{(m)}(q,x)) &= \beta w^m\psi_0^{(0,0)}(q,x)-\alpha\psi_1^{(m)}(q,x).
\end{aligned}$$

Combining (5.11), (5.31), (5.32), we obtain

$$\begin{aligned}
\frac{d}{dt}\mu_i^{(m)} &= \mathrm{E}\left[(L\psi_i^{(m)})(q,x)\right] = \mathrm{E}\left[(m_1 a_i^{11} + m_2 a_i^{22})\psi_i^{(m)}(q,x)\right] \\
&\quad + \mathrm{E}\left[m_1 a_i^{12}\psi_i^{(m_1-1,m_2+1)}(q,x)\right] + \mathrm{E}\left[m_2 a_i^{21}\psi_i^{(m_1+1,m_2-1)}(q,x)\right] \\
&\quad + \mathrm{E}\left[\delta_{i,0}\left(\alpha v^m \psi_1^{(0,0)}(q,x) - \beta\psi_0^{(m)}(q,x)\right)\right] \\
&\quad + \mathrm{E}\left[\delta_{i,1}\left(\beta w^m \psi_0^{(0,0)}(q,x) - \alpha\psi_1^{(m)}(q,x)\right)\right] \\
&= (m_1 a_i^{11} + m_2 a_i^{22})\mu_i^{(m)}(t) + m_1 a_i^{12}\mu_i^{(m_1-1,m_2+1)}(t) + m_2 a_i^{21}\mu_i^{(m_1+1,m_2-1)}(t) \\
&\quad + \delta_{i,0}\left(\alpha v^m \mu_1^{(0,0)}(t) - \beta\mu_0^{(m)}(t)\right) + \delta_{i,1}\left(\beta w^m \mu_0^{(0,0)}(t) - \alpha\mu_1^{(m)}(t)\right) \\
&= (m_1 a_i^{11} + m_2 a_i^{22})\mu_i^{(m)}(t) + m_1 a_i^{12}\mu_i^{(m_1-1,m_2+1)}(t) + m_2 a_i^{21}\mu_i^{(m_1+1,m_2-1)}(t) \\
&\quad + \delta_{i,0}\left(\alpha v^m \pi_1(t) - \beta\mu_0^{(m)}(t)\right) + \delta_{i,1}\left(\beta w^m \pi_0(t) - \alpha\mu_1^{(m)}(t)\right). \qquad (5.33)
\end{aligned}$$

From (5.28), it is clear that we can compute the evolution of $\mathrm{E}\left[Y^2(t)\right]$ given the differential equations that govern the conditional moments $\mu^{(2,0)}(t)$, $\mu^{(0,2)}(t)$, and $\mu^{(1,1)}(t)$ (which are obtained from appropriately specified extended generators). Following a similar procedure, other moments of interest can be computed. For instance, the expected value of the reward is given by

$$\mathrm{E}[Y(t)] = \sum_{i=0}^{1} r_1(i)\mu_i^{(1,0)}(t) + r_2(i)\mu_i^{(0,1)}(t). \qquad (5.34)$$

To compute $\mu_i^{(1,0)}(t)$ and $\mu_i^{(0,1)}(t)$, we would substitute $m = (1, 0)$ and $m = (0, 1)$ in (5.33).

Remark

Notice that (5.33) also yields the Chapman-Kolmogorov differential equations that govern the evolution of the occupational probabilities $\pi_0(t)$ and $\pi_1(t)$. To see this, substitute $m = (0, 0)$ in (5.33):

$$\begin{aligned}
\frac{d}{dt}\mathrm{E}[\psi_0^{(0,0)}(q,\,x)] &= \mathrm{E}\left[\left(L\psi_0^{(0,0)}\right)(q,\,x)\right] \\
&= -\beta\mathrm{E}\left[\psi_0^{(0,0)}(q,\,x)\right] + \alpha\mathrm{E}\left[\psi_1^{(0,0)}(q,\,x)\right], \qquad (5.35)
\end{aligned}$$

$$\frac{d}{dt}\mathrm{E}[\psi_1^{(0,0)}(q,\,x)] = \mathrm{E}\left[\left(L\psi_1^{(0,0)}\right)(q,\,x)\right] = -\alpha\mathrm{E}\left[\psi_1^{(0,0)}(q,\,x)\right] + \beta\mathrm{E}\left[\psi_0^{(0,0)}(q,\,x)\right]. \tag{5.36}$$

Recognizing that $\mathrm{E}[\psi_i^{(0,0)}(q,x)] = \pi_i(t)$, we get

$$\begin{cases} \dot{\pi}_0(t) = -\beta\pi_0(t) + \alpha\pi_1(t), \\ \dot{\pi}_1(t) = -\alpha\pi_1(t) + \beta\pi_0(t), \end{cases} \tag{5.37}$$

which are precisely the Chapman–Kolmogorov differential equations for a two-state Markov chain [46].

For illustration, we chose the parameters $\alpha = 6\mathrm{s}^{-1}$, $\beta = 4\mathrm{s}^{-1}$, $v = [v_1, v_2]^T = [10,\,-3]^T$, and $w = [w_1, w_2]^T = [-10,\,8]^T$. Figure 5.2 plots the occupational probabilities $\pi_0(t)$ and $\pi_1(t)$ computed by simulating (5.37), and the results of 2000 Monte Carlo simulations. Figures 5.3 and 5.4 plot the first-, and second-order moments of the reward obtained from the SHS approach with the results of 2000 Monte Carlo simulations superimposed in each case.

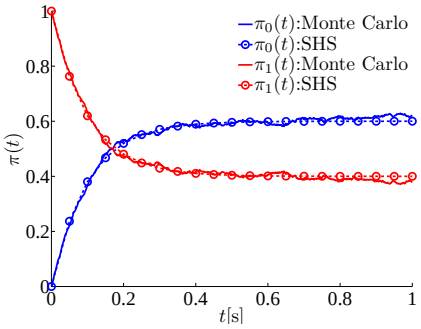

Figure 5.2: Occupational probabilities of the two modes for the model studied in Example 6.

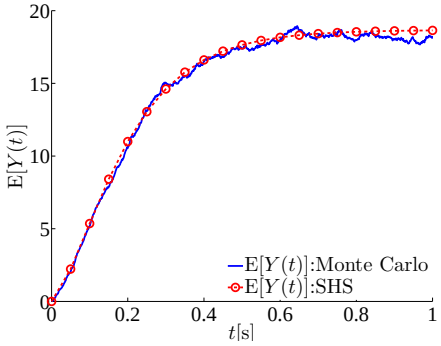

Figure 5.3: First-order moment of accumulated reward for the model studied in Example 6.

5.6 Case Studies Covering Common Reward Models

In this section, we present two case studies to demonstrate the applicability of the proposed framework in modeling system performability. To demonstrate the validity

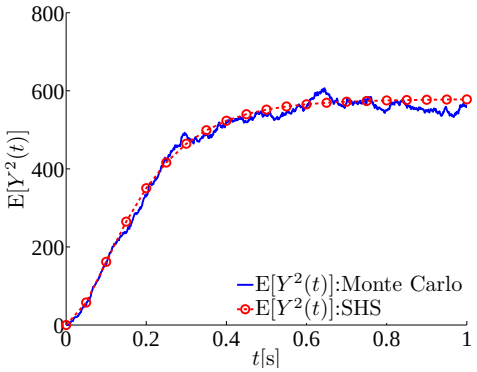

Figure 5.4: Second-order moment of the accumulated reward for the model studied in Example 6.

of the proposed approach, we compare the accuracy of the SHS framework with Monte Carlo simulations and/or results from previous literature as appropriate.

The first case study examines the repair cost expended in maintaining a system of two electric-power transformers. The system is cast as a rate-reward model with impulses in the cost (associated with the one-time expense of enlisting the services of a repair crew). Inflationary effects are modeled with a discount rate. This model is adopted from [59], where the first-order moment of the accumulated repair cost was derived using a method based on the frequency of transitions of the underlying CTMC. We develop the SHS framework for this model, and reproduce the results in [59]. In addition, we also obtain higher-order moments of the accumulated reward. In the second case study, we consider a second-order reward model that was introduced in [34] to describe the reliability of a communication network. A Laplace-transform based method was adopted in [34] to obtain the moments of the accumulated reward. We reproduce the results in [34] using the SHS framework, and in addition, consider cases where there are losses and impulses in the accumulated reward.

5.6.1 Rate Reward Model with Impulses

This case study demonstrates how the SHS framework can be applied to model impulses in a rate-reward model. We examine the accumulated repair cost to maintain a system of two electric-power transformers with common-cause failures [59]. The state-transition diagram that describes the reliability of the system is depicted in Fig 5.5. In mode 2, both transformers are operational; in mode 1, a single trans-

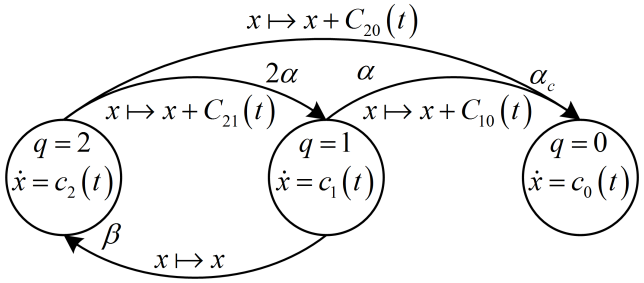

Figure 5.5: Rate reward model for transformer maintenance.

former is operational; and in mode 0, both transformers have failed. The failure rate, repair rate, and common-cause failure rate are denoted by α, β, and α_c, respectively. The reward of interest is the cost of repair, denoted by $X(t)$. The rate at which the repair cost grows in mode i is denoted by $c_i(t)$ [\$/yr]. Transitions due to failures are associated with impulses in the repair cost that model the one-time expenses in enlisting the services of a repair crew. The impulse change in repair cost as a result of a failure transition from mode i to mode j is denoted by $C_{ij}(t)$ [\$]. The cost parameters are modeled to be time-dependent to factor inflation. In particular, we presume—following along the model in [59]—that $c_i(t) = c_i e^{-\gamma t}$ and $C_{ij}(t) = C_{ij} e^{-\gamma t}$. The parameter γ is the discount rate that represents future costs by a discounted value [59]. The authors in [59] obtain analytical expressions for the expected value of the accumulated repair cost with a method that is based on the frequency of visits in a CTMC [41]. We demonstrate how to cast this problem in the SHS framework. In doing so, we obtain a family of ODEs whose solution not only yields the expected value of the accumulated cost, but also higher-order moments (the higher order moments were not tackled in [59]). We begin by defining test functions for each state of the chain

$$\psi_i^{(m)}(q,\, x) = \delta_{q,i} x^{(m)} = \begin{cases} x^{(m)} & \text{if} \quad q = i \\ 0 & \text{if} \quad q \neq i \end{cases}, \; i = 0,\, 1,\, 2. \tag{5.38}$$

The extended generators evaluated on the test functions are obtained from (5.10) and given by

$$\begin{aligned} \left(L\psi_0^{(m)}\right)(q,\, x) \;&=\; m c_0(t) \psi_0^{(m-1)}(q,\, x) + \alpha \left(\psi_1^{(1)}(q,\, x) + C_{10}(t)\psi_1^{(0)}(q,\, x)\right)^m \\ &\quad + \alpha_c \left(\psi_2^{(1)}(q,\, x) + C_{20}(t)\psi_2^{(0)}(q,\, x)\right)^m, \end{aligned} \tag{5.39}$$

$$\begin{aligned}\left(L\psi_1^{(m)}\right)(q,\,x) &= mc_1(t)\psi_1^{(m-1)}(q,\,x) - (\alpha+\beta)\,\psi_1^{(m)}(q,\,x) \\ &\quad +2\alpha\left(\psi_2^{(1)}(q,\,x) + C_{21}(t)\psi_2^{(0)}(q,\,x)\right)^m, \end{aligned} \tag{5.40}$$

$$\left(L\psi_2^{(m)}\right)(q,\,x) = mc_2(t)\psi_2^{(m-1)}(q,\,x) - (2\alpha+\alpha_c)\,\psi_2^{(m)}(q,\,x) + \beta\psi_1^{(m)}(q,\,x). \tag{5.41}$$

Applying (5.11) to (5.39), (5.40), and (5.41), we obtain the following differential equations that govern the conditional moments:

$$\begin{aligned}\frac{d}{dt}\mu_0^{(m)}(t) &= mc_0(t)\mu_0^{(m-1)}(t) + \alpha\left(C_{10}^m(t)\pi_1(t) + \sum_{k=0}^{m-1}\binom{m}{k}\mu_1^{(m-k)}(t)C_{10}^k(t)\right) \\ &\quad +\alpha_c\left(C_{20}^m(t)\pi_2(t) + \sum_{k=0}^{m-1}\binom{m}{k}\mu_2^{(m-k)}(t)C_{20}^k(t)\right), \end{aligned} \tag{5.42}$$

$$\begin{aligned}\frac{d}{dt}\mu_1^{(m)}(t) &= mc_1(t)\mu_1^{(m-1)}(t) - (\alpha+\beta)\,\mu_1^{(m)}(t) \\ &\quad +2\alpha\left(C_{21}^m(t)\pi_2(t) + \sum_{k=0}^{m-1}\binom{m}{k}\mu_2^{(m-k)}(t)C_{21}^k(t)\right), \end{aligned} \tag{5.43}$$

$$\frac{d}{dt}\mu_2^{(m)}(t) = mc_2(t)\mu_2^{(m-1)}(t) - (2\alpha+\alpha_c)\,\mu_2^{(m)}(t) + \beta\mu_1^{(m)}(t), \tag{5.44}$$

where $\pi_0(t)$, $\pi_1(t)$, and $\pi_2(t)$ are the occupational probabilities of the different modes. Notice that substituting $m = 0$ in (5.42), (5.43), and (5.44) recovers the Chapman-Kolmogorov equations: $\dot{\pi}(t) = \pi(t)\Lambda$, where $\pi(t) = [\pi_0(t),\, \pi_1(t),\, \pi_2(t)]$, and Λ is the generator matrix of the underlying CTMC given by:

$$\Lambda = \begin{bmatrix} 0 & 0 & 0 \\ \alpha & -(\alpha+\beta) & \beta \\ \alpha_c & 2\alpha & -(2\alpha+\alpha_c) \end{bmatrix}. \tag{5.45}$$

The m-order moment of the accumulated repair cost is given by (5.26), i.e., $\mathrm{E}[X^m(t)] = \mu_0^{(m)}(t) + \mu_1^{(m)}(t) + \mu_2^{(m)}(t)$. The evolution of $\mu_0^{(m)}(t)$, $\mu_0^{(m)}(t)$, and $\mu_0^{(m)}(t)$ is given by the solution of (5.42), (5.43), and (5.44).

For illustration, consider: $\alpha = 2\,\mathrm{yr}^{-1}$, $\beta = 1000\,\mathrm{yr}^{-1}$, $\alpha_c = 1\,\mathrm{yr}^{-1}$, $c_2 = \$1000/\mathrm{yr}$, $c_1 = \$10,000/\mathrm{yr}$, $c_0 = 0$, $C_{21} = \$500$, $C_{20} = \$1000$, and $C_{10} = \$500$ [59]. Figure 5.6 depicts the expected value of the accumulated repair cost for two different values of γ.

The results from the SHS approach (obtained by simulating (5.42), (5.43), and (5.44) for $m = 1$, and then using $\mathrm{E}[X(t)] = \mu_0^{(1)}(t) + \mu_1^{(1)}(t) + \mu_2^{(1)}(t)$) are superimposed on the results from [59]. To further validate the approach, Figs. 5.7-5.8 depict the second- and third-order moments of the accumulated cost (obtained by simulating (5.42), (5.43), and (5.44) for $m = 2$ and $m = 3$, respectively) superimposed on results obtained from 5000 Monte Carlo simulations. Note that it is unclear how the method proposed in [59] can be extended to obtain higher-order moments. Therefore, in these cases, we just include the Monte Carlo results for comparison and validation of the SHS approach.

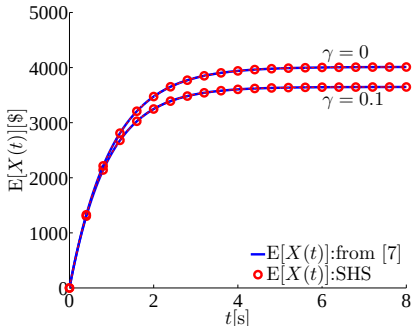

Figure 5.6: First-order moment of repair cost.

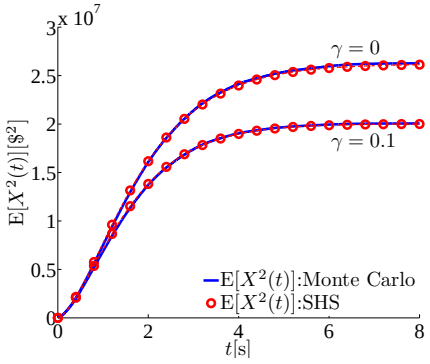

Figure 5.7: Second-order moment of repair cost.

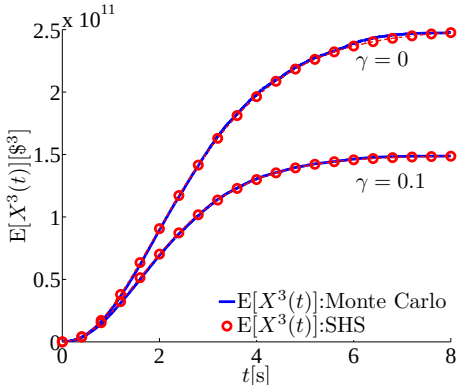

Figure 5.8: Third-order moment of repair cost.

5.6.2 Second-order Reward Model

In this case study, we examine the second-order Markov reward model illustrated by the state-transition diagram in Fig. 5.9. Note that this is a generalized version of the model presented in [34], which was employed to model the capacity of a communication channel (the reward is the available channel capacity). Transitions between different modes and the associated transition rates are also illustrated in the figure. We assume that failure transitions are associated with a reset map that can model partial total loss or impulses in the accumulated reward. In partial total loss models, a (possibly mode-dependent) fraction of the total accumulated reward is lost with each transition of the chain. With regard to the state-transition diagram presented in Fig. 5.9, setting $C_{ij} \equiv 0$, $0 \leq \kappa_i \leq 1$, we recover a model that captures partial total loss in the accumulated reward. Similarly, choosing $C_{ij} < 0$, $\kappa_i \equiv 0$, models impulses in the accumulated reward. Note that the analysis in [34] did not include losses/impulses in the accumulated reward, although loss models have been incorporated in computer tools by the same authors [35]. Furthermore, the moments of the accumulated reward are derived from a direct analysis of the Laplace transform of the accumulated-reward probability distribution in [34]. Here, we demonstrate how to formulate the model within the SHS framework.

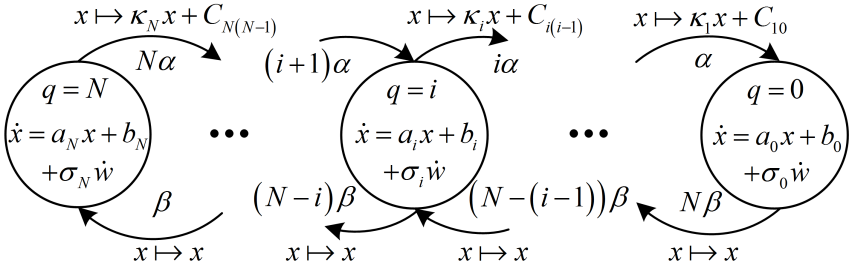

Figure 5.9: Second-order reward model for communication-channel reliability.

As before, begin by defining the test functions for each state of the chain as

$$\psi_i^{(m)}(q, x) = \begin{cases} x^m & \text{if} \quad q = i \\ 0 & \text{if} \quad q \neq i \end{cases}, \; i = 0, 1, \ldots, N. \tag{5.46}$$

The generators for the states can be obtained from (5.10) as

$$\begin{aligned}\left(L\psi_0^{(m)}\right)(q,x) &= ma_0\psi_0^{(m)}(q,x) + mb_0\psi_0^{(m-1)}(q,x) - N\beta\psi_0^{(m)}(q,x) \\ &\quad +\alpha\left(\alpha_1\psi_1^{(1)}(q,x) + C_{10}\right)^m \psi_1^{(0)}(q,x) + \frac{1}{2}\sigma_0^2 m(m-1)\psi_n^{(m-2)}(q,x), \quad (5.47)\end{aligned}$$

$$\begin{aligned}\left(L\psi_N^{(m)}\right)(q,x) &= ma_N\psi_N^{(m)}(q,x) + mb_N\psi_N^{(m-1)}(q,x) + \beta\psi_{N-1}^{(m)}(q,x), \quad (5.48) \\ &\quad -N\alpha\psi_n^{(m)}(q,x) + \frac{1}{2}\sigma_N^2 m(m-1)\psi_N^{(m-2)}(q,x) \quad (5.49)\end{aligned}$$

$$\begin{aligned}\left(L\psi_i^{(m)}\right)(q,x) &= ma_i\psi_i^{(m)}(q,x) + mb_i\psi_i^{(m-1)}(q,x) - ((N-i)\beta + i\alpha)\psi_i^{(m)}(q,x) \\ &\quad +(i+1)\alpha\left(\alpha_{i+1}\psi_{i+1}^{(1)} + C_{(i+1)i}\right)^m \psi_{i+1}^{(0)}(q,x) + (N-(i-1))\beta\psi_{i-1}^{(m)}(q,x) \\ &\quad +\frac{1}{2}\sigma_i^2 m(m-1)\psi_i^{(m-2)}(q,x), \forall i = 1,\ldots,N-1. \quad (5.50)\end{aligned}$$

As before, define the conditional moments $\mu_i^{(m)}(t) = \mathrm{E}\left[\psi_i^{(m)}(q,\, x)\right]$, $i = 0,\, 1, \ldots,\, N$. Applying (5.11), we see that the differential equations that govern the evolution of $\mu_i^{(m)}(t)$, $i = 0,\, 1, \ldots,\, N$ are given by

$$\begin{aligned}\frac{d}{dt}\mu_0^{(m)}(t) &= ma_0\mu_0^{(m)}(t) + mb_0\mu_0^{(m-1)}(t) - N\beta\mu_0^{(m)}(t) + \frac{1}{2}\sigma_0^2 m(m-1)\mu_0^{(m-2)}(t) \\ &+ \alpha\left(C_{10}^m\pi_1(t) + \sum_{k=0}^{m-1}\binom{m}{k}\kappa_1^{m-k}\mu_1^{(m-k)}(t)C_{10}^k\right), \quad (5.51)\end{aligned}$$

$$\begin{aligned}\frac{d}{dt}\mu_N^{(m)}(t) &= ma_N\mu_N^{(m)}(t) + mb_N\mu_N^{(m-1)}(t) + \beta\mu_{N-1}^{(m)}(t) \\ &\quad -N\alpha\mu_N^{(m)}(t) + \frac{1}{2}\sigma_N^2 m(m-1)\mu_N^{(m-2)}(t), \quad (5.52)\end{aligned}$$

$$\begin{aligned}\frac{d}{dt}\mu_i^{(m)}(t) &= ma_i\mu_i^{(m)}(t) + mb_i\mu_i^{(m-1)}(t) - ((N-i)\beta + i\alpha)\mu_i^{(m)}(t) \\ &+ (i+1)\alpha\left(C_{(i+1)i}^m\pi_{i+1}(t) + \sum_{k=0}^{m-1}\binom{m}{k}\kappa_{i+1}^{m-k}\mu_{i+1}^{(m-k)}(t)C_{(i+1)i}^k\right) \\ &+ (N-(i-1))\beta\mu_{i-1}^{(m)}(t) + \frac{1}{2}\sigma_i^2 m(m-1)\mu_i^{(m-2)}(t). \quad (5.53)\end{aligned}$$

As a special case, consider $a_i = 0$, $b_i = (C - ir)$, $\sigma_i = \sqrt{i}\sigma$, $\kappa_i = 1$, and $C_{ij} \equiv 0$. This recovers the model studied in [34], where there are no losses in the accumulated reward. In this case, (5.51)-(5.53) simplify to

$$\frac{d}{dt}\mu^{(m)}(t) = \mu^{(m)}(t)\Lambda + m\mu^{(m-1)}(t)\Gamma + \frac{1}{2}m(m-1)\mu^{(m-2)}(t)\Upsilon, \tag{5.54}$$

where $\mu^{(m)}(t)$ is the vector of conditional moments at time t,

$$\Gamma = \text{diag}\left(C, \ldots C - ir, \ldots, C - Nr\right), \tag{5.55}$$

$$\Upsilon = \text{diag}\left(0, \ldots i\sigma^2, \ldots, N\sigma^2\right), \tag{5.56}$$

and Λ is the generator matrix of the underlying CTMC given by

$$\Lambda = \begin{bmatrix} -N\beta & & 0 & & 0 \\ \alpha & & (N-(i-1)\beta) & & 0 \\ 0 & \cdots & -((N-1)\beta + i\alpha) & \cdots & 0 \\ 0 & & (i+1)\alpha & & \beta \\ 0 & & 0 & & -N\alpha \end{bmatrix}. \tag{5.57}$$

Note that the expression in (5.54) exactly matches Equation (6) in Theorem 2 of [34].

For illustration, consider the following: $N = 10$, $\alpha = 5$, $\beta = 2$, $\kappa_i = 0.5$, $C_{ij} = -0.1$, $a_i = i$, $b_i = N$, $\sigma_i = \sqrt{i}\sigma$. Figures 5.10, 5.11, 5.12 plot the first-, second-, and third-order moments of the reward obtained from the SHS approach (substituting $m = 1$, 2, 3, respectively in (5.51)-(5.53), and using (5.26)). The results of 75,000 Monte Carlo simulations are superimposed in each case. The simulations are repeated for different values of σ to demonstrate the validity of the SHS approach.

5.7 Moment Closure for Markov Reward Models

Recall that in the class of reward models explored in the first two case studies, the vector fields that govern the evolution of the continuous state and the reset maps are linear, while the transition rates are independent of the continuous state. If these assumptions are relaxed, the differential equations that govern the evolution of the moments are infinite dimensional and *moment-closure techniques* have to be applied

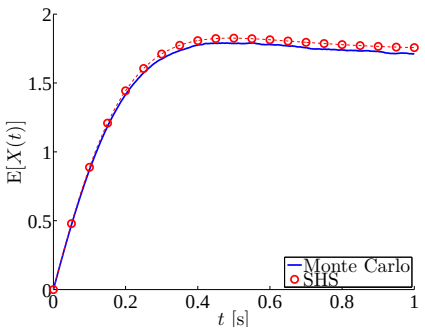

Figure 5.10: First-order moment of accumulated reward.

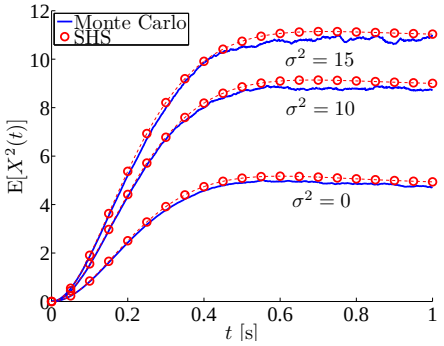

Figure 5.11: Second-order moment of accumulated reward.

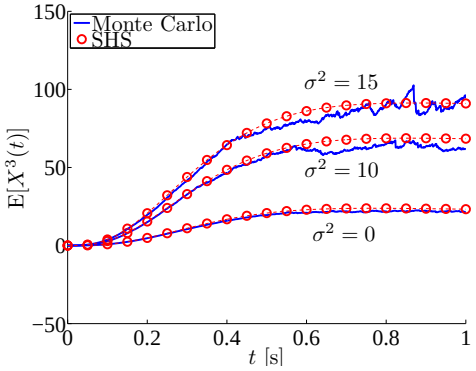

Figure 5.12: Third-order moment of accumulated reward.

to solve them.

To see the added difficulty, in all of the cases considered previously, the evolution equation for the p^{th} order moments of the process have always depended on lower-order moments, and thus the moment evolution equations always give a closed system. For example, we could always first solve the Chapman-Kolmogorov equations to obtain the zeroth-order moments; from this, the equations for the first-order moments depended only on themselves and these zeroth-order moments, the second-order moments only depend on themselves and lower order, etc. We can then always solve these systems iteratively. In general, however, we could have a case where the evolution equation for a moment of a given order depends on moments of higher orders; this system will not be closed and cannot be solved iteratively. We demonstrate this for a simple example below.

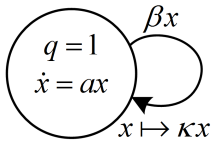

Figure 5.13: First-order single-mode model to illustrate moment closure.

Consider the state transition diagram illustrated in Fig. 5.13, for a first-order reward model with a single discrete state. The generator for this process is given by

$$\begin{aligned}\left(L\psi^{(m)}\right)(x) &= \frac{\partial}{\partial x}\psi^{(m)}(x)\cdot ax + \beta x\left(\psi^{(m)}\left(\phi(x)\right) - \psi^{(m)}(x)\right) \\ &= ma\psi^{(m)}(x) + \beta\left(\kappa^m - 1\right)\psi^{(m+1)}(x). \end{aligned} \tag{5.58}$$

Applying (5.11), we see that the differential equations that govern the moments of $X(t)$ are given by

$$\dot{\mu}^{(m)}(t) = ma\mu^{(m)}(t) + \beta\left(\kappa^m - 1\right)\mu^{(m+1)}(t). \tag{5.59}$$

Notice that $\dot{\mu}^{(m)}(t)$ depends on $\mu^{(m+1)}(t)$. Therefore, moment-closure methods are required to solve (5.59), i.e., to simulate the differential equation that governs the m-order moment, $\mu^{(m+1)}(t)$ has to be expressed as some function of $\mu^{(i)}(t)$, $1 \leq i \leq m$.

Typically, moment-closure methods rely on assumptions about the underlying distribution of the state. Methods tailored to SHS are described in [31, 32] and the references therein. For the reward models introduced in Section 5.2, moment-closure methods are unnecessary—note that as demonstrated in the previous two case studies, this class of reward models is still very powerful and can be applied to a variety of system performability modeling problems. A detailed discussion of moment-closure methods (as they apply to reward models with state-dependent transition rates and/or general polynomial vector fields governing the continuous states) is beyond the scope of this work and part of ongoing research.

Chapter 6

ESTIMATING PHOTOVOLTAIC ENERGY CONVERSION SYSTEMS PERFORMABILITY METRICS

This is the first of three chapters where we apply the methods outlined previously to renewable energy systems applications. In this chapter, we demonstrate how Markov models can be utilized to quantify reliability/performability of photovoltaic energy conversion systems (PVECS). The material we present subsequently has been published in [8].

To ensure continued growth in PVECS, it is imperative to address the high levelized cost of energy (LCOE) for PV systems. The LCOE is defined as the ratio of the present value of capital and operating costs to the energy yield over the system's lifetime and serves as a useful metric to gauge the competitiveness of different sources of energy [60]. The LCOE is inversely proportional to the net annual energy production, and directly proportional to O&M and replacement/overhaul costs [60]. Therefore, system reliability has a great impact not only on O&M and replacement/overhaul costs, but also on annual energy yield. This dependence has been evidenced by studies that demonstrated that LCOE of PVECS increases exponentially with a decrease in lifetime [61].

System reliability/performance models should provide accurate energy-yield estimation, and aid in system design to ensure favorable economics. Additionally, an important aspect is the impact of model-parameter uncertainty, which will in turn propagate to the LCOE estimate. The methods presented in this chapter address the problems discussed above by providing: i) a modeling framework to integrate reliability considerations into energy-yield and cost estimations using Markov reward model formalisms [47]; and ii) an analytical approach for parametric sensitivity analysis based on generalized matrix inversion techniques [18]. The sensitivity analysis is based on the results presented in Chapter 2.

The literature on system-level probabilistic reliability analysis for power systems is very extensive (see, e.g., [1, 11, 62] and the references therein). In the context

of PVECS, combinatorial-based methods for PV system reliability assessment have been attempted in [63, 64], but they do not yield insight into other performance metrics such as energy yield and are limited in scope and application. Reliability-oriented design approaches for off-grid, remote PVECS are explored in [6], where the authors use Markov reliability models among other methods. The idea to utilize Markov chains in PVECS reliability modeling was also proposed in [7, 65]. Our work is related to the ideas presented in [59], where the authors develop a model to integrate economic aspects in power system reliability and apply the concepts to a two-transformer example. The Markovian framework proposed in this work goes beyond standard Markov reliability models which provide metrics such as availability and mean-time-to-failure, and provides performance-related metrics such as energy yield, although other metrics that, for example, include cost as in [59] can be easily defined.

The impact of parametric uncertainty on reliability and performance metrics has already been stressed. Apart from identifying model parameters that are likely to cause modeling errors, such analyses also aid in optimal system design [20, 66]. The case studies highlight how sensitivity analysis can be used to formulate optimal maintenance policies, estimate the impact of parameter variations, and aid in optimizing economic policies in residential-scale, utility-scale, and emerging distributed microinverter systems.

6.1 Reliability and Performability Metrics of Interest in PVECS

A variety of reliability/performability metrics can be defined by Markov reward models by appropriately formulating the reward vector ρ. We provide a few examples below, and note that some of these will be used in the ensuing case studies. Recall that the stochastic behavior due to component failures and repairs is described by an ergodic Markov chain (i.e., the system is perfectly repaired) with states $i = 0, 1, 2, \ldots, N-1$ indexing system configurations that arise due to faults, and $i = N$ indexing the non-faulty configuration.

6.1.1 Expected System Capacity

Consider a PVECS with power rating P. Denote by π_i the long-term probability that the system is operating in configuration i, and the corresponding power rating by P_i. The expected system capacity is denoted by Ξ, and following (2.7), it can be defined as

$$\Xi = \pi\rho^T = [\pi_0\, \pi_1 \ldots \pi_n]\, [P_0\, P_1 \ldots P_n]^T . \tag{6.1}$$

Effectively, this metric ensures that systems with the same power rating but different reliability models can be uniformly and unambiguously compared.

6.1.2 Energy Yield

Consider a grid-tied PVECS installed at a location characterized by a capacity factor CF which is defined as

$$CF = \frac{(\text{h/day of 1-sun})}{24\,\text{h/day}}, \tag{6.2}$$

where 1-sun is defined as an insolation of 1 kW/m^2 [67]. For example, if the average incident energy density at a given location is 5 kWh/m^2-day, this corresponds to 5 h/day of 1-sun insolation, and a capacity factor of 20.8 %. Average capacity factors for different locations are computed using historical data and can be obtained from a variety of sources (see, e.g., [67]). Over some period of time T, if the system satisfies the conditions in (2.8), an estimate of its energy yield is given by

$$\Gamma = \Xi \cdot CF \cdot T. \tag{6.3}$$

Multiplying the energy yield by the average price of electricity yields the monetary gain over the period T.

Remark

In Section 6.5.1, we describe a method for explicitly considering uncertainty in the PV source and how it can be propagated to reliability and performance metrics. This method reformulates the entries of the reward vector as random variables whose distributions are derived from those of incident insolation and ambient temperature—uncertain inputs to the PVECS.

6.1.3 System Availability

By appropriate choice of the reward function, a Markov reward model can also provide standard reliability metrics. For example, system availability for an $N+1$ state model can be recovered by choosing ρ so that $\rho_i = 1$ if the system is operational in state i and $\rho_i = 0$ otherwise.

Next, we present several case studies that demonstrate the applicability of the Markov modeling framework to PVECS. The first case study applies to a utility-level system, and explores the impact of parameter variations and repair strategies on system capacity and energy yield. Next, sensitivity analysis is utilized to optimize repair rates for a residential-scale system. Finally, the sensitivity approach is utilized for design trade-off analysis in emerging distributed system architectures.

6.2 Utility-Scale Installations

Utility-owned installations constituted 8% of grid-tied PVECS in 2008 [68]. This number is expected to increase as federal legislation has incentivized utilities to own PV projects without separate investors [60]. The average installed capacity in utility installations is typically in the range of hundreds of kilowatts. While economies of scale guarantee lower operation and maintenance (O&M) costs (0.12% as compared to 1.47% for residential systems according to [60]), the large size and complexity of these systems presents various challenges to ensure high reliability.

The benchmark installation considered here is a P =225 kW grid-tied inverter analyzed in [69]. The system architecture is depicted in Fig. 6.1, where it can be seen that the inverter has nine string blocks (with rated power, $P_s = P/9 = 25$kW), each of which consist of ten strings of series-connected PV modules. Each string has twelve series-connected modules. In this case study, we assume there are two different failure modes: inverter and string blocks failures, with failure rates denoted by λ_i and λ_s, respectively. The inverter and string blocks are repairable with repair rates denoted by μ_i and μ_s, respectively, and repair brings the system back to its full functionality (although alternate repair strategies are explored subsequently). The state-transition diagram for the system stochastic behavior due to failures and repairs is depicted in Fig. 6.2. Note that other failure mechanisms including failures in series strings (e.g. due to arc faults), individual PV modules (e.g. due to faulty junction boxes

or bypass diodes), blocking diodes, and protection equipment, can be incorporated in the model by appropriately defining additional states. If representative transition rates can be identified, phenomena such as soiling and partial shading can also be modeled similarly.

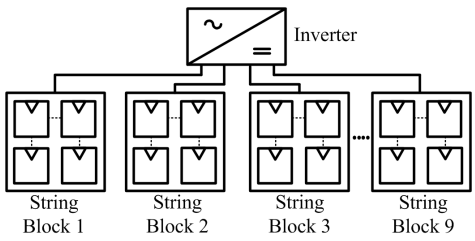

Figure 6.1: Electrical block diagram of utility-scale system with a central inverter and nine string blocks.

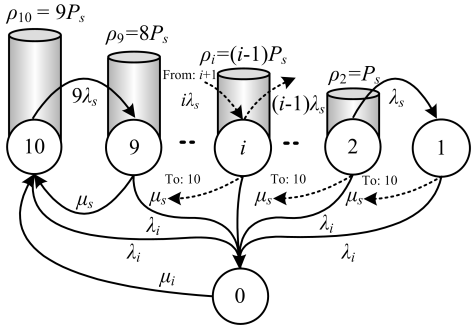

Figure 6.2: State-transition diagram that describes reliability of the utility-scale system.

6.2.1 Base Case

The performance metrics of interest are system capacity Ξ, and energy yield Γ. Following the notation in (6.1), it follows that $\rho_i = P_i = (i-1)P_s = (i-1)P/9$, $i = 1, ..., 10$, and $\rho_0 = 0$ (this configuration corresponds to inverter failure, which causes the whole system to fail at once). The failure and repair rate values are adopted from [69], and given by $\lambda_i = (1/3)$ yr^{-1}, $\lambda_s = (1/270)$ yr^{-1}, $\mu_i = (365/15)$ yr^{-1}, and $\mu_s = (365/8)$ yr^{-1}. The system capacity is $\Xi = 221.94$ kW. Then, assuming a capacity factor, $CF = 18\%$, and for a period $T = 10$ yr, an estimate of the energy yield is $\Gamma = 3.51$ GWhr.

6.2.2 Failure/Repair Rate Uncertainty Analysis

Given the uncertainty in accurately determining transition rates [61], sensitivity analysis can reveal what parameters have the largest impact on system capacity (and therefore energy yield). Figures 6.3 (a)-(d) depict the system capacity sensitivity with respect to transition rates. Notice that system capacity is most sensitive to

the inverter failure rate, followed by the string failure rate, inverter repair rate, and string repair rate. This follows intuitively, as a failure in the inverter brings the system down, whereas the system still delivers power if several strings have failed. Also, note that $\partial\Xi/\partial\mu_s$ and $\partial\Xi/\partial\mu_i$ vary by over two orders of magnitude over the range of μ_s and μ_i, respectively. This suggests that accurate estimates of repair rates (or at least an accurate estimate on their range) are required for any analysis that employs sensitivity analysis. To validate the accuracy of the analytical results on sensitivity, we plot on the same figures the sensitivities computed numerically ($\partial\Xi/\partial\theta_i \approx \Delta\Xi/\Delta\theta_i$) which are seen to match those computed using the analytical approach very well.

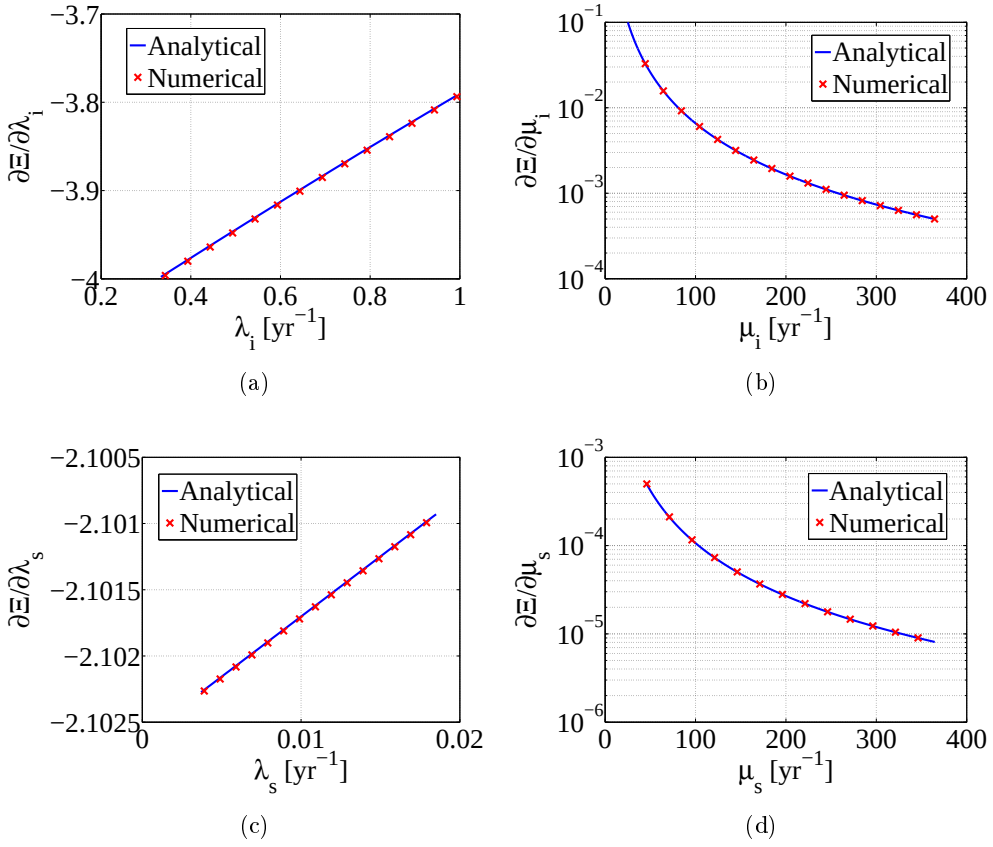

Figure 6.3: Capacity sensitivity as a function of failure/repair rates.

6.2.3 Impact of Repair Strategy on Repair Costs

Denote by n_s the largest number of operational strings for which repair is initiated. Figure 6.4 depicts the investigated repair strategies as n_s is varied from 8 to 1. Transitions due to inverter failure still exist but are not depicted in the figure for simplicity. The energy yield is calculated using (6.3) for the different repair strategies over a period of T =10 yr and capacity factor 18%. The results are plotted in Fig. 6.5. As expected, if more strings are allowed to fail before repair is initiated, the expected energy yield is reduced. Energy-yield estimates can be used to determine an alternative to the perfect repair strategy (corresponding to $n_s = 8$). To do so, we introduce the marginal utility of repair for the j repair strategy which is denoted by MUR_j and defined as

$$MUR_j = \frac{p(\Gamma_8 - \Gamma_j)}{CF \cdot T} \frac{\$}{\text{yr}}, \tag{6.4}$$

where Γ_j is the energy yield in kWhr when $n_s = j$, p is the price of electricity in \$/kWhr. Essentially the marginal utility of repair suggests the added dollar amount by which the cost of the repair strategy when $n_s = j$ can be relaxed with no monetary loss to the system operator. Hence, one way to pick a repair strategy (or pick an n_s) given an added repair cost c_r \$/yr over the perfect repair strategy, is to solve the optimization problem

$$\begin{aligned} \max \quad & j \\ \text{s.t.} \quad & c_r < MUR_j \\ & 1 \leq j \leq 8. \end{aligned} \tag{6.5}$$

The MUR for the utility-scale system is plotted in Fig. 6.6 assuming that the price of electricity is \$0.087/kW-hr. For the illustrative repair cost (denoted by c_r and sketched as a dashed line in the figure), we would pick the repair strategy corresponding to $n_s = 6$.

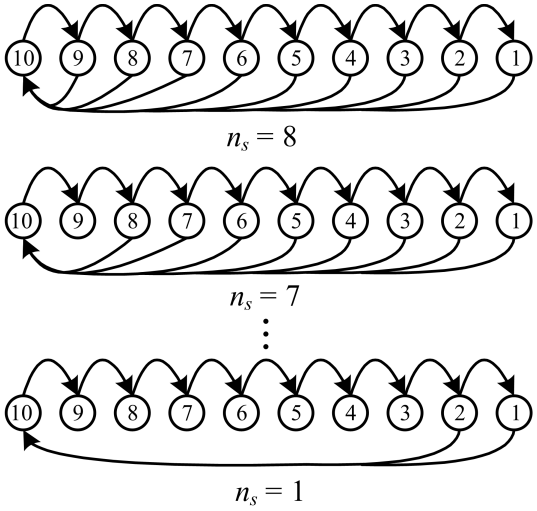

Figure 6.4: Alternate repair strategies

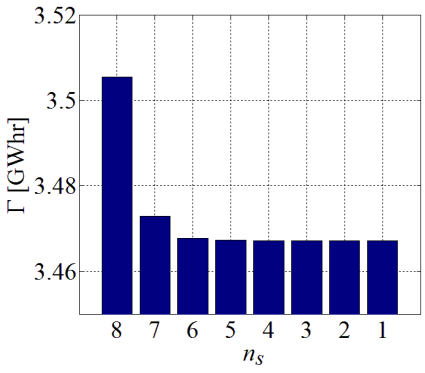

Figure 6.5: Energy yield as a function of repair strategy

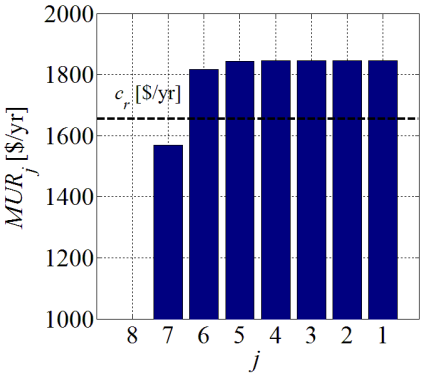

Figure 6.6: Marginal utility of repair to pick repair strategy

6.3 Optimum Repair Strategies for Residential PV Systems

Residential-scale systems had an average rating of 4.9 kW and constituted 27% of all new grid-connected systems installed in 2008 [68]. While traditionally such systems have been installed and operated by the homeowner, utilities have started to enter this sector. For example, San Diego Gas and Electric owns multi-family residential-scale PVECS, and Southern California Edison has similar initiatives to deploy utility-owned systems [70]. To encourage growth in this sector, technical advances have to

be coupled with improvements in economics. Focusing on this aspect, this case study demonstrates how the proposed framework—especially the approach to sensitivity analysis—can optimize repair rates for residential-scale systems.

The benchmark PV installation studied here is installed in the Gable Home—a net-zero solar-powered home constructed by the University of Illinois for the 2009 Solar Decathlon Competition [71]. The system is comprised of a 9 kW PV array with forty 225 W modules. Two 5 kW inverters are utilized to interface with the utility grid. A block diagram of the system architecture is shown in Fig. 6.7. The system could operate (albeit at a lower power rating) with a single inverter should one fail. The Markov model developed to study this system focuses on inverter reliability as inverter failure has been singled out as one of the chief reasons for low energy yield in grid-connected PVECS [72]. Figure 6.8 depicts the Markov-model state-transition diagram that captures inverter failures and repairs. Each state in the diagram represents the number of functional inverters. The failure rate of the inverters is denoted by λ. The repair rates corresponding to state 0 (the failed state) and state 1 (single functional inverter) are denoted by μ_0 and μ_1, respectively. This model captures the possibility that the time taken to repair two inverters could be longer than that to repair a single inverter. From the above description, it follows that $\rho = [\rho_0\ \rho_1\ \rho_2] = [0\ P/2\ P]$, $P = 10$ kW.

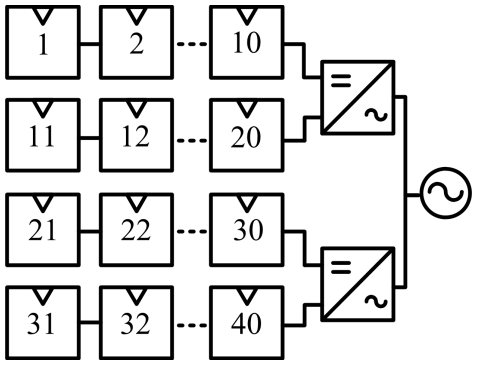

Figure 6.7: Gable Home electrical system block diagram.

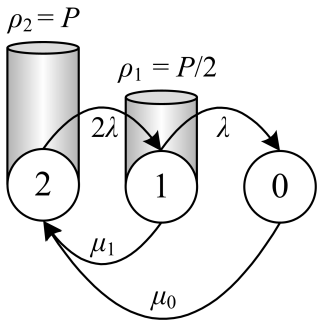

Figure 6.8: State-transition diagram capturing Gable Home inverter reliability.

To demonstrate how repair rates might be chosen, let us begin by assuming that the mean time to inverter failure is 10 yr ($\lambda = (1/10)\ \text{yr}^{-1}$) [60]. Assume that the mean time to repair the inverters is 10 days ($\mu_0 = \mu_1 = (365/10)\ \text{yr}^{-1}$). The sensitivities

of the system capacity to the failure and repair rates are: $\partial\Xi/\partial\lambda = -2.724\text{x}10^{-2}$, $\partial\Xi/\partial\mu_1 = 7.424\text{x}10^{-5}$, and $\partial\Xi/\partial\mu_0 = 4.068\text{x}10^{-7}$. From these numbers it is clear that Ξ is not sensitive to the mean time to repair both inverters. This makes intuitive sense, as the inverters are very reliable and restored to operation rather quickly. These observations suggest that μ_0 need not equal μ_1. The quantities $\partial\Xi/\partial\mu_0$ and Ξ are plotted in Fig. 6.9 as a function of μ_0. The capacity is normalized as $\Xi = \Xi \cdot (100/P)$ to express it in %. Notice that the performance of the system is unaffected as long as the mean time to repair both inverters is between 10 and 30 days (corresponds to μ_0 between $36.5\,\text{yr}^{-1}$ and $12.16\,\text{yr}^{-1}$). This suggests that the mean time to repair two inverters could be relaxed to 30 days without significantly affecting the expected energy yield.

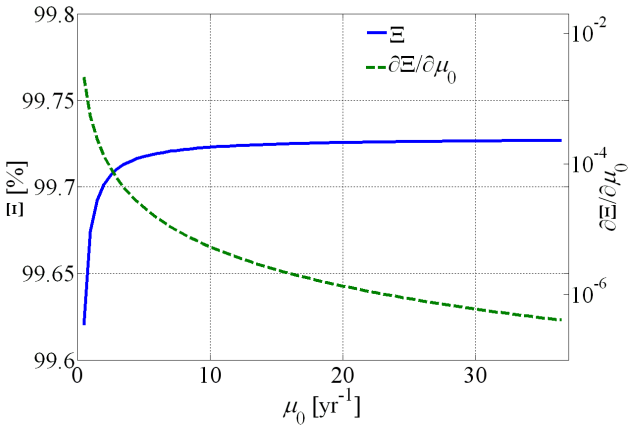

Figure 6.9: System capacity and its sensitivity to time to repair both inverters.

Similar case studies can provide invaluable insight to manufacturers and installers in determining replacement, repair, and shipment policies to minimize costs. On the other hand, system owners can not only compare the performance of several different systems with a unified performance metric but also negotiate power purchase agreements, warranties and repair policies. With proper data, the models can easily be extended to include a detailed economic analysis by coupling the repair rates with shipping and wage-related costs.

6.4 Emerging Distributed Inverter Systems

Conventional installations where large PV arrays were connected to central inverters (Fig. 6.10(a)) are expected to be replaced by distributed systems in which PV modules are coupled with module-integrated microinverters (Fig. 6.10(b)). Proponents of such systems have touted various advantages to justify the added installed cost over central systems [73]. Of particular interest is the reliability of microinverter-based architectures. The main goals of this case study are to evaluate the impact of failure and repair rates on system capacity.

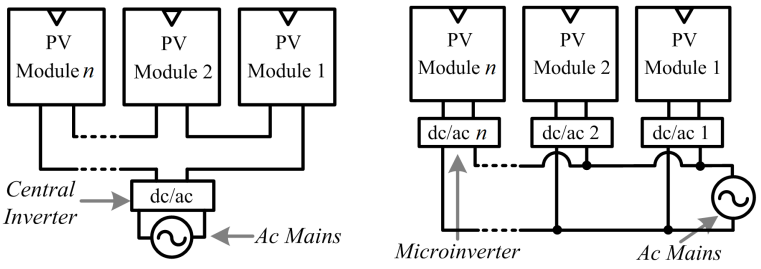

Figure 6.10: Block diagrams of the (a) central and (b) distributed inverter architectures.

Consider a grid-tied PV system built with N microinverters. The state-transition diagram for this system is shown in Fig. 6.11. As before, each state corresponds to the number of operational microinverters. Repairs in each state are assumed to restore the operation of all failed microinverters. The mean time to repair the microinverters is denoted by μ, and their failure rate is denoted by λ. Such a repair model is reasonable if the shipping time (which is ideally independent of the number of microinverters) is greater than the time taken to replace the faulty units. The stationary distribution for this chain is

$$\pi_0 = \left[1 + \sum_{i=1}^{n} \left(\prod_{k=1}^{i} \frac{\mu + (k-1)\lambda}{k\lambda} \right) \right]^{-1}, \tag{6.6}$$

$$\pi_i = \frac{\mu + (i-1)\lambda}{i\lambda} \pi_{i-1} \quad \forall\, 1 \leq i \leq n. \tag{6.7}$$

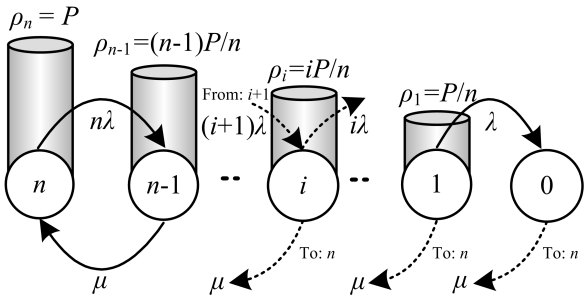

Figure 6.11: State-transition diagram for an n-microinverter PVECS.

For a system rated at P W comprising n microinverters, the reward vector and system capacity are given by

$$\rho = [\rho_0\, \rho_1 \ldots \rho_i \ldots \rho_n] = \left[0\, \frac{P}{n} \ldots \frac{iP}{n} \ldots P\right], \tag{6.8}$$

$$\Xi = \sum_{i=1}^{n} \rho_i \cdot \pi_i = \sum_{i=1}^{n} \frac{i}{n} \cdot P \cdot \pi_i, \tag{6.9}$$

where the stationary distribution follows from (6.6)-(6.7). In light of the complicated expressions above, the utility of the proposed numerical method in computing the stationary distribution and its sensitivity to variations in system parameters is immediately obvious.

6.4.1 Performance Metrics Variation with Number of Inverters

We evaluate the relationship between the number of inverters n, and the system capacity Ξ. Figure 6.12 depicts the system capacity as a function of the number of microinverters for three cases. In case 1, λ and μ are assumed to be the same as the base values, $\lambda = 1/10\,\mathrm{yr}^{-1}$ and $\mu = 365/10\,\mathrm{yr}^{-1}$, for all n. In case 2, λ is fixed to the base value, while μ is varied as shown in Fig. 6.13. In case 3, μ is fixed to the base value, while λ is varied as shown in Fig. 6.13. The monotonic reduction in λ captures possible circuit-level reliability improvements, while the monotonic increase in μ aims to quantify better repair policies. It emerges that with invariant failure and repair rates, Ξ is not a function of the number of microinverters, n. Improvements can only be made by reducing the failure rates or increasing the repair rates.

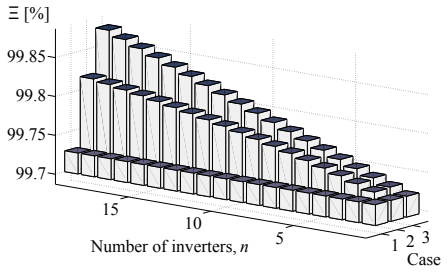

Figure 6.12: System capacity as a function of number of inverters.

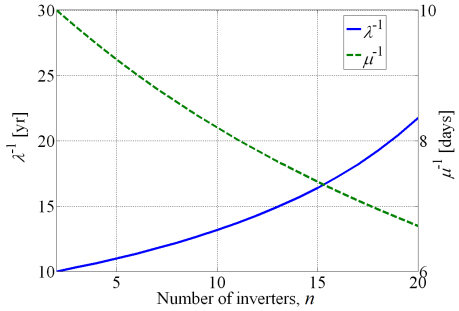

Figure 6.13: Illustrative failure and repair rates as a function of number of inverters adopted for case study.

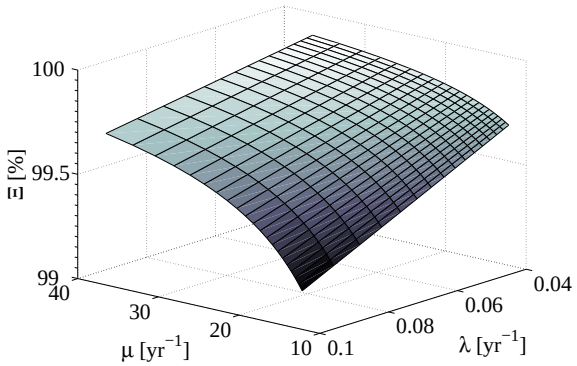

Figure 6.14: System capacity as a function of failure and repair rates for a microinverter system.

6.4.2 Application of Sensitivity Analysis to System Design

Consider the design of a grid-tied 5 kW PV array to be implemented with microinverters. Suppose the system is built with twenty module-integrated microinverters. System capacity is plotted as a function of λ and μ in Fig. 6.14. A particularly useful application of the sensitivity analysis is to suggest necessary failure and repair rates to meet a specified performance requirement. To the first order, the sensitivity formulation implies that

$$\Delta\Xi \approx \frac{\partial \Xi}{\partial \theta}\Delta\theta^T = \left[\frac{\partial \Xi}{\partial \theta_1}\,\frac{\partial \Xi}{\partial \theta_2}\ldots\frac{\partial \Xi}{\partial \theta_m}\right]\left[\Delta\theta_1\,\Delta\theta_2\,\ldots\Delta\theta_m\right]^T. \tag{6.10}$$

For instance, a performance change due to variations in failure rate can be estimated through

$$\Xi_1 \approx \Xi_0 + \frac{\partial \Xi}{\partial \lambda}(\lambda_1 - \lambda_0), \tag{6.11}$$

where variables subscripted by 0 are the nominal values. Referring to the 5 kW system considered above, it was noted that $\lambda_0 = 1/10\,\mathrm{yr}^{-1}$ and $\mu_0 = 365/10\,\mathrm{yr}^{-1}$, yielded $\Xi_0 = 99.73\%$. Suppose this were to be improved to $\Xi_1 = 99.90\%$ (with the same repair rate), (6.11) suggests that the required failure rate, $\lambda_1 = 1/26.667\,\mathrm{yr}^{-1}$. This can be verified numerically by calculating Ξ through (6.1).

6.5 Extensions and Future Work

In this section, we propose some avenues for future work to extend the methods proposed in this chapter.

6.5.1 Propagating PV Source Uncertainty to Reliability/Performability Metrics

As an alternative to the energy-yield estimation approach presented in the case studies, this section explores an explicit method to propagate input uncertainty to reliability metrics and PV energy-yield estimates. The first step is to reformulate the reward vector $\rho = [\rho_0, \rho_1, \ldots, \rho_n]$ as $R = [R_0, R_1, \ldots R_n]$, where R_i, $i = 0, 1, \ldots n$, are random variables. Then, we seek the mapping

$$R_i = f_i(S, \Delta), \tag{6.12}$$

where S and Δ are also random variables describing the incident insolation and ambient temperature at the given location. The function f_i captures the PV-system output in the i state and it can be formulated from standard PV performance models (see, e.g., [74]). Subsequently, system capacity, $\Xi = \pi \cdot R^T$, and energy yield, $\Gamma = \Xi \cdot T$, are also random variables. The pdfs of S and Δ, $f_S(s)$ and $f_\Delta(\delta)$, can be determined from field data or from analytical models. Then, the pdfs of the reward vector, system capacity, and energy yield, ($f_R(\rho)$, $f_\Xi(\xi)$, and $f_\Gamma(\gamma)$, respectively) can be determined through random variable transformation methods. Note that we tackle this problem (of propagating input uncertainty to reliability/performability

indices) in the context of wind energy conversion systems in the next chapter.

6.5.2 Considering Extenuating Distribution-System Conditions and Common-Cause Failures

PV inverters are designed to meet the IEEE 1547 standard, which prescribes active power curtailment in case there are sustained over-voltage, under-voltage, over-frequency, or under-frequency conditions in the distribution system. The Markov reward modeling framework can be easily extended to accommodate these phenomena as described next. Consider Fig. 6.15, which depicts a three-state example (similar to the one presented in Section III-B of the manuscript) augmented with an additional state 0_F in which the power output is curtailed due to the extenuating phenomena described above. The power output is ρ_i in state i, ρ_j in state j and zero in state 0_F and state 0—which corresponds to the state in which no power is produced due to component failures. Transitions between the states i, j and state 0_F are introduced at the rates λ_F and μ_F, which can be determined from statistics of field data. As in the models described in the case studies, transitions between the states i, j and state 0 are due to component failure and repair (governed by transition rates λ_i, λ_j, and μ). Finally, catastrophic failures that cause the entire system to fail (e.g., failure in protection equipment, simultaneous failure in multiple inverters) can be modeled by introducing common-cause failures at the rate λ_C. Now, the system capacity $\Xi = \pi_i\rho_i + \pi_j\rho_j$ factors in the probability of over/under voltage/frequency conditions that cause active power curtailment, as well as common-cause failures.

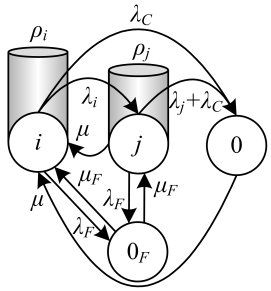

Figure 6.15: Addressing common-cause failures and under/over voltage/frequency conditions with Markov reward models.

Chapter 7

ESTIMATING WIND ENERGY CONVERSION SYSTEMS PERFORMABILITY METRICS

In this chapter, we provide a framework to quantify the impact of parametric and input uncertainty on the reliability/performability of wind farms (referred interchangeably as WECS). Parametric uncertainty in these models relates to the uncertainty in failure and repair rates of the constituent wind turbines in the farm. Input uncertainty relates to uncertainty in wind speed. The models presented here apply on longer time scales (months to years) and are useful for planning purposes; they cannot be applied, e.g., to quantify the uncertainty in wind farm power output on an hourly basis. The methods we will use to quantify the impact of parametric uncertainty are adopted from Chapter 3. The material presented here is partially adopted from [75].

7.1 Overview of Proposed Framework

The framework we propose is schematically illustrated in Fig. 7.1. Inputs to the framework are pdfs of the failure rate, repair rate, and wind speed (blocks 1, 2, and 5, respectively in Fig. 7.1). The two models that characterize the operation of the wind farm are: i) a Markov reliability/reward model (block 3 in Fig. 7.1) that describes failures and repairs in constituent wind turbines, and ii) the power versus wind speed characteristic (henceforth referred to as the $p - v$ characteristic) of the wind farm (block 6 in Fig. 7.1).

The Markov reliability models we explore are described by two parameters—the wind-turbine failure rate λ, and repair rate μ. The proposed methodology can easily be extended to more involved models with other transitions (e.g., common-cause failures [13]). Since λ and μ are not perfectly known, they are described by random variables L and M, with pdfs $f_L(\lambda)$ and $f_M(\mu)$, respectively, that are assumed to be known (blocks 1 and 2). These distributions are typically determined from

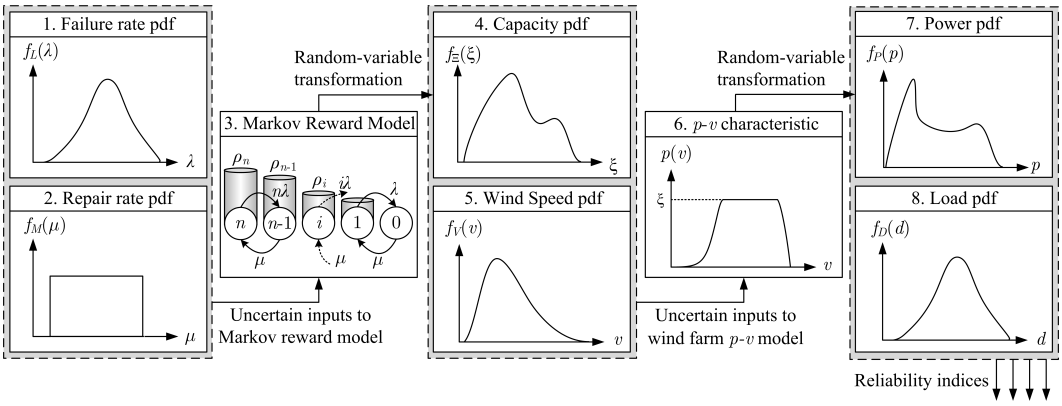

Figure 7.1: Block diagram illustrating proposed framework.

engineering experience or from field data [12,16,17]. State i of the underlying Markov chain corresponds to i operational turbines. The steady-state probability π_i captures the average time in state i, i.e., the average time with i operational turbines. The output of the Markov reward model is the wind farm capacity ξ, which is a measure of the expected rated power output of the wind farm. It is determined as the weighted sum of the rated power in each state of the chain—the weighting factors are the steady-state probabilities. Since the transition rates are uncertain, the steady-state probabilities are uncertain. Therefore, the wind farm capacity ξ is also uncertain and described by a random variable Ξ, with pdf $f_\Xi(\xi)$ that can be determined through random-variable transformations as explained in Section 7.3.2. The method relies on a Taylor-series expansion of the capacity as a function of the transition rates, since closed-form expressions are not assumed to be known. Taylor series coefficients are determined from the group inverse of the underlying Markov chain generator matrix as explained in Section 7.3.1.

The inputs to the $p - v$ characteristic are the wind farm capacity and the wind speed. Wind speed is described by a random variable V, with pdf $f_V(v)$, which is assumed to be known. The power output of the wind farm p is uncertain, and described by a random variable P. The pdf of P, $f_P(p)$, is also obtained through random-variable transformations. We propose a $p - v$ characteristic that has an analytical closed form, and further, it is invertible—consequently, it is straightforward to apply well-known numerical methods for random-variable transformation. Finally, the load d is described by a random variable D with pdf $f_D(d)$.

Given this framework, we compute wind generation indices such as the capacity

factor and expected generated wind energy, as well as generation adequacy indices such as the loss of load probability and expected energy not supplied. We will solve the above problem in two parts. First, we will concentrate on blocks 5, 6, and 7, i.e., we will assume that the wind farm capacity ξ is fully determined (no uncertainty in failure and repair rates), and that the only uncertainty is in the wind speed. Subsequently, we model the uncertainty in capacity due to uncertainty in failure and repair rates.

7.2 Quantifying Uncertainty in Wind Speed

The building blocks that capture this subset of the overall proposed framework are illustrated in the block diagram shown in Fig. 7.2. The first input to the framework is wind speed, modeled as a continuous random variable V, with pdf $f_V(v)$, which is assumed to be known. The framework also requires a statistical availability model for the wind farm; i.e., for a wind farm comprised of n turbines, the probabilities π_m, $m = 0, 1, \ldots, n$, where π_m is the probability that m turbines are operational. These inputs are propagated through the wind farm $p - v$ characteristic to obtain the pdf of the wind-farm power, denoted by $f_P(p)$. It is worth reiterating that since we do not model uncertainty in failure and repair rates, the probabilities π_m are not uncertain, and consequently, the system capacity is a fixed number.

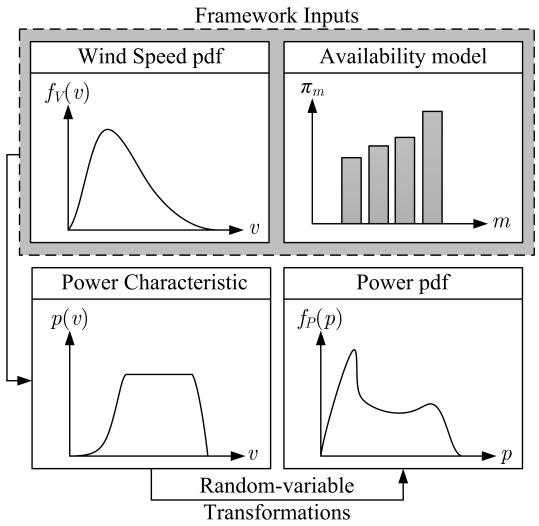

Figure 7.2: Propagating wind speed uncertainty to wind farm power output.

7.2.1 Wind Turbine $p - v$ Characteristic

Following standard terminology (see, e.g., [67]), denote the cut-in, rated, and furling wind speed of a wind turbine by v_c, v_r, and v_f, respectively. Further, denote the rated output power of the turbine by P_r. Let us consider the following piecewise continuous function to model the power output of the wind turbine p, as a function of wind speed v

$$p(v) = \begin{cases} p_1(v) & \text{for} \quad 0 \leq v \leq v_{lim}, \\ p_2(v) & \text{for} \quad v_{lim} < v \leq v_f, \end{cases} \tag{7.1}$$

where

$$p_1(v) = P_r - P_r \left[1 + \exp\left(\frac{v - v_{mid}}{c}\right)\right]^{-1}, \tag{7.2}$$

$$p_2(v) = P_r - P_r \alpha \left(v - v_{lim}\right)^q, \tag{7.3}$$

and where v_{mid}, c, α, and q are parameters that determine the shape of the functions [76]. We provide a brief note below on how the different parameters can be determined.

- The parameter v_{mid} is the wind speed at which the power output of the turbine is half the rated value, i.e., $p_1(v_{mid}) = P_r/2$. Hence it can be determined by inspecting wind-turbine data sheets.

- The parameter c can be tuned to ensure that the characteristic is within some predetermined percentage of the rated power, P_r, at the rated wind speed, v_r. For instance, if we require $p_1(v_r) = \beta \cdot P_r$ (typically $\beta \geq 0.99$ to ensure $p_1(v_r) \approx P_r$), it is easy to show

$$c = (v_r - v_{mid}) \left[\log\left(\frac{\beta}{1-\beta}\right)\right]^{-1}. \tag{7.4}$$

- The coefficient α that governs the polynomial dropoff is obtained by solving $p_2(v_f) = 0$, and is given by

$$\alpha = (v_f - v_{lim})^{-q}. \tag{7.5}$$

The function $p_2(v)$ is formulated to model a q-order drop-off in power output for wind speeds greater than a limiting wind speed, v_{lim}. The limiting wind speed can be chosen to be arbitrarily close to the furling speed. As will be shown in the case

studies in Section 7.2.5, a quadratic drop off ($q = 2$) models the output of an actual operating wind farm better than conventional models in which $v_{lim} = v_f$ so that $p_2(v) = 0 \; \forall v \geq v_f$. Figure 7.3 illustrates the $p - v$ characteristic for the Vestas V90-2.0 MW turbine [77]. Relevant turbine specifications and model parameters—extracted following the approach outlined above—are listed in Table 7.1.

Table 7.1: Parameters for the Vestas V90-2.0 MW wind turbine.

Symbol	Parameter	Value
P_r	Rated power	2 MW
v_c	Cut-in wind speed	4 m/s
v_r	Rated wind speed	12 m/s
v_{lim}	Limiting wind speed	24 m/s
v_f	Furling wind speed	25 m/s
c	Shape parameter that ensures $p_1(v_r) = \beta \cdot P_r$	0.7617 m/s
v_{mid}	Wind speed such that $p_1(v_{mid}) = P_r/2$	8.5 m/s
q	Order of drop off for $v > v_{lim}$	2
α	Parameter that ensures $p_2(v_f) = 0$	1 $(\text{m/s})^{-2}$

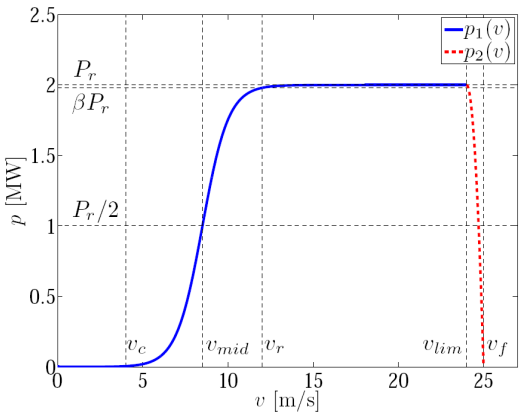

Figure 7.3: Sample $p - v$ characteristic for the Vestas V90-2.0 MW wind turbine.

7.2.2 Wind Farm $p - v$ Characteristic

Let us consider a wind farm comprising n identical wind turbines, with $p - v$ characteristics modeled by (7.1)-(7.3). If the turbines are staggered appropriately, interference effects can be minimized [67], and the $p - v$ characteristic of the farm is given

by[1]

$$p(v) = \begin{cases} p_1(v) & \text{for} \quad 0 \leq v \leq v_{lim}, \\ p_2(v) & \text{for} \quad v_{lim} < v \leq v_f, \end{cases} \tag{7.6}$$

where

$$p_1(v) = \xi - \xi \left[1 + \exp\left(\frac{v - v_{mid}}{c} \right) \right]^{-1}, \tag{7.7}$$

$$p_2(v) = \xi - \xi\alpha \left(v - v_{lim} \right)^q. \tag{7.8}$$

The wind farm capacity (which is basically the expected rated power of the farm) is denoted by ξ, and defined as

$$\xi = \omega \cdot P_r, \tag{7.9}$$

where P_r is the rated power output of a single turbine, and ω is the expected number of turbines during the period of study given by

$$\omega = \pi_0 \cdot 0 + \pi_1 \cdot 1 + \cdots + \pi_n \cdot n, \tag{7.10}$$

where π_m is the probability that m turbines are operational. As described in the introduction to this chapter, the probabilities π_i, $i = 0, 1, \ldots, n$, can be obtained from a Markov availability model (see, e.g., [3,4]). Alternately, they can be obtained from field data. Also note that the wind farm capacity in this model is a fixed number (since we do not model uncertainty in failure and repair rates yet). Subsequently, in Section 7.3, we will assume that the wind turbine failure and repair rates are uncertain. Consequently, the capacity will be described by a random variable Ξ, whose pdf $f_\Xi(\xi)$, will be determined following the methods outlined in Chapter 3.

7.2.3 Propagating Wind-Speed Uncertainty to the Wind-Farm Power Output

Suppose the wind speed is described by a random variable V, with pdf $f_V(v)$, which is assumed to be known. Applying random-variable transformations to (7.6), we get

$$f_P(p) = \frac{f_V(v_1)}{|p_1'(v_1)|} + \frac{f_V(v_2)}{|p_2'(v_2)|}, \tag{7.11}$$

[1] We abuse notation and denote the $p - v$ characteristic of the wind farm by $p(v)$. However, as expressed in (7.6)-(7.8), the rated power is different from that in (7.1)-(7.3). Subsequently, we will only be dealing with the $p - v$ characteristic of the wind farm as described in (7.6)-(7.8).

where v_1 and v_2 can be obtained by inverting the $p_1(v)$, $p_2(v)$ characteristics in (7.7)-(7.8) as follows:

$$v_1 = v_{mid} + c \cdot \log\left(\frac{p}{\xi - p}\right), \tag{7.12}$$

$$v_2 = v_{lim} + \left(\frac{1}{\alpha}\frac{\xi - p}{\xi}\right)^{1/q}. \tag{7.13}$$

The expressions for $p_1'(v)$ and $p_2'(v)$ in (7.11) can be obtained by differentiating (7.7)-(7.8) which results in

$$p_1'(v) = \frac{\xi}{c}\exp\left(\frac{v - v_{mid}}{c}\right)\left[1 + \exp\left(\frac{v - v_{mid}}{c}\right)\right]^{-2}, \tag{7.14}$$

$$p_2'(v) = -2\alpha\xi(v - v_{lim}). \tag{7.15}$$

The equation in (7.11) follows from well-known random-variable transformation methods [51]. In the context of propagating wind-speed uncertainty, these methods require inverting the $p - v$ characteristic for each value of p—which is easy given the form of $p(v)$ in (7.7)-(7.8).

Wind speed pdf $f_V(v)$ can be obtained by fitting field data with standard distributions. For instance the Weibull distribution

$$f_V(v) = \frac{b}{a^b}v^{b-1}\exp\left(-\frac{v}{a}\right)^b, \tag{7.16}$$

where b is called the *shape parameter* and a is called the *scale parameter*, has been widely adopted to model wind-speed statistics [67, 78]. By way of notation, $V \sim \mathcal{W}(a, b)$ denotes a Weibull-distributed random variable V with scale parameter a, and shape parameter b. While we utilize the Weibull distribution in the case studies that follow, note that the method proposed above is agnostic to the wind-speed distribution.

We want to point out that the above method is accurate when the maximum wind speed at the location is less than the cut-out speed. As part of future work, we will augment the $p - v$ characteristic to model the extenuating case when the maximum wind speed at the location is expected to be significantly higher than the cut-out speed. If the power output is assumed to be zero beyond this value, mixed distributions will be obtained.

7.2.4 Computer Implementation

Algorithm 4 provides the pseudocode for computer implementation of the method outlined in (7.11)-(7.15) to compute $f_P(p)$. Since (7.11) has to be evaluated pointwise, p is appropriately discretized between p_{min} and p_{max} in steps of dp to obtain the vector $\bar{p} = [p_{min} : dp : p_{max}]$. In the for loop, $f_P(p)$ is evaluated pointwise for each entry of $\bar{p}$, which we denote by $\hat{p}$. This involves computing v_1 and v_2 through (7.12)-(7.13), $p_1'(v_1)$ and $p_1'(v_1)$ through (7.14)-(7.15), and then applying (7.11).

Algorithm 4 Computation of $f_P(p)$.

define $\bar{p} = [p_{min} : dp : p_{max}]$
Model parameters: v_c, v_r, v_{lim}, v_f, α, β, c, q, P_r
Expected number of operational wind turbines ω
Wind farm capacity $\xi = \omega P_r$
Wind-speed pdf $f_V(v)$
for $\hat{p} = p_{min} : dp : p_{max}$ **do**
compute $v_1 = v_{mid} + c \cdot \log\left(\frac{\hat{p}}{\xi - \hat{p}}\right)$
$v_2 = v_{lim} + \left(\frac{1}{\alpha}\frac{\xi - \hat{p}}{\xi}\right)^{1/q}$
compute $p_1'(v_1) = \frac{\xi}{c}\exp\left(\frac{v_1 - v_{mid}}{c}\right)\left[1 + \exp\left(\frac{v_1 - v_{mid}}{c}\right)\right]^{-2}$
$p_2'(v_2) = -2\alpha\xi(v_2 - v_{lim})$.
compute $f_P(\hat{p}) = \frac{f_V(v_1)}{|p_1'(v_1)|} + \frac{f_V(v_2)}{|p_2'(v_2)|}$
end for

7.2.5 Model Validation

In this section, we validate the proposed approach by comparing the wind farm power pdf with results obtained from actual field data. We have access to 1-second data for number of operational turbines, wind speed, and wind-farm power output recorded at a wind farm comprising $n = 75$ turbines over a period of two months. The goal of this case study is to demonstrate that the method proposed in Algorithm 4 can be used to accurately extract the pdf of the wind-farm power output by comparing the results with the field data.

The methodology comprises the following steps: i) obtain a statistical availability model of the turbines in the farm, ii) fit the pdf of recorded wind speed at the site with a Weibull distribution, iii) formulate the $p - v$ characteristic of the wind farm through (7.6)-(7.8), iv) propagate wind speed uncertainty through (7.11)-(7.15).

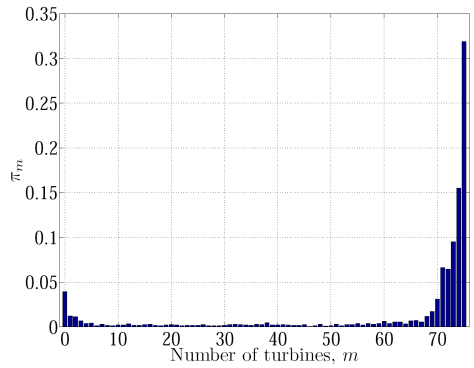

Figure 7.4: Availability of turbines in the wind farm.

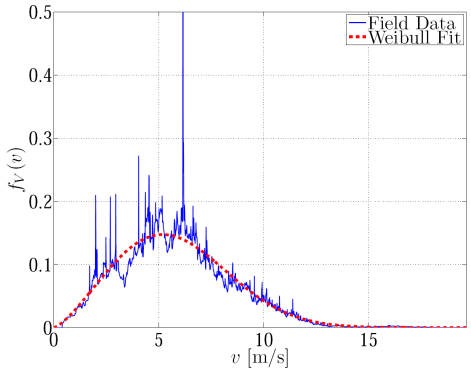

Figure 7.5: Weibull fit to distribution of wind speeds collected in the field.

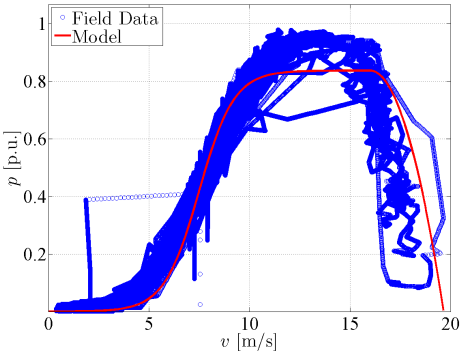

Figure 7.6: Field data compared to proposed $p - v$ characteristic.

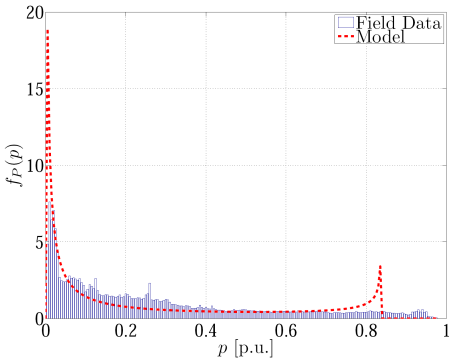

Figure 7.7: Distributions for power compared.

These steps follow along Algorithm 4, and they are explained in detail subsequently.

As stated above, we first determine a statistical availability model for the wind farm. In the context of the discussion in Section 7.2.2, this involves determining the probabilities π_m, $m = 0, 1, \ldots, n$, where π_m is the probability that the wind farm has m operational turbines. From the available data on number of wind turbines, π_m can be computed as

$$\pi_m = \frac{N_m}{N}, \tag{7.17}$$

where N_m is the number of seconds with m operational turbines, and $N = 2 \cdot 30 \cdot 24 \cdot 60 \cdot 60$ s, the number of seconds in 2 months—which is the duration of the observed period. The results are plotted in Fig. 7.4, and from (7.10), we get the expected number of operational turbines, $\omega = 62.7461$.

In the next step, a Weibull distribution is fitted to the distribution of wind speed

utilizing MATLAB's *dfittool* function. The resulting scale and shape parameters are $a = 6.54818$ m/s, and $b = 2.35952$, respectively. Figure 7.5 plots the Weibull fit and the distribution computed from the raw wind speeds. The results show excellent agreement.

Next, we determine the $p - v$ characteristic of the wind farm. Figure 7.6 plots the $p - v$ characteristic of the wind farm computed from (7.6)-(7.8) and it also plots the raw power data as a function of wind speed. Finally, we follow along the steps in Algorithm 4 to determine the distribution $f_P(p)$ and compare the results with the field data. Results plotted in Fig. 7.7 show good agreement over a wide power range. The mean power from the field data is equal to 0.2673 p.u., while that computed using the proposed method is 0.2374 p.u.

7.3 Quantifying Uncertainty in Failure and Repair Rates

In this section, we describe how to extend the uncertainty model presented in Section 7.2 to accommodate uncertainty in turbine failure and repair rates. This will allow us to completely describe the uncertainty propagation method depicted in Fig. 7.1.

7.3.1 Wind Farm Markov Reward Model[2]

The wind-farm Markov reward model is comprised of a Markov chain that takes values in a set $\mathcal{Q}$, and a reward function $\varrho : \mathcal{Q} \to \mathbb{R}$ that maps each element i of $\mathcal{Q}$ into a real-valued quantity ρ_i that quantifies some notion of wind farm performance while in configuration i. A long-term measure of performance can be described by the reward

$$\xi = \sum_{i=0}^{n} \rho_i \pi_i = \pi \cdot \rho^T, \tag{7.18}$$

where $\pi = [\pi_0, \pi_1, \ldots, \pi_n]$ is the Markov-chain stationary distribution and $\rho = [\rho_0, \rho_1, \ldots, \rho_n]$ is the reward vector. In the context of the models we describe here, the reward is the wind farm capacity. To explicitly represent the dependence of the stationary distribution and system capacity on the failure and repair rates, they are expressed as $\pi(\theta)$ and $\xi(\theta)$, respectively, where $\theta = [\lambda, \mu]$. Also recall from Section

[2]For a comprehensive overview of Markov reward models, please refer Chapter 2. Here, we provide a brief overview of key aspects.

2.4, that the sensitivity of the reward to the i parameter, θ_i, can be expressed as

$$\frac{\partial^k \xi(\theta)}{\partial \theta_i^k} = \frac{\partial^k \pi(\theta)}{\partial \theta_i^k} \rho^T = k! \, (-1)^k \, \pi(\theta) \left(\frac{\partial \Lambda}{\partial \theta_i} \Lambda^{\#} \right)^k \rho^T, \tag{7.19}$$

where $\Lambda^{\#}$ is the group inverse of the generator matrix and $\pi(\theta)$ is the stationary distribution of the chain.

Reliability and performability indices of interest can be easily recovered from the above formulation by appropriate choice of the reward. For instance, if the values that the reward function ϱ takes are defined in per-unit time, e.g., energy produced per unit time, then ξ describes the average rate at which the system will deliver/consume some quantity that measures the system performance, e.g., energy production [8]. In the context of this work, we recover the definition of system capacity in (7.9) by choosing

$$\rho_i = i \cdot P_r, \, i = 0, \, 1, \ldots, \, n. \tag{7.20}$$

7.3.2 Propagating Uncertainty in Failure and Repair Rates to Wind-Farm Capacity

In this section, we summarize numerical methods proposed in Chapter 3 to compute the pdf of the wind farm capacity, given the Markov chain generator matrix and the model-parameter pdfs. Let $\Theta = [\Theta_1, \, \Theta_2] = [L, \, M]$ be the vector of random variables that describe the failure and repair rates. It is assumed that L and M are independent, and that their pdfs, $f_L(\lambda)$ and $f_M(\mu)$, are known. Therefore, the steady-state probabilities are random variables that can be collectively described by a random vector $\Pi = [\Pi_0, \, \Pi_1, \, \ldots, \, \Pi_n]$, where $\Pi_i = \pi_i(\Theta)$ with pdf $f_{\Pi_i}(\pi_i)$. Similarly, the capacity, $\Xi = \xi(\Theta) = \Pi(\Theta) \cdot \rho^T$, is a random variable with pdf $f_\Xi(\xi)$. Following the method proposed in Chapter 3, to derive $f_\Xi(\xi)$, $\xi(\Theta)$ is first approximated by a Taylor-series polynomial expansion. The Taylor series coefficients are the sensitivities $\partial^k \xi(\theta)/\partial \theta^k$. In general, obtaining these sensitivities is a difficult task; however, they can be computed from the generator-matrix group inverse as shown in (7.19). Once the polynomial characterization is available, an extension of Lemma 1—that accommodates multiple parameters—can be applied to compute $f_\Xi(\xi)$ by evaluating the roots of the polynomial approximations, which are easy to obtain numerically. The procedure was described in detail for general reward models in Section 3.4, and

is summarized below for the specific two-parameter case (the parameters in this case are the failure rate and the repair rate).

7.3.2.1 Determining the pdf of $f_{\Xi}(\xi)$

First, we pick a parameter, say the failure rate λ, and seek the Taylor series expansion of ξ around μ_L, the mean of L, with the other parameter, μ, fixed. To do so, begin by expressing Θ as

$$\Theta = \mu_\Theta + \Delta\Theta, \tag{7.21}$$

where $\mu_\Theta = [\mu_L, \mu]$ and $\Delta\Theta = [\Delta L, 0]$—$\Delta L$ is a zero-mean random variable with pdf $f_{\Delta L}(\Delta\lambda) = f_L(\mu_L + \Delta\lambda)$. Then, applying a Taylor-series expansion, we can express

$$\begin{aligned} \Xi &= \xi(\Theta) = \xi(\mu_\Theta + \Delta\Theta) = \xi(\mu_\Theta) + \sum_{k=1}^{\infty} \frac{c_k}{k!} \Delta L^k \\ &= \pi(\mu_\Theta)\rho^T + \sum_{k=1}^{\infty} \frac{c_k}{k!} \Delta L^k. \end{aligned} \tag{7.22}$$

The k-order Taylor series coefficient, c_k, follows from (7.19):

$$c_k = k!\,(-1)^k\,\pi(\theta)\left(\frac{\partial\Lambda(\theta)}{\partial\lambda}\Lambda^{\#}\right)^k \rho^T\Big|_{\theta=\mu_\Theta}. \tag{7.23}$$

We then express $\Xi = x(\Delta L)$, where x is a polynomial function with real coefficients obtained by truncating the Taylor series in (7.22) at the t term:

$$\Xi = x(\Delta L) = \pi(\mu_\Theta)\rho^T + \sum_{k=1}^{t} \frac{c_k}{k!} \Delta L^k. \tag{7.24}$$

Then, applying Lemma 1 we get

$$f_{\Xi|M}(\xi|\mu) = \sum_{j=1}^{r} \frac{f_{\Delta L}(\Delta\lambda_j)}{|x'(\Delta\lambda_j)|}, \tag{7.25}$$

where $\Delta\lambda_1, \Delta\lambda_2, \ldots \Delta\lambda_r$ are the $r \leq t$ roots of $\xi = x(\Delta\lambda)$ and

$$x'(\Delta\lambda_j) := \left.\frac{dx(\Delta\lambda)}{d\Delta\lambda}\right|_{\Delta\lambda=\Delta\lambda_j} = \sum_{k=1}^{t} \frac{c_k}{(k-1)!}\Delta\lambda_j^{k-1}. \tag{7.26}$$

Applying the total probability theorem, and acknowledging the independence of L and M, it follows that

$$f_{\Xi}(\xi) = \int_{\mu} f_{\Xi|M}(\xi|\mu)\, f_M(\mu) d\mu. \tag{7.27}$$

7.3.2.2 Computer implementation

Algorithm 5 provides the pseudocode for computer implementation of the method outlined in (7.21)-(7.27) to compute $f_{\Xi}(\xi)$ given $f_L(\lambda)$ and $f_M(\mu)$. The vector $\bar{\xi} = [0 : d\xi : \|\rho\|_1 \cdot P_r]$ is formulated based on the one-norm of ρ, since $\xi = \left(\pi\rho^T\right) \cdot P_r$ and $0 \leq \pi_i \leq 1$, $\forall i = 0, 1, \ldots, n$. The vector $\bar{\mu} = \left[\mu^{start} : d\mu : \mu^{end}\right]$ is defined so that it spans several standard deviations on both sides of μ_M, the mean of M. The nested for loops ensure that the conditional pdf in (7.25) is evaluated point wise for the entries in $\bar{\mu}$. The QR factorization of the generator matrix is evaluated for every $[\mu_L, \hat{\mu}]$, where $\hat{\mu}$ denotes an entry of the vector $\bar{\mu}$. Next $\pi_i(\hat{\theta})$ is obtained from (2.12) by normalizing the last column of Q, the group inverse $\Lambda^{\#}$ is obtained from (2.13), and the Taylor series coefficients, c_k, $k = 1, 2, \ldots, t$ are computed using (7.23). The r real roots of the equation $\hat{\xi} = x(\Delta\lambda)$ are computed and the conditional $f_{\Xi|M}\left(\hat{\xi}|\hat{\mu}\right)$ follows from (7.25)-(7.26). The integrals at the end of the nested for loop can be implemented using some numerical integration scheme, e.g., the trapezoidal method.

7.3.3 Determining the Wind Farm Power Output pdf

Given the pdfs of the capacity $f_{\Xi}(\xi)$ and the pdf of the wind speed $f_V(v)$ (recall (7.16)), we can now determine the wind farm power output pdf $f_P(p)$. The approach closely mirrors the method outlined in Section 7.2.3. Applying random-variable transformations to (7.6), we get

$$f_{P|\Xi}(p|\xi) = \frac{f_V(v_1)}{|p_1'(v_1)|} + \frac{f_V(v_2)}{|p_2'(v_2)|}, \tag{7.28}$$

Algorithm 5 Computation of $f_{\Xi}(\xi)$ given $f_L(\lambda)$ and $f_M(\mu)$.

define $\rho = [\rho_0, \rho_1, \ldots, \rho_n]$, $\bar{\xi} = [0 : d\xi : \|\rho\|_1 \cdot P_r]$, $\bar{\mu} = \left[\mu^{start} : d\mu : \mu^{end}\right]$.
define Taylor series order t
compute $\frac{\partial \Lambda}{\partial \lambda}$
for $\hat{\xi} = 0 : d\xi : \|\rho\|_1$ **do**
  for $\hat{\mu} = \mu^{start} : d\mu : \mu^{end}$ **do**
    compute $QR = \Lambda(\hat{\theta})$ where $\hat{\theta} = [\mu_{\Theta_1}, \hat{\mu}]$
    compute $\xi(\hat{\theta}) = \pi(\hat{\theta}) \cdot \rho^T$ (2.12), $\Lambda^{\#}$ (2.13), c_k, $k = 1, 2, \ldots, t$ (7.23)
    compute real roots of $\xi(\hat{\theta}) - \hat{\xi} + \sum_{k=1}^{t} \frac{c_k}{k!} \Delta\lambda^k = 0$, $\Delta\lambda_j$, $j = 1, \ldots, r$
    for $j = 1$ to r **do**
      compute $f_{\Delta L}(\Delta\lambda_j)$, and $x'(\Delta\lambda_j) = \sum_{k=1}^{t} \frac{c_k}{(k-1)!} \Delta\lambda_j^{k-1}$
    end for
    compute $f_{\Xi|M}\left(\hat{\xi}|\hat{\mu}\right) = \sum_{j=1}^{r} \frac{f_{\Delta L}(\Delta\lambda_j)}{|x'(\Delta\lambda_j)|}$
  end for
compute $f_{\Xi}(\hat{\xi}) = \int_{\mu} f_{\Xi|M}(\hat{\xi}|\mu) f_M(\mu) d\mu$
end for

where v_1 and v_2 are given by (7.12), (7.13), and $p_1'(v)$ and $p_2'(v)$ are given by (7.14), (7.15). Assuming that wind speed and system capacity are independent, by applying the total probability theorem we can obtain the pdf of the wind-farm output from $f_{P|\Xi}(p|\xi)$ (7.28) and $f_{\Xi}(\xi)$ (7.27) as follows:

$$f_P(p) = \int_{\xi} f_{P|\Xi}(p|\xi) f_{\Xi}(\xi) d\xi. \tag{7.29}$$

7.3.3.1 Computer implementation

Algorithm 6 provides the pseudocode for computer implementation of the method outlined in (7.28)-(7.29) to compute $f_P(p)$. Since (7.28) has to be evaluated pointwise, p is appropriately discretized between p_{min}(chosen to be close to 0) and p_{max} (chosen to be close to P_r^{ξ}) in steps of dp to obtain the vector $\bar{p} = [p_{min} : dp : p_{max}]$. In the for loop, $f_P(p)$ is evaluated pointwise for each entry of $\bar{p}$, which we denote by $\hat{p}$. This involves computing v_1 and v_2 through (7.12), (7.13), $p_1'(v_1)$ and $p_1'(v_1)$ through (7.14), (7.15), and then applying (7.28). Notice that this algorithm closely follows along Algorithm 4, except in this case we model the uncertainty in the wind

farm capacity.

Algorithm 6 Computation of $f_P(p)$.

define $\bar{p} = [p_{min} : dp : p_{max}]$
define model parameters: v_c, v_r, v_{lim}, v_f, α, β, c, q, P_r
define Capacity pdf, $f_\Xi(\xi)$ obtained from Algorithm 5
define Wind-speed pdf, $f_V(v)$
for $\hat{p} = p_{min} : dp : p_{max}$ **do**
  for $\hat{\xi} = 0 : d\xi : \|\rho\|_1 \cdot P_r$ **do**
    compute $v_1 = v_{mid} + c \cdot \log\left(\frac{\hat{p}}{\hat{\xi}-\hat{p}}\right)$
    compute $v_2 = v_{lim} + \left(\frac{1}{\alpha}\frac{\hat{\xi}-\hat{p}}{\hat{\xi}}\right)^{1/q}$
    compute $p_1'(v_1) = \frac{\hat{\xi}}{c}\exp\left(\frac{v_1-v_{mid}}{c}\right)\left[1+\exp\left(\frac{v_1-v_{mid}}{c}\right)\right]^{-2}$
    compute $p_2'(v_2) = -2\alpha\hat{\xi}(v_2 - v_{lim})$.
    compute $f_{P|\Xi}(\hat{p}|\hat{\xi}) = \frac{f_V(v_1)}{|p_1'(v_1)|} + \frac{f_V(v_2)}{|p_2'(v_2)|}$
  end for
  compute $f_P(\hat{p}) = \int_\xi f_{P|\Xi}(\hat{p}|\xi)\, f_\Xi(\xi) d\xi$
end for

7.3.4 Wind Generation Indices

The proposed framework can be utilized to compute common wind generation indices that gauge the reliability/performability of wind farms [3, 4]. We introduce some metrics of interest below and explain how they can be computed.

7.3.4.1 Installed Wind Power, IWP

The installed wind power is the sum of nominal rated power of all turbines

$$\text{IWP} = n \times P_r\,[\text{MW}]. \tag{7.30}$$

7.3.4.2 Installed Wind Energy, IWE

The installed wind energy is the maximum possible energy that can be extracted in one year from the wind farm

$$\text{IWE} = \text{IWP}\,[\text{MW}] \times 8760\,\left[\frac{\text{hr}}{\text{yr}}\right]. \tag{7.31}$$

7.3.4.3 Expected Available Wind Energy, EAWE

The energy expected to be generated by the wind farm in one year without considering wind-turbine failure is

$$\text{EAWE} = \int_{p} p \cdot \left. f_P(p) \right|_{\omega=n} dp \,[\text{MW}] \times 8760 \left[\frac{\text{hr}}{\text{yr}}\right]. \tag{7.32}$$

To compute this index, we need the expected power output of the wind-farm without considering wind-turbine failure. The pdf of the power output without any failures, $\left. f_P(p) \right|_{\omega=n}$, can be computed following the procedure in Section 7.2.3, with $\omega = n \Rightarrow \xi = n \cdot P_r$.

7.3.4.4 Expected Generated Wind Energy, EGWE

The energy expected to be generated by the wind farm in one year considering wind-turbine failures and repairs is

$$\text{EGWE} = \int_{p} p \cdot f_P\left(p\right) dp \,[\text{MW}] \times 8760 \left[\frac{\text{hr}}{yr}\right]. \tag{7.33}$$

To compute this index, we need the expected power output of the wind-farm while accommodating failures and repairs through an availability model.

7.3.4.5 Capacity Factor, CF

The capacity factor of the wind farm without considering wind-turbine failure is

$$\text{CF} = \frac{\text{EAWE}}{\text{IWE}}. \tag{7.34}$$

7.3.4.6 Wind Generation Availability Factor, WGAF

The capacity factor of wind farm considering failures and repairs is

$$\text{WGAF} = \frac{\text{EGWE}}{\text{IWE}}. \tag{7.35}$$

This is the capacity factor of the the wind farm while factoring in failures and repairs of the wind turbines.

7.3.4.7 Loss of Load Probability, LOLP

The loss of load probability (LOLP) is the probability of the event that the demand exceeds the generation capacity. Denote the demand/load over the period of study by d. We model the demand as a random variable D with pdf $f_D(d)$, which can be determined from historical data. Given distributions for P and D, define the unserved load, $U = P - D$. The loss of load probability, LOLP $= \Pr\{U = P - D < 0\}$. To compute this metric, we first determine the pdf of $U = P - D$ by convolving $f_P(p)$ and $f_D(-d)$, and then integrate over the region that $P - D$ is negative.

7.3.4.8 Expected Energy Not Supplied (EENS):

The EENS provides an estimate of the energy not supplied to the load over the period of investigation. This metric can be computed from the pdf of the random variable $U = P - D$ as follows:

$$\text{EENS} = \left| \int_{u_{min}}^{0} u f_U(u) du \right| [\text{MW}] \times 8760 \left[\frac{\text{hr}}{\text{yr}} \right], \tag{7.36}$$

where $u_{min} < 0$ is the minimum value that the random variable U takes.

7.4 Case Studies that Demonstrate Impact of Input and Parametric Uncertainty

In this section, we present two case studies. The first describes how the proposed framework can be utilized to compute the wind generation indices explained above, when there is no uncertainty in turbine failure and repair rates. The next case study examines the case where there is uncertainty in both wind speed and turbine failure and repair rates.

7.4.1 Computing Wind Generation Indices

In this case study, we demonstrate the applicability of the proposed framework in computing the wind generation indices listed in Section 7.3.4. Consider a wind farm comprised of $n = 50$ wind turbines with specifications in Table 7.1. We will investigate wind-generation indices for wind regimes characterized by the Weibull distributions in Fig. 7.8. The installed wind power can be computed from (7.30) as $\text{IWP} = n \cdot P_r = 50 \times 2 = 100\,\text{MW}$. Similarly, the installed wind energy can be computed from (7.31) as $\text{IWE} = \text{IWP} \times 8760 = 8.76 \times 10^5\,\text{MWhr}$.

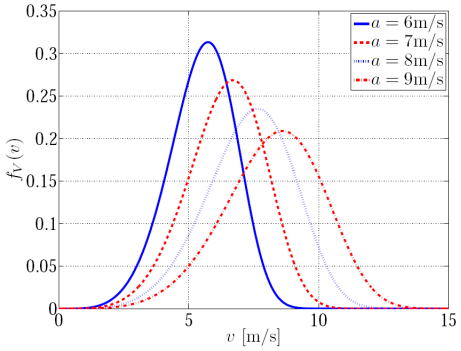

Figure 7.8: Representative Weibull distributions (a varied, $b = 5$) to model wind speeds.

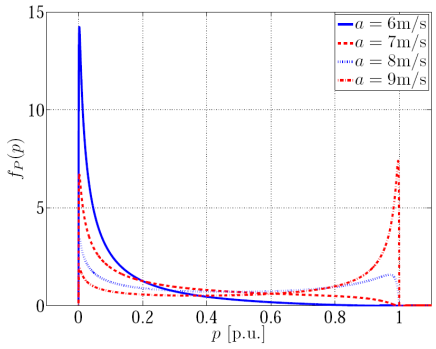

Figure 7.9: Power distribution computed for the wind-speed distributions in Fig. 7.8

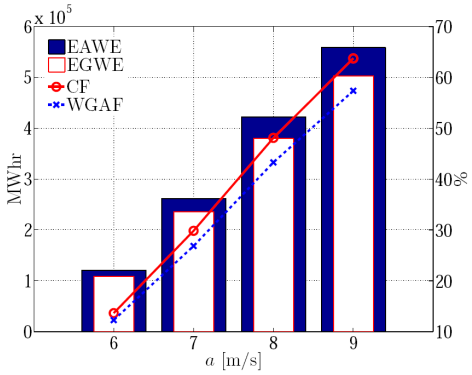

Figure 7.10: Wind generation indices as a function of the scale parameter.

Figure 7.9 depicts the pdfs $f_P(p)$ computed for wind speeds modeled by Weibull distributions in Fig. 7.8 assuming no wind-turbine failures. The base power corre-

sponding to 1 p.u. is 100 MW, the IWP. Figure 7.10 depicts the expected available wind energy (EAWE), expected generated wind energy (EGWE), capacity factor (CF), and wind generation availability factor (WGAF) as a function of the scale parameter a, assuming $\xi = 0.9 \times n$, i.e., 45 turbines are expected to operate on average. These indices are computed from (7.32)-(7.35).

7.4.2 Quantifying the impact of Input and Peripatetic Uncertainty

Consider a wind farm comprised of $n = 100$ turbines. The wind-turbine parameters are listed in Table 7.1. Without loss of generality, wind speed is modeled by a Weibull distribution, turbine failure rate and the load are modeled by normal distributions, and the turbine repair rate is modeled by a uniform distribution. Details on the distributions are provided in Table 7.2. The results below demonstrate how the proposed framework can be applied to compute the generation-adequacy and wind-generation indices described in Section 7.3.4.

Table 7.2: Distributions of uncertain inputs and model parameters used in the case study described in Section 7.4.2.

Symbol	Parameter	Value
$L \sim \mathcal{N}(\mu_L, \sigma_L^2)$	Wind-turbine failure rate	$\mu_L = 1$ yr^{-1}, $\sigma_L = 10\% \cdot \mu_L$
$M \sim \mathcal{U}(a_M, b_M)$	Wind-turbine repair rate	$a_M = 80$ yr^{-1}, $b_M = 100$ yr^{-1}
$V \sim \mathcal{W}(a, b)$	Wind speed	$a = 7$ m/s, $b = 9$
$D \sim \mathcal{N}(\mu_D, \sigma_D^2)$	Wind-farm load	$\mu_D = 25$ MW, $\sigma_D = 10\% \cdot \mu_D$

Figures 7.11 (a), (b) depict the generation adequacy and wind generation indices as a function of the mean wind speed, μ_V. Figures 7.11 (c), (d) depict the generation adequacy and wind generation indices computed for different mean wind-turbine failure rates. And finally, Figs. 7.11 (e), (f) depict the generation adequacy and wind generation indices as the mean repair rate is increased. An interesting observation is the precipitous change in the LOLP index as the mean repair rate changes from 2-3 and the mean failure rate changes from 1-2.

In Fig. 7.11, we also superimpose relevant results from repeated Monte Carlo simulations to demonstrate the validity of the analytical approach. These are obtained by repeatedly sampling distributions of the parameters and inputs and computing

the relevant indices with the $p - v$ characteristic.

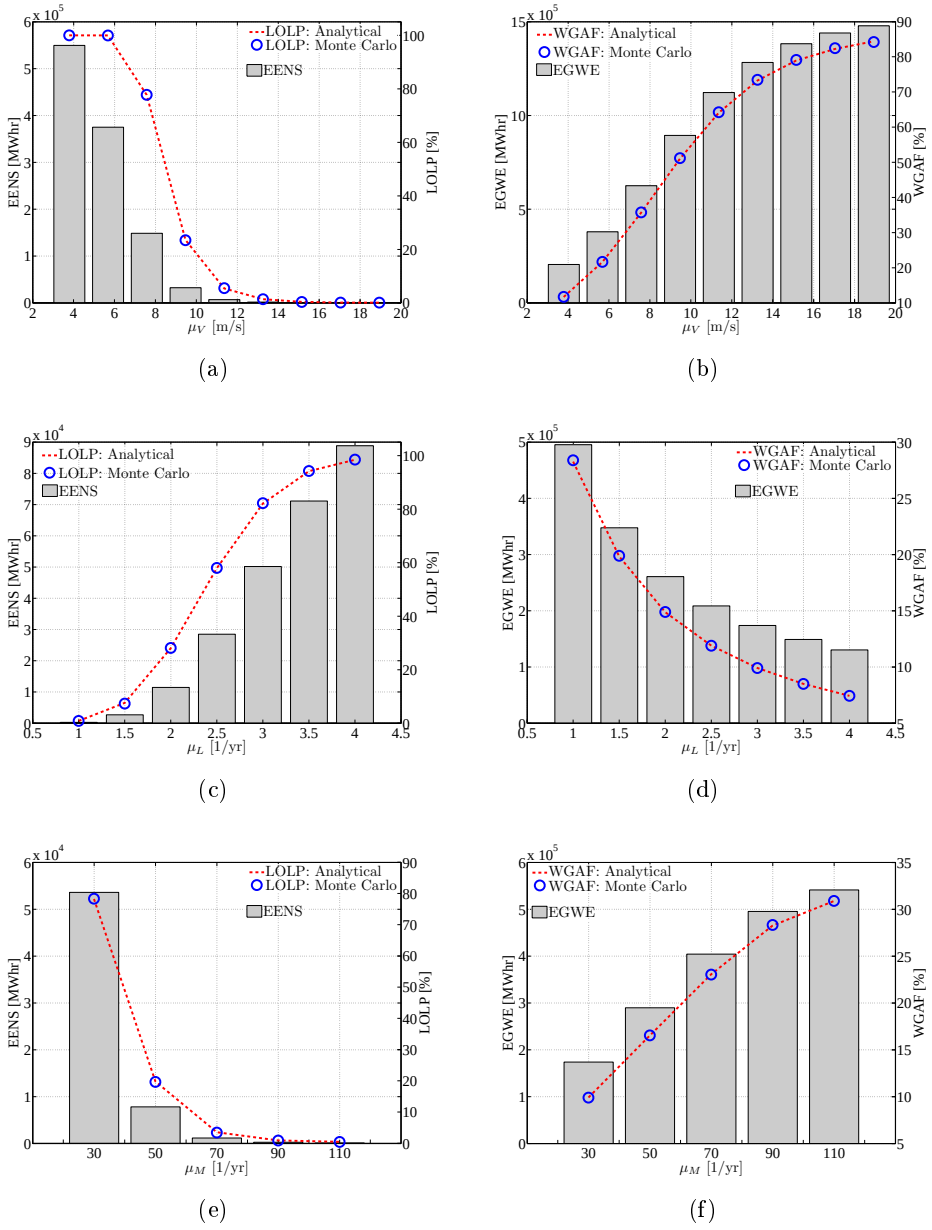

Figure 7.11: Reliability and performability indices as a function of mean wind speed, repair rate, and failure rate.

Chapter 8

IMPACT OF RENEWABLE RESOURCE VARIABILITY ON POWER SYSTEM DYNAMICS—AN SHS APPROACH

In this chapter, we explore a stochastic small-signal power system model cast in the SHS framework. The general DAE model that describes the evolution of the electromechanical states of the power system is linearized around nominal values of real/reactive power injections (corresponding to some nominal mode). With regard to the SHS model prescribed in (5.2), this implies that f and g are linear/affine in the state. As the mode $Q(t)$ evolves (governed by the transition rates), so do the real/reactive power injections—we describe how this can be used to model renewable resource variability in Section 8.3. Subsequently, we apply results from [30, 32] to obtain the moments of the electromechanical states of the power system. We further assume that the transition rates are not a function of the continuous state. Under these assumptions, the differential equations that govern the evolution of the moments of the state are finite dimensional, and moment-closure methods are unnecessary.

The assumptions that we make are not restrictive. Indeed, linear models are widely used to study the impact of small-signal disturbances on power-system stability. Similarly, with constant/time-dependent transition rates, we can model a wide class of stochastic disturbances in power injections. It is worth noting that moment-closure methods tailored to SHS (which as we have mentioned above, need to be applied when, e.g., the transition rates are a function of the continuous state) are well developed (see, e.g., [31, 32] and the references therein). Since this work represents the first application of SHS to stochastic small-signal power systems analysis, we restrict attention to linearized models, with state-independent transition rates so that moment closure methods are unnecessary.

We want to point out that our methodology is closely related to [79] (see also [80, 81] for related work), which established a framework for probabilistic steady-state and dynamic security assessment of power systems. The authors in [79] consider

different modes that the power system can transition between in a stochastic fashion, and derive a linear differential equation whose solution yields the distribution of a performance metric—this is done from first principles, and SHS tools are not employed. In [82], decentralized control methods for stabilization of power systems are presented where uncertainties are modeled within a Markov jump linear systems framework. It is worth noting that the models in [79, 82] can all be described with SHS formalisms; in particular, it is very easy to show that jump linear Markov processes are a type of SHS.

8.1 Linearized Power System Dynamics

In this section, we formulate the linearized electromechanical power-system model to explicitly capture variations in power injections. Towards this end, we first consider the standard DAE power-system model

$$\begin{aligned} \dot{x} &= f(x, y), \\ 0 &= g(x, y, u), \end{aligned} \tag{8.1}$$

where $x \in \mathbb{R}^n$ is the vector of synchronous machine dynamic states, $y \in \mathbb{R}^p$ is the vector of bus-voltage magnitudes and angles, $u = [P_1, Q_1, \ldots, P_r, Q_r]^T \in \mathbb{R}^{2r}$ is the vector of real/reactive power injections at the r PQ buses of the power system, $f : \mathbb{R}^{n+p} \to \mathbb{R}^n$, and $g : \mathbb{R}^{n+p+2r} \to \mathbb{R}^p$. Denote the stable equilibrium point of the above DAE by (x^*, y^*, u^*). Assuming that the power-flow Jacobian is non-singular, we can linearize (8.1) to obtain the following linear system:

$$\dot{x} = Ax + Bu + C, \tag{8.2}$$

where the entries of A, B, and C are a function of the entries of the Jacobians of $f(\cdot, \cdot)$ and g$(\cdot, \cdot, \cdot)$ evaluated at (x^*, y^*, u^*). The complete derivation of (8.2), and the expressions for A , B , and C, are provided in Appendix A.5.

8.2 Linearized Power System Dynamics as SHS

Recall that the stochastic process $Q(t)$ takes values in the set $\mathcal{Q} = \{0, 1, , \ldots, N\}$, where mode 0 is the nominal mode of the power system (with some nominal value of real/reactive power injections), and in modes $1, \ldots, N$ the real/reactive power injections differ from the nominal value, i.e., these modes capture disturbances in the power system. In each mode $q \in \mathcal{Q}$, we define the vector of power injections $u_q = [P_1^q, Q_1^q, \ldots, P_r^q, Q_r^q]^T \in \mathbb{R}^{2r}$. We then define the stochastic process $U(Q(t))$, $U : \mathcal{Q} \to \mathbb{R}^{2r}$, which at each instant of time t, defines the power injections in the PQ buses of the power system. In particular, if at some time $t \geq 0$, $Q(t) = i$, then $U(i) = u_i = \left[P_1^i, Q_1^i, \ldots, P_r^i, Q_r^i\right]^T$ denotes the vector of real and reactive power injections in the r power-system PQ buses. As described above, without loss of generality, assume the nominal mode of the system is $q = 0$.

The DAE model in (8.1) is linearized about the equilibrium point $(x^*, y^*, u^* = u_0)$ to obtain the linear system in (8.2). Since the power injections are described by a stochastic process, the electromechanical states of the power system are also described by a stochastic process $X(t)$, whose evolution is governed by the following linear ODE:[1]

$$dX(t) = (A\,X(t) + BU(Q(t)) + C)\,dt. \tag{8.3}$$

Recall that we assume that the transition rates are independent of the state $X(t)$; i.e., they are of the form

$$\lambda_j(q,t),\ \lambda_j : \mathcal{Q} \times \mathbb{R}^+ \to \mathbb{R}^+,\ \forall j \in \mathcal{J}, \tag{8.4}$$

where $\mathcal{J}$ is the set of transitions in the SHS. Also, as in Chapter 5, we consider the transition reset maps

$$\phi_j(q,x),\ \phi_j \colon \mathcal{Q} \times \mathbb{R}^d \to \mathcal{Q} \times \mathbb{R}^d,\ j \in \mathcal{J}. \tag{8.5}$$

The intuitive explanation of this model is as follows. The power system undergoes transition j with rate λ_j, and if it undergoes this transition, then it instantaneously applies the map ϕ_j to the current discrete and continuous states and

[1] In the power-system SHS model, we do not include an additive noise term (i.e., the term $g(q,x,t)dW_t$ in (5.2), although, this could straightforwardly be incorporated into the model to capture mode-dependent uncertainty in real/reactive power injections.

changes their values at that moment.[2] More specifically, for any time $t > 0$, we say that the probability of transition j occurring in the time domain $[t, t + \Delta t)$ is $\lambda_j(Q(t), X(t))\Delta t + o(\Delta t)$, and if it does occur, then we define $(Q(t+\Delta t), X(t+\Delta t)) = \phi_j(Q((t+\Delta t)^-), X((t+\Delta t)^-))$, thus obtaining a new value of the discrete and continuous state. The evolution of the continuous states of the power system is governed by (8.3) between transitions when the real/reactive power injections change. Also, note that since we do not consider the transition rates to be explicit functions of the continuous state, the discrete process $Q(t)$ is a continuous time Markov chain—in particular, the path-wise evolution of $Q(t)$ is independent of $X(t)$.

8.3 Renewable Resource Variability

The stochastic power injections described in the model above can straightforwardly model variability in renewable resources. A variety of stochastic models have been proposed to model renewable resources, and in many cases these can be cast in the SHS framework we propose (i.e., different real/reactive power injections in different modes with constant/time-dependent transition rates determined from field data). For example, in [83–85] Markov models are proposed to model PV production. Stochastic models for wind energy conversion systems are available in [3,86,87] (these include SHS and Markov models). In the subsequent discussion, we abstract out the particulars of the renewable resource (i.e., we do not make the explicit connection to common stochastic models for renewables), but present our method with a level of generality that allows it to be applied in general to stochastic small-signal power systems studies.

We present a short example next to illustrate ideas.

Example 7

The state-transition diagram in Fig. 8.1 depicts an SHS model for a representative stochastic small-signal power systems study. This particular SHS model has three modes $\mathcal{Q} = \{0, 1, 2\}$, and two transitions $\mathcal{J} = \{1, 2\}$.[3] As described above, the nominal mode is $q = 0$ with the nominal real/reactive power injections

[2] With each transition, the real/reactive power injections in the buses change.

[3] We will label the transition by the mode that it maps into. Along these lines, note that in this example, transition 1 maps into mode 1, and transition 2 maps into mode 2.

$u(0) = [P_i^0, Q_i^0]^T = [P_i^*, Q_i^*]^T$. The disturbance in the power injections evolves with transitions in $Q(t)$ (which in turn is governed by the transition rates λ_1 and λ_2). Consequently, the moments of the electromechanical states of the power system $X(t)$, are of interest. We follow the methods outlined in Chapter 5 to compute the moments of $X(t)$.

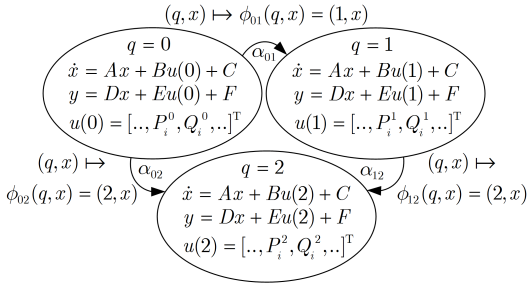

Figure 8.1: Sample SHS model for stochastic power-system small-signal analysis.

We end this section by illustrating the notation introduced so far with a single-machine infinite-bus example. We revert to this example in Section 8.4 where we compute the moments of the electromechanical states.

Example 8

Consider the single-machine infinite-bus (SMIB) system depicted in Fig. 8.2. The synchronous-generator dynamic states are given by $x = [\delta, \omega]^T$, where δ and ω are the rotor angular position and velocity, respectively. We assume the classical model for the generator dynamics; in particular, the DAEs that describe this SMIB system are given by

$$\begin{aligned}
\dot{\delta} &= \omega - \omega_s, \\
\dot{\omega} &= \frac{1}{M}\left(P_M - \frac{EV}{X_M}\sin(\delta - \theta) - D(\omega - \omega_s)\right), \\
0 &= \frac{EV}{X_M}\sin(\delta - \theta) - \frac{V_\infty V}{X_L}\sin(\theta) - P_1, \\
0 &= \frac{EV}{X_M}\cos(\delta - \theta) - \frac{V^2}{X_M} + \frac{V_\infty V}{X_L}\cos(\theta) - \frac{V^2}{X_L} - Q_1,
\end{aligned} \tag{8.6}$$

where P_1 and Q_1 are the real and reactive power input injections (we make no distinctions between constant power sources/loads), respectively, at the PQ bus, V_∞ is the voltage of the slack bus (1 p.u.), $V\angle\theta$ is the PQ bus voltage, and ω_s, M, D, P_m, E, X_m, and X_l are relevant machine and network constants/parameters. The values of the constants/parameters are adopted from [88]. All quantities (except the angular velocity) are in per unit.

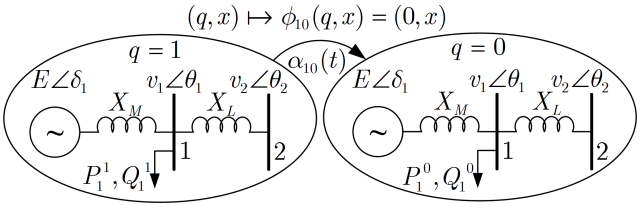

Figure 8.2: SMIB SHS model studied in Example 8.

We will assume that the real/reactive power injections are uncertain. Particularly, in a nominal mode $q = 0$, the nominal real/reactive power injections at the PQ bus are denoted by $P_1^0 = P_1^*$, $Q_1^0 = Q_1^*$, respectively. The corresponding equilibrium values of the system states are given by: $\delta^*, \omega^*, V^*, \theta^*$. Linearizing (8.6) about this equilibrium point, assuming small variations in P_1, Q_1, we get the linear system in (8.2) with the A, B, and C matrices derived following the approach prescribed in Appendix A.5.

Now, consider a disturbance in this system, where the real/reactive power injections are given by $P_1^1 = 0.5 \cdot P_1^*$, and $Q_1^1 = 0.5 \cdot Q_1^*$. The duration of this disturbance is uncertain, and described by a random variable T, with pdf and cdf denoted by $f_T(t)$ and $F_T(t)$, respectively. The above model can be cast as an SHS with two modes: a nominal mode $q = 0$ (with real/reactive power injections given by the nominal values P_1^0, Q_1^0), and a mode $q = 1$ (with a disturbance in the real/reactive power injections P_1^1, Q_1^1). There is a single transition from mode 1 to 0 that models the clearing of the disturbance, with the transition rate given by the hazard rate of the normal distribution, $\lambda_0(q, x, t) = \delta_{q1} \left(f_T(t)/1 - F_T(t) \right) =: \delta_{q1}\alpha(t)$. Finally, note that since δ and ω do not jump due to the transition, the reset map is given by $\phi_0(q, x) = (0, x)$. The SHS described above is schematically illustrated in Fig. 8.2.

8.4 Moment Evolution

In this section, we examine the evolution of the moments of the continuous state $X(t)$. Towards this end, we first define the extended generator of the stochastic process, and then describe a general method to formulate appropriate test functions that yield the moments of interest. The discussion in this section mirrors that presented for general SHS in Chapter 5. We restate some of the key results in Chapter 5, so this section is self contained and can be read independent of Chapter 5.

8.4.1 Extended Generator of the Power Systems SHS Model

For the power-system SHS model described in Section 8.2, we consider test functions of the form $\psi(q, x)$, for which the extended generator $(L\psi)(q, x)$ (computed by applying (5.10)), is given by

$$\begin{aligned}(L\psi)(q,\, x) &= \frac{\partial}{\partial x}\psi(q,\, x)\cdot(Ax + Bu(q) + C) \\ &+ \sum_{j\in\mathcal{J}} \lambda_j(q, x, t)\left(\psi\left(\phi_j\left(q,\, x\right)\right) - \psi(q,\, x)\right). \end{aligned} \tag{8.7}$$

As described in Chapter 5, we can specify a family of test functions to obtain relevant moments of the continuous states. The evolution of the moments is governed by Dynkin's formula (5.11).

8.4.2 Test Functions for the Power Systems SHS Model

For a SHS where $Q(t)$ takes values in the set $\mathcal{Q} = \{0,\, 1, \ldots,\, N\}$, we define the following family of test functions:

$$\psi_i^{(m)}(q,\, x) := \delta_{qi}x^m = \begin{cases} x^m & \text{if} \quad q = i \\ 0 & \text{if} \quad q \neq i \end{cases}, \forall i \in \mathcal{Q}, \tag{8.8}$$

where $m := (m_1,\, m_2, \ldots,\, m_n) \in \mathbb{N}^{1\times n}$, and $x^m := x_1^{m_1}x_2^{m_2}\ldots x_n^{m_n}$. We also define the conditional moments at time t, $\mu_i^{(m)}(t)$, $\forall i \in \mathcal{Q}$ by

$$\mu_i^{(m)}(t) := \mathrm{E}\left[\psi_i^{(m)}(q, x)\right] = \mathrm{E}\left[X^m(t)|Q(t) = i\right]\pi_i(t), \tag{8.9}$$

where $\pi_i(t)$ denotes the occupational probability of mode i, i.e., $\pi_i(t) := \Pr\{Q(t) = i\}$. As described in Section 5.4, by appropriately picking the m_i's, we can isolate the conditional moments of interest. We demonstrate this next, in the context of the two-mode SMIB example introduced in Example 8.

Example 8 (continued)

Recall the SMIB model introduced in Section 8.2. Associated with the two discrete modes, $i = \{0, 1\}$, define the following test functions $\psi_i^{(m)}(q, x) = \delta_{qi}x^m$, where $m \in \mathbb{N}^{1\times 2}$ and $x^m = \delta^{m_1}\omega^{m_2}$. By appropriately picking m, we can recover many conditional moments of interest. For instance, note that choosing $m = (0, 0)$ recovers the occupational probabilities of the modes,

$$\mu_i^{(0,0)}(t) = \Pr\{Q(t) = i\} = \pi_i(t). \tag{8.10}$$

Similarly, picking $m = (2, 0)$ isolates the second-order conditional moment of $\Delta(t)$:

$$\mu_i^{(2,0)}(t) = \mathbb{E}\left[X^{(2,0)}(t)|Q(t) = i\right] \cdot \pi_i(t) = \mathbb{E}\left[\Delta^2(t)|Q(t) = i\right] \cdot \pi_i(t). \tag{8.11}$$

Finally, picking $m = (1, 1)$ yields the conditional expectation of the product $\Delta(t)\Omega(t)$:

$$\mu_i^{(1,1)}(t) = \mathbb{E}\left[X^{(1,1)}(t)|Q(t) = i\right] \cdot \pi_i(t) = \mathbb{E}\left[\Delta(t)\Omega(t)|Q(t) = i\right] \cdot \pi_i(t) \tag{8.12}$$

8.4.3 Evolution of the Moments of $X(t)$

Suppose we are interested in the evolution of a particular moment of the continuous state, i.e., the evolution of $\mathrm{E}\left[X^m(t)\right]$ for some $m \in \mathbb{N}^{1\times n}$. Applying the law of total expectation, we can get this from the conditional moments μ_i:

$$\mathrm{E}[X^m(t)] = \sum_{i\in\mathcal{Q}} \mathrm{E}\left[X^m(t)|Q(t) = i\right] \pi_i(t) = \sum_{i\in\mathcal{Q}} \mu_i^{(m)}(t). \tag{8.13}$$

Therefore, at each time t, to obtain $\mathrm{E}[X^m(t)]$, we need to know $\mu_i^{(m)}(t)$, $\forall i \in \mathcal{Q}$. The time evolution of each $\mu_i^{(m)}(t)$ can be obtained by first applying (8.7) to obtain expressions for $N + 1$ extended generators $\left(L\psi_i^{(m)}\right)(q, x)$, $i \in \mathcal{Q}$, and then using

Dynkin's formula as follows:

$$\frac{d}{dt}\mu_i^{(m)}(t) = \frac{d}{dt}\mathrm{E}\left[\psi_i^{(m)}(q,\, x)\right] = \mathrm{E}\left[\left(L\psi_i^{(m)}\right)(q,\, x)\right]. \tag{8.14}$$

We revert to Example 8 to illustrate how (8.14) applies in practice.

Example 8 (continued)

Let us again consider Example 8. Suppose we are interested in computing $\mathrm{E}\left[X^m(t)\right] = \mathrm{E}\left[\Delta^{m_1}(t)\Omega^{m_2}(t)\right]$ for some $m \in \mathbb{N}^{1\times 2}$. We go through this derivation in detail next. First, we use the definition of L from (8.7) to obtain

$$\begin{aligned}\left(L\psi_i^{(m)}\right)(q,\, x) &= \frac{\partial}{\partial x}\psi_i^{(m)}(q,\, x)\cdot(Ax + Bu(i) + C) \\ &+ \lambda_0(q,x,t)\left(\psi_i^{(m)}(\phi_1(q,\, x)) - \psi_i^{(m)}(q,\, x)\right)\end{aligned} \tag{8.15}$$

Let us denote the entries in the i^{th} row and j^{th} column of A, B, and C as a_{ij}, b_{ij}, and c_{ij}, respectively. From the definition of the test functions in (8.8) and the linearized power-system dynamic model in (8.2), we get

$$\frac{\partial}{\partial x}\psi_i^{(m)}(q,\, x) = \delta_{qi}\begin{bmatrix} m_1\delta^{m_1-1}\omega^{m_2} \\ m_2\delta^{m_1}\omega^{m_2-1}\end{bmatrix}^T, \tag{8.16}$$

$$Ax + Bu(i) + C = \begin{bmatrix} a_{11}\delta + a_{12}\omega + b_{11}P_1^i + b_{12}Q_1^i + c_{11} \\ a_{21}\delta + a_{22}\omega + b_{21}P_1^i + b_{22}Q_1^i + c_{21}\end{bmatrix}. \tag{8.17}$$

So, the first term in (8.15) is given by the dot product of (8.16) and (8.17):

$$\begin{aligned}&\frac{\partial}{\partial x}\psi_i^{(m)}(q,\, x)\cdot(Ax + Bu(i) + C) \\ &= \delta_{qi}\left((m_1a_{11} + m_2a_{22})x^m\right. \\ &+ m_1a_{12}x^{(m_1-1,m_2+1)} + m_2a_{21}x^{(m_1+1,m_2-1)} \\ &+ m_1x^{(m_1-1,m_2)}\left(b_{11}P_1^i + b_{12}Q_1^i + c_{11}\right) \\ &+ \left. m_2x^{(m_1,m_2-1)}\left(b_{21}P_1^i + b_{22}Q_1^i + c_{21}\right)\right).\end{aligned} \tag{8.18}$$

We now consider the second term of (8.15). Recalling that $\lambda_0(q,x,t) = \delta_{q1}\alpha(t)$, and $\phi_0(q,x) = (0,x)$, we get

$$\begin{aligned}
&\lambda_0(q,x,t)\left(\psi_i^{(m)}(\phi_1(q,\,x)) - \psi_i^{(m)}(q,\,x)\right) \\
&= \delta_{q1}\alpha(t)\left(\psi_i^{(m)}(0,x) - \psi_i^{(m)}(q,\,x)\right) \\
&= \delta_{q1}\alpha(t)\left(\delta_{0i}x^m - \delta_{qi}x^m\right) \\
&= \delta_{i0}\left(\alpha(t)\psi_1^{(m)}(q,\,x)\right) + \delta_{i1}\left(-\alpha(t)\psi_1^{(m)}(q,\,x)\right). \qquad (8.19)
\end{aligned}$$

Combining (8.18), (8.19), while acknowledging $\mu_i^{(m)}(t) = \mathrm{E}\left[\psi_i^{(m)}(q,x)\right]$, we get

$$\begin{aligned}
\dot{\mu}_i^{(m)}(t) \;=\; & \mathrm{E}\left[\left(L\psi_i^{(m)}\right)(q,\,x)\right] = (m_1a_{11} + m_2a_{22})\mu_i^{(m)}(t) \\
& + m_1a_{12}\mu_i^{(m_1-1,m_2+1)}(t) + m_2a_{21}\mu_i^{(m_1+1,m_2-1)}(t) \\
& + m_1\left(b_{11}P_1^i + b_{12}Q_1^i + c_{11}\right)\mu_i^{(m_1-1,m_2)}(t) \\
& + m_2\left(b_{21}P_1^i + b_{22}Q_1^i + c_{21}\right)\mu_i^{(m_1,m_2-1)}(t) \\
& + \delta_{i0}\left(\alpha(t)\mu_1^{(m)}(t)\right) + \delta_{i1}\left(-\alpha(t)\mu_1^{(m)}(t)\right). \qquad (8.20)
\end{aligned}$$

By substituting different values of $m = (m_1, m_2)$ in (8.20), we can obtain ODEs that govern the corresponding moments. For illustration, suppose the duration of the disturbance is normally distributed with mean $m_T = 5$s , and standard deviation $\sigma_T = \frac{20}{100}m_T$. To illustrate the validity of the SHS approach, we will compare results with Monte Carlo simulations implemented for the linearized system in (8.2). Figures 8.3-8.4 depict the first-order moments of the rotor angle and speed, respectively. Superimposed in dashed lines are standard deviation bounds. Figures 8.5-8.6 depict the second-order moments of the rotor angle and speed, respectively. The results show excellent agreement, hence validating the SHS approach.

8.5 Three-machine Nine-bus Power System

In this section, we examine a three-machine nine-bus power system model. A reduced, third-order model is utilized to model the mechanical equations of motion and the governor of each synchronous generator. The real/reactive power injections at the PQ buses are uncertain, and modeled as a Markov process (i.e., adopting SHS terminology, the transition rates of the discrete process are constant). We utilize

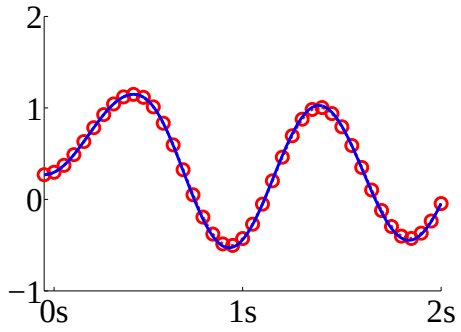

Figure 8.3: First-order moment of rotor angle for SMIB system.

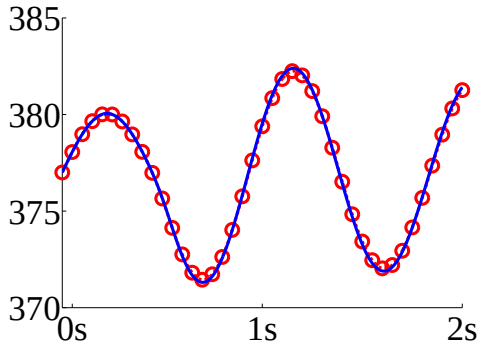

Figure 8.4: First-order moment of rotor speed for SMIB system.

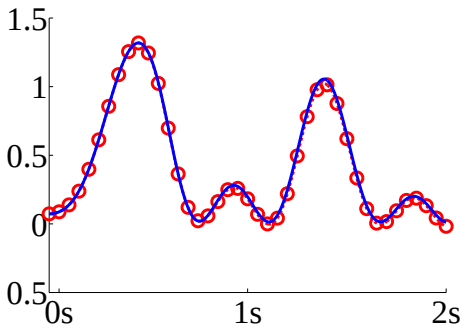

Figure 8.5: Second-order moment of rotor angle for SMIB system.

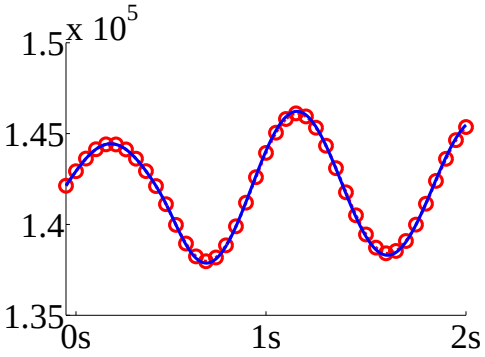

Figure 8.6: Second-order moment of rotor speed for SMIB system.

the SHS framework to compute the moments of the synchronous-generator states. First, we describe the power-system electromechanical model. Next, we describe the stochastic load model, and finally present simulation results for a number of different cases. In each case, the results from Monte Carlo simulations are included to demonstrate the validity of the SHS approach.

8.5.1 Electromechanical Model Description

Consider the three-machine nine-bus system depicted in Fig. 8.7. We utilize a reduced-order model for the synchronous machines in the power system. Particularly, the conventional nine-state synchronous machine model [89]—that includes mechanical equations of motion, exciter, voltage regulator, turbine, governor, and

models for the damper windings—is reduced to a three-state model that captures the governor dynamics and the mechanical equations of motion. For the i synchronous machine, the system states of interest are the rotor angular position δ_i, rotor angle velocity ω_i, and the turbine power ξ_i. The evolution of these states is governed by

$$\begin{aligned}
\dot{\delta}_i &= \omega_i - \omega_s, \\
\dot{\omega}_i &= \frac{1}{M_i}\left(\xi_i - \frac{E_i V_i}{X_{Mi}}\sin\left(\delta_i - \theta_i\right) - D_i\left(\omega - \omega_s\right)\right), \\
\dot{\xi}_i &= \frac{1}{T_i}\left(-\left(\xi_i - P_i^{ref}\right) - \frac{1}{R_{Di}\omega_s}\left(\omega_i - \omega_s\right)\right),
\end{aligned} \tag{8.21}$$

where ω_s is the synchronous speed (377 rad/s), M_i is the machine inertia constant, X_{Mi} is the machine impedance, D_i is the damping coefficient, E_i is the machine internal voltage, T_i is the governor time constant, R_{Di} is the slope of the machine speed-droop characteristic, and P_i^{ref} is a function of the unit base-point generation [90]. The states of the i generator are described by the vector $x_i = [\delta_i, \omega_i, \xi_i]^T$, and the vector $x = [x_1, x_2, x_3]^T$, $x \in \mathbb{R}^{9\times 1}$ captures all dynamic states of interest. The power flow equations for the buses $j = 1, \ldots, 9$ are given by

$$\sum_{k=1}^{9} V_k V_j \left(G_{kj}\cos\left(\theta_k - \theta_j\right) + B_{kj}\sin\left(\theta_k - \theta_j\right)\right) - P_j = 0, \tag{8.22}$$

$$\sum_{k=1}^{9} V_k V_j \left(G_{kj}\sin\left(\theta_k - \theta_j\right) - B_{kj}\cos\left(\theta_k - \theta_j\right)\right) - Q_j = 0, \tag{8.23}$$

where G_{kj} and B_{kj} are the conductance and susceptance, respectively, of the transmission line between bus k and j.

8.5.2 Stochastic Real/Reactive Power-Injection Model

We will assume that the real/reactive power injections in the buses ($j = 1, \ldots, 9$) are uncertain. Towards this end, consider a nominal mode $q = 0$, where the nominal real/reactive power injections at the buses are denoted by

$$u(0) = [P_1^0, Q_1^0, \ldots, P_9^0, Q_9^0]^T = [P_1^*, Q_1^*, \ldots, P_9^*, Q_9^*]^T. \tag{8.24}$$

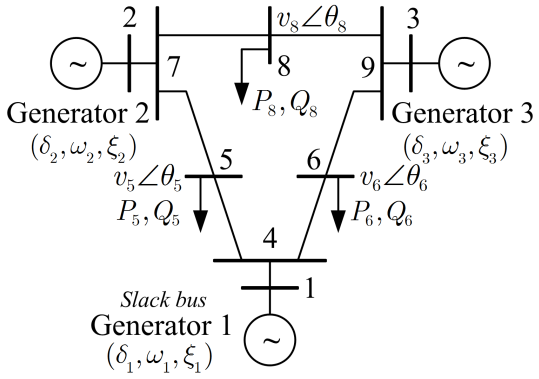

Figure 8.7: One-line diagram of three-machine nine-bus power system studied in Section 8.5.

The corresponding equilibrium values of the system states are given by: $\delta_i^*, \omega_i^*, V_j^*, \theta_j^*$, $i = 1, 2, 3$, $j = 1, \ldots, 9$. Linearizing (8.21) about this equilibrium point, assuming small variations in P_j, Q_j, we get the linear system in (8.2) with the A, B, and C matrices derived following the approach prescribed in Appendix A.5.

Now, consider a disturbance in this system, where the real/reactive power injections are denoted by

$$u(1) = [P_1^1, Q_1^1, \ldots, P_9^1, Q_9^1]^T \tag{8.25}$$

We assume that the disturbance is described by a Markov model. In particular, the transition rate that governs the disturbance occurrence is denoted by $\lambda_1(q, x) = \alpha$, and the rate that governs the clearance of the disturbance is given by $\lambda_0(q, x) = \beta$. The above model can be cast as a SHS with two modes: a nominal mode $q = 0$ (with real/reactive power injections given by the nominal values P_j^0, Q_j^0), and a mode $q = 1$ (with a disturbance in the real/reactive power injections P_j^1, Q_j^1). Finally, note that since δ and ω do not jump due to the transition, the reset maps are given by $\phi_0(q, x) = (0, x)$ and $\phi_1(q, x) = (1, x)$. The SHS described above is schematically illustrated in Fig. 8.8.

8.5.3 Moments of Generator Rotor Speed

The line and machine impedances for the system in Fig. 8.7 are adopted from [82]; Machine inertias, terminal voltages, and damping coefficients are adopted from [88]; and finally, the governor parameters are adopted from [91]. The base values of

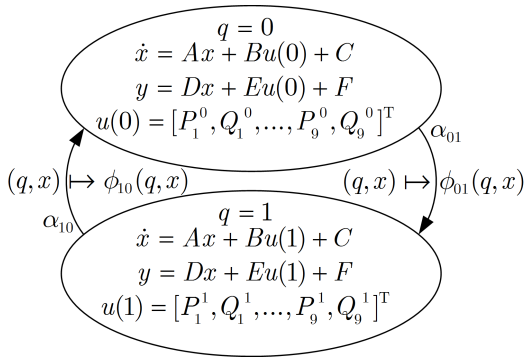

Figure 8.8: State-transition diagram for the SHS model of the three-machine nine-bus power system studied in Section 8.5.

the bus loads corresponding to the nominal $q = 0$ mode (see (8.24)) are adopted from [82], and given by

$$u(0) = [0,\ 0,\ 0,\ 0,\ 0,\ 0,\ 0.25,\ 0.5,\ 0,\ 0,\ 0,\ 0,\ 0.3,\ 0.3,\ 0,\ 0,\ 0.20.35]^T.$$

The values of the loads corresponding to mode $q = 1$ (see (8.25)) are given by

$$u(1) = [0, 0, 0, 0, 0, 0, 0, 0.25, 0.5, 1, 0.5, 0, 0, 0.3, 0.3, 0.5, 0.2, 0.2, 0.35]^T.$$

For these simulation parameters, Figures 8.9-8.10 depict the first- and second-order moments, respectively, of Generator 1 speed for $\alpha = 5\mathrm{s}^{-1}$ and $\beta = 5\mathrm{s}^{-1}$. Figures 8.11-8.12 depict the first- and second-order moments, respectively, of Generator 1 speed for $\alpha = 5\mathrm{s}^{-1}$ and $\beta = 10\mathrm{s}^{-1}$. Finally, Figs. 8.13-8.14 depict the first- and second-order moments, respectively, of Generator 1 speed for $\alpha = 10\mathrm{s}^{-1}$ and $\beta = 5\mathrm{s}^{-1}$. In each case the SHS results are superimposed on results of 1000 Monte Carlo simulations. In Figs. 8.9, 8.11, and 8.13, standard-deviation bounds are superimposed. The results indicate the validity of the SHS approach. Additionally, as expected by intuition, notice that when the mean time to transition to the perturbed mode ($q = 1$) is much higher than the mean time to transition to the nominal mode, i.e., when $\alpha < \beta$, the expected system frequency deviates significantly from the nominal value. Interestingly, the standard deviation bounds are independent of the transition rates. Further analysis of this stochastic system, integration of renewable models described in Section 8.3, stochastic control design, etc., while excellent opportunities for future work, are beyond the scope of this dissertation.

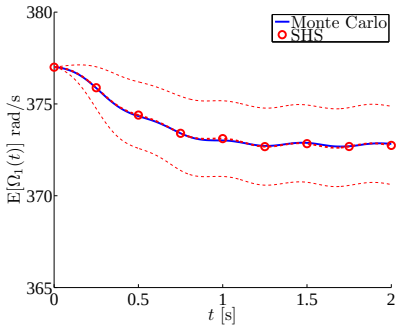

Figure 8.9: First-order moment of Generator 1 rotor speed for $\alpha = 5\mathrm{s}^{-1}$, $\beta = 5\mathrm{s}^{-1}$.

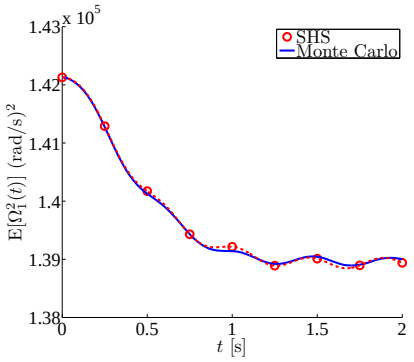

Figure 8.10: Second-order moment of Generator 1 rotor speed for $\alpha = 5\mathrm{s}^{-1}$, $\beta = 5\mathrm{s}^{-1}$.

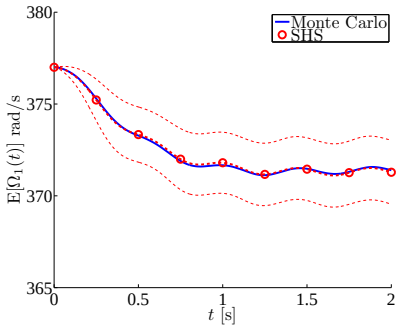

Figure 8.11: First-order moment of Generator 1 rotor speed for $\alpha = 5\mathrm{s}^{-1}$, $\beta = 10\mathrm{s}^{-1}$.

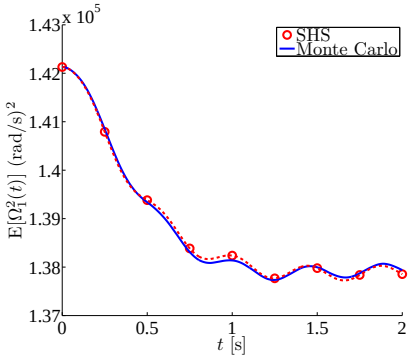

Figure 8.12: Second-order moment of Generator 1 rotor speed for $\alpha = 5\mathrm{s}^{-1}$, $\beta = 10\mathrm{s}^{-1}$.

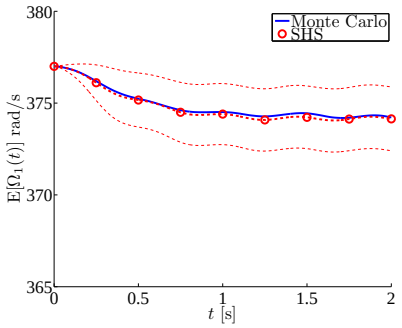

Figure 8.13: First-order moment of Generator 1 rotor speed for $\alpha = 10\mathrm{s}^{-1}$, $\beta = 5\mathrm{s}^{-1}$.

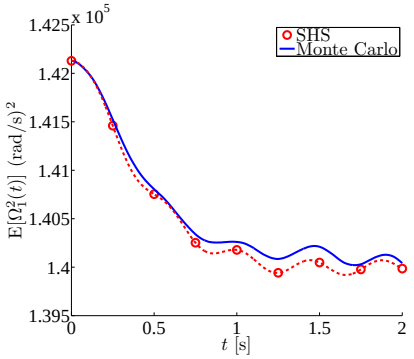

Figure 8.14: Second-order moment of Generator 1 rotor speed for $\alpha = 10\mathrm{s}^{-1}$, $\beta = 5\mathrm{s}^{-1}$.

Chapter 9

CONCLUDING REMARKS AND FUTURE WORK

In this chapter, we first summarize the work presented in the dissertation with a few concluding remarks. Next, we present several avenues for future work related to the numerical methods we have developed, and their applications to power and energy systems models.

9.1 Concluding remarks

This dissertation presented performability models for analysis of renewable electric power systems. In particular, we demonstrated how Markov reward models and stochastic hybrid systems can be applied to study the energy yield, reliability, availability, and performance of wind energy conversion systems and photovoltaic energy conversion systems.

In the domain of Markov models, it is widely recognized that the failure and repair rates—the model parameters—are never perfectly known. Therefore, the model outputs, i.e., performability measures, are also not perfectly known. To address this, we developed analytical expressions for the sensitivity of performability measures to model parameters. These were then utilized to formulate a Taylor-series approximation of the Markov chain stationary distribution that was employed in two approaches for uncertainty analysis. The first is a probabilistic approach, where it is assumed that the failure and repair rates are random numbers with known distributions, and these distributions are propagated through the Taylor-series expansion of the Markov chain stationary distribution to obtain distributions of performability measures. The second is a set-theoretic approach, where we assume that model parameters are constrained to an ellipsoidal set, and this set is propagated through the stationary distribution Taylor-series expansion to obtain a set that constrains all the values that the performability measures can take. We demonstrated several

applications of the methods described above to study the performability of wind and photovoltaic energy conversion systems subject to parametric uncertainty.

With regard to stochastic hybrid systems, we applied this modeling framework to study a wide class of system performability problems. In this regard, we developed dynamic reliability models to extend basic Markov reward models. Ongoing work in this domain relates to the investigation of the impact of stochastic disturbances on power system dynamics. Here, a linearized version of the nonlinear power system DAE model is cast as a stochastic hybrid system, and moments of the power system electromechanical states are derived using Dynkin's formula and the extended generator of the stochastic process.

9.2 Future Work

This thesis presents several avenues for future work for both Markov models and stochastic hybrid systems models. With regard to the uncertainty propagation methods developed in Chapters 3 and 4, we could further investigate the multivariate Taylor-series expansion. To do so, general expressions for the higher-order sensitivities of performability indices to model parameters need to be formulated. A related problem is to compare the efficiency and accuracy of the method we propose to compute the sensitivities with that suggested in the literature.

With regard to the probabilistic approach to uncertainty analysis, we recognized the proposed method applies very well for large models with a few uncertain parameters. Presumably, we could identify parameters that have minimal impact on the performability indices and utilize that information to extend the methods to cases where there are many uncertain parameters (perhaps by systematically ranking the parameters in order of the impact they have). In the domain of set-theoretic methods, we need to develop numerically efficient tools to solve optimization programs for the propagation of ellipsoidal-shaped sets through the second-order Taylor-series expansion (this has obvious applications to other areas of study). We could also investigate other sets, e.g., zonotopes, to capture the parametric uncertainty.

A major challenge that was highlighted in our investigation of stochastic hybrid systems relates to the problem of moment closure. We demonstrated that this problem arises, e.g., when the transition rates are functions of the continuous state. Presumably, if we had numerically efficient and accurate moment closure methods at

hand, the stochastic hybrid systems framework could be applied to an even broader class of problems relevant to power and energy systems. This is because we could model systems with polynomial vector fields that governed the state evolution as well as transition rates that were a function of the state. Inspiration could be sought from previous work on infinite-dimensional systems of differential equations to address this problem. The alternative is to go along with present methods for moment closure by investigating distributions for the continuous state tailored to the problem at hand based on engineering judgment. In summary, the key challenge that needs to be addressed is to scale the numerical methods we have developed when the dimension of the model parameters (with regard to Markov models) or the number of moments (with regard to stochastic hybrid systems) increases.

From the application perspective, there are several directions to extend the presented models. We have already highlighted in Chapter 6 some avenues to extend the work on performability modeling of photovoltaic systems. For instance, similar to the methods presented in Chapter 7, we could propagate uncertainty in inputs (ambient temperature, incident solar insolation, etc.) through common photovoltaic performance models. Similarly, a wide variety of faults (extending beyond faults in inverters and PV strings) could be modeled by augmenting the state space. With regard to wind energy conversion systems, we need to develop and apply better performance models to capture the wind power output that account for interference effects. We can also investigate the sensitivity of common wind generation indices to model parameters and inputs; this could be applied to improve the design of wind farms.

Finally, with regard to the application of stochastic hybrid systems in power system dynamics modeling, we need to develop the computational platform to integrate a wide class of machine dynamic models. Also, since the moment dynamics are governed by a linear system, we can apply a wide class of tools that have been developed for general linear systems to get further insights into the stochastic behavior of power systems. For instance, we could investigate problems such as: correlation of dynamic states, eigenvalue sensitivity of the moment equations, and the impact of model parameters on steady-state statistics. We also need to formulate the appropriate stochastic models to integrate the renewable resource uncertainty directly into the stochastic hybrid systems modeling framework. A related problem is to model dynamics in the power injections by augmenting the state space of the stochastic hybrid systems.

Appendix A

DERIVATIONS OF IMPORTANT RESULTS

A.1 Derivation of Result in (2.9)

Consider the definition of the accumulated reward in (2.8). Let t_0 be the time at which the effect of initial conditions in (2.4) has vanished, i.e., $\pi(t) \approx \pi \, \forall t \geq t_0$. Then, for $\tau \gg t_0$, it follows that

$$\begin{aligned} \gamma &= \int_0^{\tau} \pi(t)\rho^T dt \\ &= \int_0^{t_0} \pi(t)\rho^T dt + \int_{t_0}^{\tau} \pi(t)\rho^T dt \\ &\approx \int_0^{t_0} \pi(t)\rho^T dt + \pi\rho^T(\tau - t_0). \end{aligned} \tag{A.1}$$

Now, by applying the mean-value theorem for integration to the first term of the last equality above, we obtain

$$\begin{aligned} \gamma &\approx \pi(s)\rho^T t_0 + \pi\rho^T(\tau - t_0) \\ &= \left(\pi(s)\rho^T - \pi\rho^T\right) t_0 + \pi\rho^T\tau \\ &\approx \pi\rho^T\tau, \end{aligned} \tag{A.2}$$

where $\pi(s) = \pi(t)|_{t=s}$ for some $s \in [0, t_0]$. Since $0 \leq \pi_i(s) \leq 1$ and $0 \leq \pi_i \leq 1$, $\forall i = 0, 1, \ldots, N$, and $\tau \gg t_0$, the term $\pi\rho^T\tau$ dominates $\left(\pi(s)\rho^T - \pi\rho^T\right) t_0$, and as a result, $\gamma \approx \pi\rho^T\tau$ as claimed in (2.9).

A.2 Derivation of Stationary Distribution Sensitivities in (2.14)-(2.15)

Theorem 1

The k-order sensitivity of the stationary distribution, $\pi(\theta)$ of an ergodic continuous time Markov chain (CTMC) described by (2.4) with respect to the i model parameter, θ_i, is given by

$$\frac{\partial^k \pi(\theta)}{\partial \theta_i^k} = k!\,(-1)^k\,\pi(\theta)\left(\frac{\partial \Lambda}{\partial \theta_i}\Lambda^{\#}\right)^k, \tag{A.3}$$

The second-order mixed partial derivative is given by

$$\frac{\partial \pi_i^2(\theta)}{\partial \theta_j \partial \theta_k} = \pi(\theta)^T\left(\frac{\partial \Lambda}{\partial \theta_j}\Lambda^{\#}\frac{\partial \Lambda}{\partial \theta_k}\Lambda^{\#} + \frac{\partial \Lambda}{\partial \theta_k}\Lambda^{\#}\frac{\partial \Lambda}{\partial \theta_j}\Lambda^{\#}\right)e_i^T, \tag{A.4}$$

where $e_i \in \mathbb{R}^{n+1}$ is a vector with 1 as the i entry and zero otherwise.where $\Lambda^{\#}$ is the group inverse of the generator matrix Λ.

Proof

Consider that the ergodic CTMC is associated with a discrete time Markov chain (DTMC) whose distribution is governed by

$$p[k+1] = p[k]P, \tag{A.5}$$

where $P = I + \delta\Lambda$ is a row-stochastic, irreducible, and primitive matrix (with an appropriate choice of δ). Define the matrix

$$A = I - P = -\delta\Lambda, \tag{A.6}$$

and denote the group inverse of A by $A^{\#}$. The stationary distribution of the DTMC satisfies $pA = 0$. If we consider linear perturbations, i.e., $\partial^k A/\partial\theta_i^k = 0, \forall k > 1$, differentiating the expression $pA = 0$ a total of k times yields

$$\frac{\partial^k p}{\partial \theta_i^k}A = -k\frac{\partial^{k-1} p}{\partial \theta_i^{k-1}}\frac{\partial A}{\partial \theta_i}. \tag{A.7}$$

Following along the lines of Theorem 3.2 in [50], since $\mathbf{dim}\, N(A) = 1$ (the null space of a matrix A is denoted by $N(A)$), we can express

$$\frac{\partial^k p}{\partial \theta_i^k} = -k \frac{\partial^{k-1} p}{\partial \theta_i^{k-1}} \frac{\partial A}{\partial \theta_i} A^{\#} + \alpha p \text{ for some } \alpha. \tag{A.8}$$

We can determine α by noting that $pe^T = 1 \Rightarrow \partial^k p / \partial \theta_i^k e^T = 0$. Since $e^T \in N(A) = N(A^{\#})$,

$$\frac{\partial^k p}{\partial \theta_i^k} e^T = -k \frac{\partial^{k-1} p}{\partial \theta_i^{k-1}} \frac{\partial A}{\partial \theta_i} A^{\#} e^T + \alpha p e^T = \alpha p e^T = 0 \Rightarrow \alpha = 0. \tag{A.9}$$

Thus the k-order sensitivity of the stationary distribution of the DTMC to the i parameter is given by

$$\frac{\partial^k p}{\partial \theta_i^k} = -k \frac{\partial^{k-1} p}{\partial \theta_i^{k-1}} \frac{\partial A}{\partial \theta_i} A^{\#}. \tag{A.10}$$

Expressing $\partial^{k-1} p / \partial \theta_i^{k-1}$ as a function of $\partial^{k-2} p / \partial \theta_i^{k-2}$ and so on, we get

$$\begin{aligned} \frac{\partial^k p}{\partial \theta_i^k} &= k!(-1)^{k-1} \frac{\partial p}{\partial \theta_i} \left(\frac{\partial A}{\partial \theta_i} A^{\#} \right)^{k-1} \\ &= k!(-1)^k p(\theta) \left(\frac{\partial A}{\partial \theta_i} A^{\#} \right)^k, \end{aligned} \tag{A.11}$$

which follows from the result

$$\frac{\partial p}{\partial \theta_i} = -p(\theta) \frac{\partial A}{\partial \theta_i} A^{\#}, \tag{A.12}$$

derived in Theorem 3.2 in [50]. Now, consider that the group inverse of the CTMC generator matrix, Λ, denoted by $\Lambda^{\#}$, is given by

$$\Lambda^{\#} = -\delta A^{\#}, \tag{A.13}$$

which can be shown by noting that $\Lambda^{\#}$ satisfies the definition of the group inverse given in (2.10). From (A.13) and (A.6),

$$\frac{\partial \Lambda(\theta)}{\partial \theta_i} \Lambda^{\#} = \left(-\delta^{-1} \frac{\partial A(\theta)}{\partial \theta_i} \right) \left(-\delta A^{\#} \right) = \frac{\partial A(\theta)}{\partial \theta_i} A^{\#}. \tag{A.14}$$

Since the stationary distributions of the CTMC and the DTMC match, from (A.11) and (A.14), we get the result in (2.14)

$$\frac{\partial^k \pi(\theta)}{\partial \theta_i^k} = k! \, (-1)^k \, \pi(\theta) \left(\frac{\partial \Lambda}{\partial \theta_i} \Lambda^{\#} \right)^k. \tag{A.15}$$

Now differentiate (A.12) with respect to θ_j, $j \neq i$ to obtain

$$\frac{\partial^2 p}{\partial \theta_j \partial \theta_i} A + \frac{\partial p}{\partial \theta_i} \frac{\partial A}{\partial \theta_j} + \frac{\partial p}{\partial \theta_j} \frac{\partial A}{\partial \theta_i} + p \frac{\partial^2 A}{\partial \theta_j \partial \theta_i} = 0. \tag{A.16}$$

Given the assumption of linear parameter perturbations, (A.16) simplifies as follows:

$$\frac{\partial^2 p}{\partial \theta_j \partial \theta_i} A = p \frac{\partial A}{\partial \theta_i} A^{\#} \frac{\partial A}{\partial \theta_j} + p \frac{\partial A}{\partial \theta_j} A^{\#} \frac{\partial A}{\partial \theta_i}. \tag{A.17}$$

Following along the lines of Theorem 3.2 in [50], we get:

$$\frac{\partial^2 p}{\partial \theta_j \partial \theta_i} = p \frac{\partial A}{\partial \theta_i} A^{\#} \frac{\partial A}{\partial \theta_j} A^{\#} + p \frac{\partial A}{\partial \theta_j} A^{\#} \frac{\partial A}{\partial \theta_i} A^{\#}, \tag{A.18}$$

where $A^{\#}$ is the group inverse of A. Since the stationary distributions of the CTMC and DTMC match, we get the result in (2.15)

$$\frac{\partial \pi^2}{\partial \theta_j \partial \theta_i} = \pi^T \left(\frac{\partial \Lambda}{\partial \theta_j} \Lambda^{\#} \frac{\partial \Lambda}{\partial \theta_i} \Lambda^{\#} + \frac{\partial \Lambda}{\partial \theta_i} \Lambda^{\#} \frac{\partial \Lambda}{\partial \theta_j} \Lambda^{\#} \right). \tag{A.19}$$

A.3 Derivation of Result in (3.22)

The expression in (3.22) can be derived as follows:[1]

$$\begin{aligned} & \Pr\left\{ \pi_i \leq \Pi_i \leq \pi_i + \Delta(\pi_i) \,|\, \Theta_2 = \theta_2, \ldots, \Theta_m = \theta_m \right\} \\ = & \sum_{j \in \mathcal{J}^-} \Pr\left\{ \Delta\theta_{1,j} + \Delta(\Delta\theta_{1,j}) < \Delta\Theta_1 < \Delta\theta_{1,j} \,|\, \Theta_2 = \theta_2, \ldots, \Theta_m = \theta_m \right\} \\ + & \sum_{j \in \mathcal{J}^+} \Pr\left\{ \Delta\theta_{1,j} < \Delta\Theta_1 < \Delta\theta_{1,j} + \Delta(\Delta\theta_{1,j}) \,|\, \Theta_2 = \theta_2, \ldots, \Theta_m = \theta_m \right\}, \end{aligned} \tag{A.20}$$

[1] The operator $\Delta(x)$ denotes an incremental change (possibly negative) in the quantity x.

where $\Delta\theta_{1,j}$, $j = 1, \ldots, t$ are the roots of the equation $\pi_i = p_i(\Delta\theta_1)$, with $p_i(\Delta\theta_1)$ defined in (3.21), and

$$\mathcal{J}^+ = \left\{ j \,:\, p_i'(\Delta\theta_{1,j}) > 0 \right\}, \mathcal{J}^- = \left\{ j \,:\, p_i'(\Delta\theta_{1,j}) < 0 \right\}. \tag{A.21}$$

It follows that $\Delta(\Delta\theta_{1,j}) > 0 \ \forall j \in \mathcal{J}^+$ and similarly, $\Delta(\Delta\theta_{1,j}) < 0 \ \forall j \in \mathcal{J}^-$. Using this fact and the independence of the Θ_i's, we can simplify (A.20) as

$$\begin{aligned} &\Pr\left\{\pi_i \le \Pi_i \le \pi_i + \Delta(\pi_i) \,|\, \Theta_2 = \theta_2, \Theta_3 = \theta_3, \ldots, \Theta_m = \theta_m\right\} \\ &\quad = \sum_{j \in \mathcal{J}^-} \Pr\left\{\Delta\theta_{1,j} - |\Delta(\Delta\theta_{1,j})| < \Delta\Theta_1 < \Delta\theta_{1,j}\right\} \\ &\quad + \sum_{j \in \mathcal{J}^+} \Pr\left\{\Delta\theta_{1,j} < \Delta\Theta_1 < \Delta\theta_{1,j} + |\Delta(\Delta\theta_{1,j})|\right\}. \end{aligned} \tag{A.22}$$

Further, since $\Pr\{x \le X \le x + |\Delta(x)|\} = \Pr\{x - |\Delta(x)| \le X \le x\} \approx f_X(x) \cdot |\Delta(x)|$, it follows from (A.22) that

$$\begin{aligned} f_{\Pi_i|\Theta_2,\ldots,\Theta_m}(\pi_i \,|\, \theta_2, \ldots, \theta_m) \cdot \Delta\pi_i &= \sum_{j \in \mathcal{J}^-} f_{\Delta\Theta_1}(\Delta\theta_{1,j}) \cdot |\Delta(\Delta\theta_{1,j})| \\ &+ \sum_{j \in \mathcal{J}^+} f_{\Delta\Theta_1}(\Delta\theta_{1,j}) \cdot |\Delta(\Delta\theta_{1,j})| \\ &= \sum_{j=1}^{t} f_{\Delta\Theta_1}(\Delta\theta_{1,j}) \cdot |\Delta(\Delta\theta_{1,j})|. \end{aligned} \tag{A.23}$$

By construction, $\Delta\pi_i > 0$, which implies $|\Delta\pi_i| = \Delta\pi_i$, and therefore

$$\begin{aligned} f_{\Pi_i|\Theta_2,\ldots,\Theta_m}(\pi_i \,|\, \theta_2, \ldots, \theta_m) &= \sum_{j=1}^{t} f_{\Delta\Theta_1}(\Delta\theta_{1,j}) \cdot \frac{|\Delta(\Delta\theta_{1,j})|}{|\Delta\pi_i|} \\ &= \sum_{j=1}^{t} f_{\Delta\Theta_1}(\Delta\theta_{1,j}) \cdot \left| \frac{\Delta\pi_i}{\Delta(\Delta\theta_{1,j})} \right|^{-1}. \end{aligned} \tag{A.24}$$

In the limit, as $\Delta(\Delta\theta_{1,j}) \to 0$,

$$\begin{aligned} f_{\Pi_i|\Theta_2,\ldots,\Theta_m}(\pi_i \,|\, \theta_2, \ldots, \theta_m) &= \sum_{j=1}^{t} f_{\Delta\Theta_1}(\Delta\theta_{1,j}) \cdot \lim_{\Delta(\Delta\theta_{1,j})\to 0} \left| \frac{\Delta\pi_i}{\Delta(\Delta\theta_{1,j})} \right|^{-1} \\ &= \sum_{j=1}^{t} f_{\Delta\Theta_1}(\Delta\theta_{1,j}) \cdot \left| \lim_{\Delta(\Delta\theta_{1,j})\to 0} \frac{\Delta\pi_i}{\Delta(\Delta\theta_{1,j})} \right|^{-1} \\ &= \sum_{j=1}^{t} \frac{f_{\Delta\Theta_1}(\Delta\theta_{1,j})}{|p_i'(\Delta\theta_{1,j})|}. \end{aligned} \tag{A.25}$$

A.4 The Case of Dependent Model Parameters Considered in (3.25)

In order to obtain $f_{\Pi_i}(\pi_i)$, (pdfs of the other indices follow similarly), we first compute $f_{\Pi_i|\Theta_2,\ldots,\Theta_m}(\pi_i|\theta_2, \ldots, \theta_m)$ as

$$f_{\Pi_i|\Theta_2,\ldots,\Theta_m}(\pi_i|\theta_2, \ldots, \theta_m) = \sum_{j=1}^{r} \frac{f_{\Delta\Theta_1|\Theta_2,\ldots,\Theta_m}(\Delta\theta_{1,j}|\theta_2, \ldots, \theta_m)}{|p_i'(\Delta\theta_{1,j})|}, \tag{A.26}$$

where $\Delta\theta_{1,1}$, $\Delta\theta_{1,2}, \ldots \Delta\theta_{1,r}$ are the $r \leq t$ real roots of $\pi_i = \pi_i(m_\Theta) + \sum_{k=1}^{t} \frac{b_{ki}}{k!} \Delta\Theta_1^k$, and $m_\Theta = [m_{\Theta_1}, \theta_2, \ldots, \theta_m]$. Note that the above result follows from (A.22). Since the model parameters are dependent, the numerator in (A.26) does not simplify to $f_{\Delta\Theta_1}(\Delta\theta_{1,j})$ (as was the case in (3.22)). If the joint pdf of the model parameters is known, $f_{\Delta\Theta_1|\Theta_2,\ldots,\Theta_m}(\Delta\theta_{1,j}|\theta_2, \ldots, \theta_m)$ can be obtained as

$$\begin{aligned} f_{\Delta\Theta_1|\Theta_2,\ldots,\Theta_m}(\Delta\theta_1|\theta_2, \ldots, \theta_m) &= f_{\Theta_1|\Theta_2,\ldots,\Theta_m}(m_{\Theta_1} + \Delta\theta_1|\theta_2, \ldots, \theta_m) \\ &= \frac{f_{\Theta_1,\Theta_2,\ldots,\Theta_m}(m_{\Theta_1} + \Delta\theta_1, \theta_2, \ldots, \theta_m)}{f_{\Theta_2,\ldots\Theta_m}(\theta_2, \ldots, \theta_m)} \\ &= \frac{f_{\Theta_1,\Theta_2,\ldots,\Theta_m}(m_{\Theta_1} + \Delta\theta_1, \theta_2, \ldots, \theta_m)}{\int_{\theta_1} f_{\Theta_1,\Theta_2,\ldots,\Theta_m}(\theta_1, \theta_2, \ldots, \theta_m) d\theta_1} \end{aligned} \tag{A.27}$$

The last step in the derivation above is necessary, since we assume only the joint distribution is known. Once $f_{\Pi_i|\Theta_2,\ldots,\Theta_m}(\pi_i|\theta_2, \ldots, \theta_m)$ is computed, it is straight-

forward to obtain $f_{\Pi_i}(\pi_i)$ from the total probability theorem as

$$\begin{aligned} f_{\Pi_i}(\pi_i) &= \int_{\theta_2} \cdots \int_{\theta_m} f_{\Pi_i|\Theta_2,\ldots,\Theta_m}(\pi_i|\theta_2,\ldots,\theta_m)\, f_{\Theta_2,\ldots\Theta_m}(\theta_2,\ldots\theta_m) d\theta_2 \ldots d\theta_m \\ &= \int_{\theta_2} \cdots \int_{\theta_m} f_{\Pi_i|\Theta_2,\ldots,\Theta_m}(\pi_i|\theta_2,\ldots,\theta_m) \left(\int_{\theta_1} f_{\Theta_1,\ldots,\Theta_m}(\theta_1,\ldots\theta_m) d\theta_1 \right) d\theta_2 \ldots d\theta_m \end{aligned} \tag{A.28}$$

Since $f_{\Pi_i|\Theta_2,\ldots,\Theta_m}(\pi_i|\theta_2,\ldots,\theta_m)$ does not depend on θ_1, we can express (A.28) as follows:

$$f_{\Pi_i}(\pi_i) = \int_{\theta_1} \cdots \int_{\theta_m} f_{\Pi_i|\Theta_2,\ldots,\Theta_m}(\pi_i|\theta_2,\ldots,\theta_m)\, f_{\Theta_1,\ldots\Theta_m}(\theta_1,\ldots\theta_m) d\theta_1 d\theta_2 \ldots d\theta_m. \tag{A.29}$$

A.5 Derivation of Linearized Power-System Model in (8.2)

Recall the standard power-system DAE model in (8.1). Denote the Jacobian of $f(\cdot,\cdot)$ and $g(\cdot,\cdot,\cdot)$ evaluated at (x^*, y^*, u^*) by

$$J_f|_{(x^*,y^*)} = \left[\frac{\partial f}{\partial x}, \frac{\partial f}{\partial y}\right]\Bigg|_{(x^*,y^*)}^T =: [f_x,\, f_y]^T, \tag{A.30}$$

$$J_g|_{(x^*,y^*,u^*)} = \left[\frac{\partial g}{\partial x}, \frac{\partial g}{\partial y}, \frac{\partial g}{\partial u}\right]\Bigg|_{(x^*,y^*,u^*)}^T =: [g_x,\, g_y,\, g_u]^T. \tag{A.31}$$

Linearizing $f(\cdot,\cdot)$ about the equilibrium point, up to first order, we get

$$\dot{x} \approx f(x^*, y^*) + f_x(x - x^*) + f_y(y - y^*) = f_x x + f_y y - f_x x^* - f_y y^*, \tag{A.32}$$

where we have used the fact $f(x^*, y^*) = 0$. Similarly, linearizing $g(\cdot,\cdot,\cdot)$ about the equilibrium point,

$$0 \approx g(x^*, y^*, u^*) + g_x(x - x^*) + g_y(y - y^*) + g_u(u - u^*). \tag{A.33}$$

Assuming that $g_y = \partial g/\partial y|_{(x^*,y^*,u^*)}$ is invertible, and recognizing that $g(x^*, y^*, u^*) = 0$, we get

$$y \approx g_y^{-1}\left(-g_x(x - x^*) - g_u(u - u^*) + g_y y^*\right). \tag{A.34}$$

Finally, substituting for y from (A.34) in (A.32), we get the linear system $\dot{x} = Ax + Bu + C$, with A , B , and C given by

$$A = f_x - g_y^{-1} g_x \tag{A.35}$$

$$B = f_y - g_y^{-1} g_u, \tag{A.36}$$

$$C = \left(g_y^{-1} g_x - f_x\right) x^* + \left(I - f_y\right) y^* + g_y^{-1} g_u u^*. \tag{A.37}$$

REFERENCES

[1] G. J. Anders, *Probability Concepts in Electric Power Systems*. New York, NY: John Wiley and Sons, 1990.

[2] R. Billinton, M. Fotuhi-Firuzabad, and L. Bertling, "Bibliography on the application of probability methods in power system reliability evaluation 1996-1999," *IEEE Transactions on Power Systems*, vol. 16, no. 4, pp. 595–602, November 2001.

[3] A. P. Leite, C. L. T. Borges, and D. M. Falcão, "Probabilistic wind farms generation model for reliability studies applied to Brazilian sites," *IEEE Transactions on Power Systems*, vol. 21, no. 4, pp. 1493–1501, November 2006.

[4] F. Castro Sayas and R. Allan, "Generation availability assessment of wind farms," *IEE Proceedings-Generation, Transmission and Distribution*, vol. 143, no. 5, pp. 507–518, September 1996.

[5] C. L. T. Borges and R. J. Pinto, "Small hydro power plants energy availability modeling for generation reliability evaluation," *IEEE Transactions on Power Systems*, vol. 23, no. 3, pp. 1125–1135, August 2008.

[6] H. A. M. Maghraby, M. H. Shwehdi, and G. K. Al-Bassam, "Probabilistic assessment of photovoltaic generation systems," *IEEE Transactions on Power Systems*, vol. 17, no. 1, pp. 205–208, February 2002.

[7] S. V. Dhople, A. Davoudi, P. L. Chapman, and A. D. Domínguez-García, "Integrating photovoltaic inverter reliability into energy yield estimation with Markov models," in *IEEE 12th Workshop on Control and Modeling for Power Electronics*, June 2010, pp. 1 –5.

[8] S. V. Dhople and A. D. Domínguez-García, "Estimation of photovoltaic system reliability and performance metrics," *IEEE Transactions on Power Systems*, vol. 27, no. 1, pp. 554–563, February 2012.

[9] G. A. Hamoud, "Assessment of spare transformer requirements for distribution systems," *IEEE Transactions on Power Systems*, vol. 26, no. 1, pp. 174–180, February 2011.

[10] H. Ge and S. Asgarpoor, "Reliability evaluation of equipment and substations with fuzzy Markov processes," *IEEE Transactions on Power Systems*, vol. 25, no. 3, pp. 1319–1328, August 2010.

[11] J. Endrenyi, *Reliability Modeling in Electric Power Systems.* New York, NY: John Wiley and Sons, 1978.

[12] L. Yin, M. A. J. Smith, and K. S. Trivedi, "Uncertainty analysis in reliability modeling," *Reliability and Maintainability Symposium*, pp. 229–234, 2001.

[13] S. V. Dhople and A. D. Domínguez-García, "A parametric uncertainty analysis method for Markov reliability and reward models," *IEEE Transactions on Reliability*, vol. 61, no. 3, pp. 634–648, September 2012.

[14] S. V. Dhople, Y. C. Chen, and A. D. Domínguez-García, "A set-theoretic method to propagate parametric uncertainty in Markov reliability models," *IEEE Transactions on Reliability*, in review.

[15] A. Devaraj, K. Mishra, and K. S. Trivedi, "Uncertainty propagation in analytic availability models," in *Proc. IEEE Symposium on Reliable Distributed Systems*, 2010, pp. 121–130.

[16] B. R. Haverkort and A. M. H. Meeuwissen, "Sensitivity and uncertainty analysis of Markov-reward models," *IEEE Transactions on Reliability*, vol. 44, no. 1, pp. 147–154, March 1995.

[17] M. L. Shooman, *Probabilistic Reliability: An Engineering Approach.* Malabar, FL: Robert E. Krieger Publishing Company, 1990.

[18] S. L. Campbell and C. D. Meyer Jr., *Generalized Inverses of Linear Transformations.* Mineola, NY: Dover Publications, 1991.

[19] B. R. Haverkort and A. M. H. Meeuwissen, "Sensitivity and uncertainty analysis in performability modeling," *Symposium on Reliable Distributed Systems*, pp. 93–102, 1992.

[20] J. T. Blake, A. L. Reibman, and K. S. Trivedi, "Sensitivity analysis of reliability and performability measures for multiprocessor systems," *Proceedings of the ACM Sigmetrics*, pp. 177–186, 1988.

[21] K. Takaragi, R. Sasaki, and S. Shingai, "A probability bound estimation method in Markov reliability analysis," *IEEE Transactions on Reliability*, vol. 34, no. 3, pp. 257–261, August 1985.

[22] A. Gandini, "Importance and sensitivity analysis in assessing system reliability," *IEEE Transactions on Reliability*, vol. 39, no. 1, pp. 61–70, April 1990.

[23] F. C. Schweppe, *Uncertain Dynamic Systems.* Englewood Cliffs, NJ: Prentice-Hall, Inc., 1973.

[24] H. S. M. Coxeter, *Regular Polytopes.* New York, NY: Dover Publications Inc., 1973.

[25] E. R. Hansen, "Bounding the solution of interval linear equations," *SIAM Journal on Numerical Analysis*, vol. 29, no. 5, pp. 1493–1503, Oct. 1992.

[26] S. Galdino and P. Maciel, "Outer estimates of interval system of linear equations: ISPN models in dependability evaluation," in *IEEE International Conference on Systems Man and Cybernetics (SMC), 2008*, Oct. 2008, pp. 2075–2080.

[27] ——, "Availability with input uncertainties using an interval-based approach," in *IEEE International Conference on Systems Man and Cybernetics (SMC), 2010*, Oct. 2010, pp. 298–303.

[28] D. K. Mohanta, P. K. Sadhu, and R. Chakrabarti, "Fuzzy Markov model for determination of fuzzy state probabilities of generating units including the effect of maintenance scheduling," *IEEE Transactions on Power Systems*, vol. 20, no. 4, pp. 2117–2124, November 2005.

[29] J. C. Ke, H. I. Huang, and C. H. Lin, "Parametric programming approach for a two-unit repairable system with imperfect coverage, reboot and fuzzy parameters," *IEEE Transactions on Reliability*, vol. 57, no. 3, pp. 498–506, September 2008.

[30] M. H. A. Davis, *Markov Models and Optimization.* London, UK: Chapman and Hall, 1993.

[31] J. P. Hespanha, "A model for stochastic hybrid systems with application to communication networks," *Nonlinear Analysis,* Special Issue on Hybrid Systems, vol. 62, no. 8, pp. 1353–1383, September 2005.

[32] ——, "Modelling and analysis of stochastic hybrid systems," *IEE Proceedings–Control Theory and Applications*, vol. 153, no. 5, pp. 520–535, September 2006.

[33] S. Rácz and M. Telek, "Performability analysis of Markov reward models with rate and impulse reward," in *International Conference on Numerical solution of Markov chains*, 1999, pp. 169–187.

[34] G. Horváth, S. Rácz, and M. Telek, "Analysis of second-order Markov reward models," in *International Conference on Dependable Systems and Networks*, June 2004, pp. 845–854.

[35] G. Horváth, S. Rácz, Á. Tari, and M. Telek, "Evaluation of reward analysis methods with MRMSolve 2.0," *International Conference on Quantitative Evaluation of Systems*, pp. 165–174, 2004.

[36] E. de Souza e Silva, H. R. Gail, and R. V. Campos, "Calculating transient distributions of cumulative reward," *SIGMETRICS Performance Evaluation Review*, vol. 23, no. 1, pp. 231–240, May 1995.

[37] D. P. Bertsekas and J. N. Tsitsiklis, *Introduction to Probability.* Belmont, MA: Athena Scientific, 2008.

[38] B. R. Iyer, L. Donatiello, and P. Heidelberger, "Analysis of performability for stochastic models of fault-tolerant systems," *IEEE Transactions on Computers*, vol. C-35, no. 10, pp. 902–907, October 1986.

[39] L. Donatiello and B. R. Iyer, "Analysis of a composite performance reliability measure for fault-tolerant systems," *Journal of the ACM*, vol. 34, no. 1, pp. 179–199, 1987.

[40] M. A. Qureshi and W. H. Sanders, "Reward model solution methods with impulse and rate rewards: an algorithm and numerical results," *Performance Evaluation*, vol. 20, pp. 413–436, July 1994.

[41] J. K. Muppala, M. Malhotra, and K. S. Trivedi, *Markov Dependability Models of Complex Systems: Analysis Techniques,* (ed.) S. Özekici. Berlin: Springer, 1992.

[42] F. Castella, G. Dujardin, and B. Sericola, "Moments' analysis in homogeneous Markov reward models," *Methodology and Computing in Applied Probability*, vol. 11, pp. 583–601, 2009.

[43] J. Devooght and P. E. Labeau, "Moments of the distributions in probabilistic dynamics," *Annals of Nuclear Energy*, vol. 22, no. 2, pp. 97–108, February 1995.

[44] J. Devooght and C. Smidts, "Probabilistic reactor dynamics–I: The theory of continuous event trees," *Nuclear Science and Engineering*, vol. 111, pp. 229–240, 1992.

[45] ——, "Probabilistic dynamics as a tool for dynamic PSA," *Reliability Engineering and System Safety*, vol. 52, no. 3, pp. 185–196, June 1996.

[46] M. Rausand and A. Høyland, *System Reliability Theory.* Hoboken, NJ: Wiley Interscience, 2004.

[47] R. A. Sahner, K. S. Trivedi, and A. Puliafito, *Performance and Reliability Analysis of Computer Systems.* Norwell, MA: Kluwer Academic Publishers, 2002.

[48] G. Grimmett and D. Stirzaker, *Probability and Random Processes.* Oxford University Press, 1992.

[49] C. D. Meyer Jr., "The role of the group generalized inverse in the theory of finite Markov chains," *SIAM*, vol. 17, no. 3, pp. 443–464, July 1975.

[50] G. H. Golub and C. D. Meyer Jr., "Using the QR factorization and group inversion to compute, differentiate, and estimate the sensitivity of stationary probabilities for Markov chains," *SIAM*, vol. 7, no. 2, pp. 273–281, April 1986.

[51] H. Stark and J. W. Woods, *Probability, Random Processes, and Estimation Theory for Engineers.* Englewood Cliffs, NJ: Prentice Hall, 1994.

[52] A. M. Breipohl, *Probabilistic Systems Analysis.* New York: John Wiley and Sons, 1970.

[53] A. D. Domínguez-García, J. G. Kassakian, and J. E. Schindall, "A generalized fault coverage model for linear time-invariant systems," *IEEE Transactions on Reliability*, vol. 58, no. 3, pp. 553–567, September 2009.

[54] Y. C. Chen and A. D. Domínguez-García, "Assessing the impact of wind variability on power system small-signal reachability," in *Proc. Hawaii International Conference on System Sciences*, 2011, pp. 1–8.

[55] S. Boyd and L. Vandenberghe, *Convex Optimization.* New York, NY: Cambridge University Press, 2004.

[56] H. Ge, "Maintenance optimization for substations with aging equipment," Master's thesis, University of Nebraska, Lincoln, NE, April 2010.

[57] K. Vaidyanathan, D. Selvamuthu, and K. S. Trivedi, "Analysis of inspection-based preventive maintenance in operational software systems," in *IEEE Symposium on Reliable Distributed Systems*, 2002, pp. 286–295.

[58] S. V. Dhople, L. DeVille, and A. D. Domínguez-García, "A stochastic hybrid systems framework for performability analysis," *Performance Evaluation*, in review.

[59] G. J. Anders and A. M. L. da Silva, "Cost related reliability measures for power system equipment," *IEEE Transactions on Power Systems*, vol. 15, no. 2, pp. 654–660, May 2000.

[60] S. Price and R. Margolis, "2008 Solar technologies market report," National Renewable Energy Laboratory, Tech. Rep., January 2010.

[61] J. E. Granata and M. A. Quintana, "System level reliability methodologies," Sandia National Laboratories, Tech. Rep., July 2009.

[62] R. Billinton and R. Allan, *Reliability Assessment of Large Power Systems.* Boston, MA: Kluwer Academic Publishers, 1988.

[63] M. A. Hamdy, M. E. Beshir, and S. E. Elmasry, "Reliability analysis of photovoltaic systems," *Applied Energy*, vol. 33, no. 4, pp. 253–263, 1989.

[64] W. M. Rohouma, I. M. Molokhia, and A. Esuri, "Comparative study of different PV modules configuration reliability," *Desalination*, vol. 209, pp. 122–128, April 2007.

[65] L. H. Stember, W. R. Huss, and M. S. Bridgman, "A methodology for photovoltaic system reliability and economic analysis," *IEEE Transactions on Reliability*, vol. R-31, no. 3, pp. 296–303, August 1982.

[66] A. C. G. Melo and M. V. F. Pereira, "Sensitivity analysis of reliability indices with respect to equipment failure and repair rates," *IEEE Transactions on Power Systems*, vol. 10, no. 2, pp. 1014–1021, May 1995.

[67] G. M. Masters, *Renewable and Efficient Electric Power Systems.* Hoboken, NJ: Wiley Interscience, 2004.

[68] L. Sherwood, "U. S. solar market trends 2008," Interstate Renewable Energy Council, Tech. Rep., July 2009.

[69] J. S. Stein and S. P. Miller, "Stochastic PV performance/reliability model," Sandia National Laboratories, Tech. Rep., April 2010.

[70] T. Key, "Distributed photovoltaics: Utility integration issues and opportunities," Electric Power Research Institute, Tech. Rep., August 2010.

[71] S. V. Dhople, J. L. Ehlmann, C. J. Murray, S. T. Cady, and P. L. Chapman, "Engineering systems in the gable home: A passive, net-zero, solar-powered house for the U. S. Department of Energy's 2009 Solar Decathlon," *Power and Energy Conference at Illinois (PECI), 2010*, pp. 58–62, 2010.

[72] H. Laukamp, "Reliability study of grid-connected PV systems," International Energy Agency, Tech. Rep., March 2002.

[73] S. B. Kjaer, J. K. Pedersen, and F. Blaabjerg, "A review of single-phase grid-connected inverters for photovoltaic modules," *IEEE Transactions on Industry Applications*, vol. 41, no. 5, pp. 1292–1306, September/October 2005.

[74] D. L. King, W. E. Boyson, and J. A. Kratochvil, "Photovoltaic array performance model," Sandia National Laboratories, Tech. Rep., Augustl 2004.

[75] S. V. Dhople and A. D. Domínguez-García, "A framework to determine the probability density function for the output power of wind farms," in *North American Power Symposium (NAPS)*, September 2012, pp. 1–6.

[76] J. Abelson, "Theory energy and sustainable engineering," Class notes for ENG571, University of Illinois, 2010.

[77] Vestas, "V90-1.8/2.0 MW data sheet," 2011. [Online]. Available: "http://www.vestas.com"

[78] T. Ackermann, *Wind Power in Power Systems.* West Sussex, England: John Wiley and Sons, 2005.

[79] F. F. Wu and Y.-K. Tsai, "Probabilistic dynamic security assessment of power systems-I: Basic model," *IEEE Transactions on Circuits and Systems*, vol. 30, no. 3, pp. 148–159, March 1983.

[80] F. F. Wu and S. Kumagai, "Steady-state security regions of power systems," *IEEE Transactions on Circuits and Systems*, vol. 29, no. 11, pp. 703–711, November 1982.

[81] R. Kaye and F. F. Wu, "Dynamic security regions of power systems," *IEEE Transactions on Circuits and Systems*, vol. 29, no. 9, pp. 612–623, September 1982.

[82] V. A. Ugrinovskii and H. R. Pota, "Decentralized control of power systems via robust control of uncertain Markov jump parameter systems," in *IEEE Conference on Decision and Control*, December 2004, pp. 3503–3508.

[83] Y.-Z. Li, L. Ru, and J.-C. Niu, "Forecast of power generation for grid-connected photovoltaic system based on Grey model and Markov chain," in *IEEE Conference on Industrial Electronics and Applications.*

[84] Y.-Z. Li, L. He, and R.-Q. Nie, "Short-term forecast of power generation for grid-connected photovoltaic system based on advanced Grey-Markov chain," in *International Conference on Energy and Environment Technology*, vol. 2, October 2009, pp. 275–278.

[85] P. S. Perez, J. Driesen, and R. Belmans, "Characterization of the solar power impact in the grid," in *International Conference on Clean Electrical Power*, May 2007, pp. 366–371.

[86] G. Papaefthymiou and B. Klöckl, "MCMC for wind power simulation," *IEEE Transactions on Energy Conversion*, vol. 23, no. 1, pp. 234–240, March 2008.

[87] J. Bect, Y. Phulpin, H. Baili, and G. Fleury, "On the Fokker-Planck equation for stochastic hybrid systems: Application to a wind turbine model," in *International Conference on Probabilistic Methods Applied to Power Systems*, June 2006, pp. 1–6.

[88] K. Wang and M. L. Crow, "Numerical simulation of stochastic differential algebraic equations for power system transient stability with random loads," in *IEEE Power and Energy Society General Meeting*, July 2011, pp. 1–8.

[89] P. Sauer and M. A. Pai, *Power System Dynamics and Stability.* Upper Saddle River, NJ: Prentice Hall, 1998.

[90] A. D. Domínguez-García, *"Models for Impact Assessment of Wind-Based Power Generation on Frequency Control,"* in Control and Optimization Methods for Electric Smart Grids, (ed.) A. Chakrabortty, and M. Ilić. Berlin: Springer-Verlag, 2012.

[91] Y. C. Chen and A. D. Domínguez-García, "A method to study the effect of renewable resource variability on power system dynamics," *IEEE Transactions on Power Systems*, To Appear.